PREPARATION AND CHARACTERIZATION OF VINYLSILANE CROSSLINKED THERMOPLASTIC COMPOSITES FILLED WITH NANOCLAYS

by

MOTSHABI ALINAH SIBEKO (B.Sc. Hons.)

Submitted in accordance with the requirement of the degree

MASTER OF SCIENCE (M.S.c)

Department of Chemistry

Faculty of Natural and Agricultural Sciences

at the

UNIVERSITY OF THE FREE STATE (QWAQWA CAMPUS)

SUPERVISOR: PROF A.S. LUYT

05 December 2012

DECLARATION

I hereby declare that the research in this thesis is my own independent work, and has not previously been submitted to any other University in order to obtain a degree. I further cede copyright of the dissertation in favour of the University of the Free State.

_____	_____
M.A. Sibeko	Prof. A.S. Luyt

DEDICATION

This work is dedicated to the entire Sibeko family for their undivided love, patience and support. ToMatebesi Sibeko (father), Mantseke Sibeko (mom), Madika, Mantwa, Matseko, Manakedi (sisters), Tello, Tseko, Setjhaba, Motjhakela, Tebello (brothers), Matona (brother in law), Mamaziya, Ncentseng (sisters in law), Nthabiseng, Refilwe, Retsedisitswe, Hlohonolofatso (nieces), Tumelo, Maziya, Kamohelo, Teboho (nephews), and most importantly my late grandfather Tseko Fanyane Sibeko.

ABSTRACT

The effects of dicumyl peroxide/vinyltriethoxysilane (DCP/VTES) treatment, nanoclay content and the nature of the nanoclay were investigated for low-density polyethylene (LDPE)/clay and high-density polyethylene (HDPE)/clay nanocomposites. LDPE was treated with 0.1 phr of DCP with respectively 1 phr and 3 phr VTES (System A), and with 0.2 phr of DCP with the same amounts of VTES, and then mixed with different contents (1, 3, and 5 wt. %) of modified (Cloisite 15A) and unmodified (calcium montmorillonite) clay. The HDPE nanocomposites were prepared according to System A, using Cloisite 15A. The polymer-clay nanocomposites were prepared through melt mixing in a Brabender Plastograph internal mixer, and were characterized for their morphology, thermal properties, mechanical properties, thermomechanical properties and the extent of grafting/crosslinking. FTIR analysis clearly showed that grafting in System A was not very effective, and that the 'grafted' LDPE contained an appreciable amount of ungrafted (pure or hydrolysed) VTES. However, sufficient grafting was achieved in System B, but there was also a higher extent of crosslinking. The XRD and TEM results showed that C15A was more intercalated than Ca^{2+}MMT showed, and also slightly exfoliated. Nanocomposites prepared according to System A showed intercalated structures, while those prepared according to System B showed partially exfoliated structures. The DSC results showed that the presence of DCP/VTES decreased the melting temperature and crystallinity of both the polymer matrices due to a decrease in lamellar thickness as a result of crosslinking between the polymer chains, in addition to VTES grafting. The addition of clay and its nature had no significant influence on the melting temperature and crystallinity of both polymers. The TGA results showed an improvement in the thermal stability of all the nanocomposites, but the silane treated C15A nanocomposites showed a higher degradation rate at higher clay contents. The mechanical and thermomechanical properties of the untreated nanocomposites were better than those of the treated nanocomposites at the same clay loading.

TABLE OF CONTENTS

		Page
DECLARATION		**i**
DEDICATION		**ii**
ABSTRACT		**iii**
TABLE OF CONTENTS		**iv**
LIST OF ABBREVIATIONS AND SYMBOLS		**vii**
LIST OF TABLES		**viii**
LIST OF FIGURES		**ix**
CHAPTER ONE (INTRODUCTION)		**1**
1.1	Background	1
1.2	Polymer based nanocomposites	1
1.3	Polymer-clay nanocomposites	2
1.4	Clay minerals	2
1.5	Methods used to prepare polymer-clay nanocomposites	4
1.6	Polymer-clay nanocomposites structures	5
1.7	Drawbacks and limitations of polymer-clay nanocomposites	6
1.8	Applications of polymer-clay nanocomposites	7
1.9	Aims and objectives	8
1.10	Thesis outline	8
1.11	References	9
CHAPTER TWO (LITERATURE REVIEW)		**13**
2.1	Introduction	13
2.2	Layered silicate	13
2.2.1	Structure of layered silicate	13
2.2.2	Modification of layered silicates	15

2.2.2.1 Ion exchange modification 16
2.2.2.2 Modification of clay with a silane compound 17
2.3 Techniques used to characterize polymer-clay nanocomposites 18
2.4 Factors affecting the extent of clay modification 20
2.5 Polyethylenes 23
2.5.1 Modification of polyethylene 24
2.5.2 Polyethylene reinforced nanocomposites 26
2.6 Properties of polymer-clay nanocomposites 27
2.6.1 Morphology 27
2.6.2 Mechanical and thermomechanical properties 29
2.6.3 Thermal properties 32
2.7 Properties of other polyethylene reinforced nanocomposites 34
2.7.1 Morphology 34
2.7.2 Thermal properties 35
2.7.3 Mechanical and thermomechanical properties 35
2.8 References 36

CHAPTER THREE (MATERIALS AND METHODS) 46

3.1 Materials 46
3.1.1 High-density polyethylene 46
3.1.2 Low-density polyethylene 46
3.1.3 Nanoclays 46
3.1.4 Other chemicals 47
3.1.4.1 Dicumyl peroxide 47
3.1.4.2 Vinyltriethoxysilane 47
3.2 Methods 47
3.2.1 Preparation of polyethylene-g-vinyltriethoxysilane 47
3.2.2 Preparation of polyethylene-g-vinyltriethoxysilane-clay nanocomposites 50
3.2.3 Preparation of polyethylene-clay nanocomposites 50
3.3 Characterizations 51
3.3.1 X-ray diffraction (XRD) 51
3.3.2 Transmission electron microscopy (TEM) 51
3.3.3 Differential scanning calorimetry (DSC) 52

3.3.4 Thermogravimetric analysis (TGA) 53
3.3.5 Dynamic mechanical analysis (DMA) 53
3.3.6 Tensile testing 54
3.3.7 Fourier-transform infrared (FTIR) spectroscopy 55
3.3.8 Gel content 55
3.4 References 56

CHAPTER FOUR (RESULTS AND DISCUSSION) 58

4.1 Attenuated total reflectance Fourier-transform infrared (ATR-FTIR) spectroscopy 58
4.2 X-ray diffraction (XRD) and transmission electron microscopy (TEM) 63
4.3 Thermogravimetric analysis (TGA) 72
4.4 Gel content 81
4.5 Differential scanning calorimetry (DSC) 84
4.6 Dynamic mechanical analysis (DMA) 97
4.7 Tensile testing 113
4.8 References 121

CHAPTER FIVE (CONCLUSIONS) 127

ACKNOWLEDGEMENTS 129

APPENDIX 131

LIST OF ABBREVIATIONS AND SYMBOLS

CEC	Cation exchange capacity
Ca^{2+}MMT	Calcium montmorillonite
C15A	Cloisite 15A
CPE	Chlorinate polyethylene
DCP	Dicumyl peroxide
ΔH_m^{obs}	Observed melting enthalpy
ΔH_m^{norm}	Normalized melting enthalpy
DSC	Differential scanning calorimetry
DMA	Dynamic mechanical analysis
E'	Storage modulus
E''	Loss modulus
EVA	Ethylene vinyl acetate
EVOH	Ethylene vinyl alcohol
FTIR	Fourier-transform infrared spectroscopy
MMT	Montmorillonite
MWCNT	Multi-walled carbon nanotubes
NMR	Nuclear magnetic resonance
PCNs	Polymer clay nanocomposites
POSS	Polyhedral oligomeric silsesquioxanes
PEO	Poly(ethylene oxide)
PPA	Poly(acrylic acid)
PE-g-MA	Maleic anhydride grafted polyethylene
phr	Parts per hundred rubber
SWCNT	Single-walled carbon nanotubes
TGA	Thermogravimetric analysis
TEM	Transmission electron microscopy
VTES	Vinyltriethoxysilane
VTMS	Vinyltrimethoxysilane
tan δ	Damping coefficient
T_g	Glass transition temperature
T_m	Melting temperature

LIST OF TABLES

		Page
Table 1.1	Formulae of commonly used 2:1 phylosilicates	3
Table 3.1	Properties of nanoclays	46
Table 3.2	New peaks observed in the FTIR spectrum of vinyltriethoxysilane treated LDPE	49
Table 3.3	Samples ratios used to prepare the nanocomposites	50
Table 4.1	Some important peaks in the FTIR spectra of LDPE, LDPE-g-VTES, the two clays and the different nanocomposites	58
Table 4.2	The basal spacings of the clays determined from the d_{001} peaks and 2θ in the XRD spectra	64
Table 4.3	Summary of the TGA results for the LDPE, LDPE-g-VTES and the different nanocomposites (System A and System B)	73
Table 4.4	Summary of the TGA results for the HDPE, HDPE-g-VTES and the different nanocomposites (Systems A)	79
Table 4.5	Gel content of all the samples	83
Table 4.6	Summary of the DSC heating results for all the investigated LDPE-based samples	86
Table 4.7	Summary of the DSC heating results for all the investigated LDPE-based samples (System B)	89
Table 4.8	Summary of the DSC cooling results for all the investigated LDPE-based samples	93
Table 4.9	Summary of the DSC heating results for all the investigated HDPE-based samples	94
Table 4.10	Summary of the DSC cooling results for all the investigated HDPE-based samples	96
Table 4.11	Summary of the tensile results of LDPE samples	117
Table 4.12	Summary of the tensile results of HDPE samples	118

LIST OF FIGURES

		Page
Figure 1.1	Structure of 2:1 phyllosilicates	4
Figure 1.2	Schemes of different types of composites morphology which can arise from the interaction between layered silicates and polymer	6
Figure 2.1	(a) Silica tetrahedron and tetrahedral units arranged in a hexagonal network, and (b) octahedron and octahedral units arranged in a sheet	14
Figure 2.2	The arrangement of charges on the surface of silica layers	15
Figure 2.3	Schemes representation of clay surface treatment by ion-exchange reaction	17
Figure 2.4	Schematic representation of the coupling reaction of trifunctional silane molecules on clay	18
Figure 2.5	Illustration of the different states of dispersion of organo clays in a polymer matrix observed through XRD and TEM	19
Figure 3.1	Structure of the organic modifier	47
Figure 3.2	FTIR spectrum on pure LDPE and silane grafted LDPE	48
Figure 3.3	FTIR spectrum of pure LDPE and vinyltriethoxysilane grafted LDPE (System B)	48
Figure 3.4	Dumbbell shaped tensile testing sample	54
Figure 4.1	FTIR spectra of Ca^{2+}MMT and C15A	59
Figure 4.2	FTIR spectra of LDPE, VTES grafted LDPE (system A) and the different clay nanocomposites	60
Figure 4.3	FTIR spectra of LDPE, VTES grafted LDPE (system B) and the different clay nanocomposites	60
Figure 4.4	Coupling mechanism between the silica surface and silane	62
Figure 4.5	XRD diffractograms of the clays and their nanocomposites	65
Figure 4.6	TEM images of (a) 97/3 w/w LDPE/C15A and (b) 97/3 w/w LDPE/Ca^{2+}MMT nanocomposites	65
Figure 4.7	XRD diffractograms of C15A and its VTES treated LDPE nanocomposites (System A)	66

Figure 4.8	TEM micrographs of (a) 97/3 w/w LDPE-g-VTES (1 phr)/C15A and (b) 97/3 w/w LDPE-g-VTES (3 phr)/C15A (System A), (c) 97/3 w/w LDPE-g-VTES (1 phr)/C15A and (d) 97/3 w/w LDPE-g-VTES (3 phr)/C15A (System B)	67
Figure 4.9	XRD diffractograms of C15A and its VTES treated LDPE nanocomposites (System B)	68
Figure 4.10	A proposed diagram of the interaction of an epoxy molecule with silane functionalized MMT	68
Figure 4.11	TEM micrographs of low magnification (a) 97/3 w/w LDPE-g-VTES (1 phr)/C15A and (b) 97/3 w/w LDPE-g-VTES (3 phr)/Ca^{2+}MMT (System B), 93/3 w/w LDPE-g-VTES (1 phr)/Ca^{2+}MMT (c) System A (d) System B	69
Figure 4.12	XRD diffractograms of Ca^{2+}MMT and its VTES treated LDPE nanocomposites (System A)	70
Figure 4.13	XRD diffractograms of Ca^{2+}MMT and its VTES treated LDPE nanocomposites (System B)	70
Figure 4.14	XRD diffractograms of Cloisite 15A, 97/3 HDPE-g-VTES (1 phr)/C15A and HDPE-g-VTES (3 phr)/C15A (System A)	71
Figure 4.15	TEM micrographs of (a) HDPE-g-VTES (1 phr)/C15A (b) HDPE-g-VTES (3 phr)/C15A nanocomposites	72
Figure 4.16	TGA curves of Ca^{2+}MMT and Cloisite 15A	74
Figure 4.17	TGA curves of LDPE and the LDPE/C15A nanocomposites	75
Figure 4.18	TGA curves of LDPE and the LDPE/Ca^{2+} MMT nanocomposites	75
Figure 4.19	TGA curves of LDPE, VTES grafted LDPE (1 phr, System A) and the different nanocomposites	77
Figure 4.20	TGA curves of LDPE, VTES grafted LDPE (3 phr, System A) and the different nanocomposites	77
Figure 4.21	TGA curves of LDPE, VTES grafted LDPE (1 phr, System B) and the different nanocomposites	78
Figure 4.22	TGA curves of LDPE, VTES grafted LDPE (3 phr, System B) and the different nanocomposites	78
Figure 4.23	TGA curves of HDPE, VTES grafted HDPE (1 phr, System A) and the different nanocomposites	80

Figure 4.24	TGA curves of HDPE, VTES grafted HDPE (3 phr, System A) and the different nanocomposites	81
Figure 4.25	Gel content of VTES treated LDPE/C15A and its different nanocomposites (System A)	82
Figure 4.26	Gel content of VTES treated HDPE/C15A and its different nanocomposites (System A)	82
Figure 4.27	DSC heating curves of LDPE and its clay nanocomposites	85
Figure 4.28	DSC cooling curves of LDPE and its clay nanocomposites	85
Figure 4.29	DSC heating curves of LDPE and LDPE treated different VTES contents (System A)	87
Figure 4.30	DSC heating curves of LDPE, VTES (1 phr) treated LDPE and the different nanocomposites (System A)	88
Figure 4.31	DSC heating curves of LDPE, VTES (3 phr) treated LDPE and the different nanocomposites (System A)	88
Figure 4.32	DSC heating curves of LDPE, and LDPE treated with different VTES contents (System B)	90
Figure 4.33	DSC heating curves of LDPE, VTES (1 phr) treated LDPE and the different nanocomposites (System B)	90
Figure 4.34	DSC heating curves of LDPE, VTES (3 phr) treated LDPE and the different nanocomposites (System B)	91
Figure 4.35	DSC cooling curves of LDPE, VTES (1 phr) treated LDPE and the different nanocomposites (System A)	92
Figure 4.36	DSC cooling curves of LDPE, VTES (3 phr) treated LDPE and the different nanocomposites (System A)	92
Figure 4.37	DSC heating curves of HDPE, VTES treated LDPE (1 phr) and the different nanocomposites (System A)	95
Figure 4.38	DSC heating curves of HDPE, VTES treated LDPE (3 phr) and the different nanocomposites (System A)	95
Figure 4.39	DSC cooling curves of HDPE, VTES treated LDPE (1 phr) and the different nanocomposites (System A)	96
Figure 4.40	DSC cooling curves of HDPE, VTES treated LDPE (3 phr) and different nanocomposites (System A)	97
Figure 4.41	Storage modulus of the LDPE/C15A and LDPE/Ca^{2+}MMT Nanocomposites	99

Figure 4.42	Storage modulus of LDPE and LDPE with different VTES contents	99
Figure 4.43	Storage modulus of LDPE, LDPE-g-VTES (1 phr)/C15A and the different nanocomposites	100
Figure 4.44	Storage modulus of LDPE, LDPE-g-VTES (3 phr)/C15A and the different nanocomposites	100
Figure 4.45	Storage modulus of LDPE and the different LDPE/clay nanocomposites containing 3 wt. % of clay	101
Figure 4.46	Loss modulus of LDPE/C15A and LDPE/Ca^{2+}MMT nanocomposites	102
Figure 4.47	Loss modulus of LDPE and LDPE-g-VTES prepared with different VTES contents	103
Figure 4.48	Loss modulus of LDPE, LDPE-g-VTES (1 phr)/C15A andthe different nanocomposites	103
Figure 4.49	Loss modulus of LDPE, LDPE-g-VTES (3 phr)/C15A and the different nanocomposites	104
Figure 4.50	Loss modulus of LDPE and the different LDPE/clay nanocomposites containing 3 wt. % of clay	104
Figure 4.51	tan δ of LDPE treated with different contents of VTES	105
Figure 4.52	tan δ of LDPE, LDPE-g-VTES (1 phr)/C15A and the different nanocomposites	106
Figure 4.53	tan δ of LDPE, LDPE-g-VTES (3 phr)/C15A and the different nanocomposites	107
Figure 4.54	Storage modulus of LDPE and the different LDPE/clay nanocomposite	108
Figure 4.55	Loss modulus of LDPE and the different LDPE/clay nanocomposites	108
Figure 4.56	Storage modulus of HDPE and the HDPE-g-VTES (1 phr)/C15A nanocomposites	109
Figure 4.57	Storage modulus of HDPE and the HDPE-g-VTES (3 phr)/C15A nanocomposites	109
Figure 4.58	Loss modulus of HDPE and HDPE treated with different VTES contents	111
Figure 4.59	Loss modulus of HDPE and the HDPE-g-VTES (1 phr)/C15A nanocomposites	111
Figure 4.60	Loss modulus of HDPE and the HDPE-g-VTES (3 phr)/C15A nanocomposites	112
Figure 4.61	tan δ of HDPE and the HDPE-g-VTES (1 phr)/C15A nanocomposites	112

Figure 4.62 tan δ of HDPE and the HDPE-g-VTES (3 phr)/C15A nanocomposites 113
Figure 4.63 Tensile strength of LDPE/C15A, LDPE/Ca^{2+}MMT and the LDPE-g-VTES/C15A nanocomposites 115
Figure 4.64 Elongation at break of LDPE/C15A, LDPE/Ca^{2+}MMT and the LDPE-g-VTES/C15A nanocomposites 116
Figure 4.65 Young's modulus of LDPE/C15A, LDPE/Ca^{2+}MMT and the LDPE-g-VTES/C15A nanocomposites 116
Figure 4.66 Tensile strength of HDPE-g-VTES and the HDPE-g-VTES/C15A nanocomposites 119
Figure 4.67 Young's modulus of HDPE-g-VTES and the HDPE-g-VTES/C15A nanocomposites 120
Figure 4.68 Elongation at break of HDPE and HDPE-g-VTES/C15A nanocomposites 120

Chapter 1: General introduction

1.1 Background

The beginning of research on nanotechnology and nanoscience can be traced back over 40 years [1]. However, during the past decade nanotechnology went through a variety of disciplines, from chemistry to biology and from materials science to electrical engineering. Scientists are now creating the tools and developing the expertise to bring nanotechnology out of the research labs and into the market place [1,2]. Nanotechnology is regarded as a very promising field for industrial applications. One of the first applications of nanotechnology was the production of nanofillers. Nanofillers are materials added to plastic materials, in most cases polymers, in order to improve their strength, working properties and sometimes to reduce the cost [2].

The interest of producing composite materials with nanosized fillers or reinforcement i.e. nanocomposites has grown tremendously in recent years [2]. Nanocomposites are a new generation of composite materials made up of a polymer matrix and filler. However, at least one of the constituent phases of the filler must have one dimension of less than 100 nm. Nanocomposites were first reported in the patent literature as early as 1950 and have attracted much attention because of the remarkable improvement in their material properties when compared to virgin polymers [3,4]. Nanocomposites are applicable to a wide range of polymer matrices including thermoplastics, thermosets, elastomers, and natural and biodegradable polymers [5].

1.2 Polymer based nanocomposites

Polymers are used for a number of applications, but they often require certain properties in order to satisfy their numerous application needs. Nanofillers have been used to improve properties of polymers without any impact on density, transparency and processability of the polymer. Nanofillers are dispersed in polymer matrices at low loadings (< 10 wt. %), because they are small and have high aspect ratios [2,6-8]. Another aspect of nanoparticles that sets them apart is their enormous surface area, which increases the interaction with the polymer matrix. Nanofillers include nanoclays, nanofibres, carbon nanotubes (single-walled

(SWCNT) and multi-walled (MWCNT)), metal oxide nanoparticles, cellulose nanowhiskers, and polyhedral oligomeric silsesquioxanes (POSS). When compared to conventional polymers, nanofiller-containing polymers exhibit improved properties [2,7,9]. These improved properties include increased tensile strength, high modulus, improved electrical and optical properties, good thermal stability, decreased gas permeability, improved flammability resistance, decreased water absorbtion, and increased biodegradability of biodegradable polymers [2,8-10,16].

1.3 Polymer-clay nanocomposites

Polymer-clay nanocomposites (PCNs) are composites where nanoscale silicate layers are molecularly dispersed within a polymer matrix [5]. Clay-based polymer nanocomposites have attracted considerable attention in the past decade from the field of research and in various applications. This is due to the capacity of clay to improve nanocomposite properties and the strong synergistic effects between the polymer and the silicate platelets on both molecular or nanometric scale [11]. Polymer-clay nanocomposites have several advantages: (a) they are lighter in weight than the same polymers filled with other types of fillers; (b) they have enhanced flame retardance and thermal stability; and (c) they exhibit enhanced barrier properties [6,7,8]. This system was first studied in the early 1980s by the Toyota Central Research Laboratories. They used an *in situ* polymerization method (explained in section 1.5) to synthesise nylon-6-clay nanocomposites using caprolactam [12]. With the addition of only 5% clay, these nanocomposites gave greatly enhanced mechanical properties along with a large increase in heat distortion temperature. Their success has created a lot of attention in the use of clay as a reinforcement material for polymers [3,4,13,14].

1.4 Clay minerals

Clay minerals are normally called layered silicates because of their stacked structure of 1 nm silicate sheets which are in nanoscale with a variable basal distance. Nanoclays are grouped into different classes i.e. montmorillonites, hallosides, bentonites, hectorites and kaolirites [15]. Amongst them the most commonly used layered silicates for the preparation of polymer layered silicates nanocomposites belongs to the general family of layered silicates or phyllosilicates called montmorillonites [2]. There are two natural varieties of montmorillonite: sodium montmorillonite having a high swelling capacity in water, and

calcium montmorillonite with a low swelling capacity. The growing interest in using montmorillonites as reinforcement in polymer based nanocomposites is mainly due to their high cation exchange capacity (CEC), the degree to which the clay can absorb and exchange cations, their large surface area, their high aspect ratio, their platelets' morphology, as well as their low cost and natural availability [2,16,17]. Depending on their chemical composition and the nanoparticle morphology, the layered silicates can be divided into two phyllosilicate families:

- 1:1 phyllosilicates (non-swelling clay) are made up of one tetrahedral layer and one octahedral layer. They are not commonly used because they cannot expand, hence the forces that hold the adjacent clay layers in place are strong. As a result the silicate layers cannot be separated in order to allow polymer chains between them. Examples are kaolinite and the halloysites [18].

- 2:1 phyllosilicates (swelling clay) have a crystal structure with layers made up of two tetrahedrally coordinated silicon atoms fused to an edged-shared octahedral sheet of either aluminium or magnesium hydroxide. The layered thickness is around 1 nm, and the lateral dimension of these layers may differ from 30 nm to several microns or larger. Layers organize themselves to form stacks with regular van der Waals gaps in between them, called the interlayers or the gallery [19,20]. These types of clays are mostly used because of their ability to expand or swell, allowing polymer chains to penetrate between the layers. Examples are the montmorillonites (MMT), hectorite, and saponite [21]. Details of the structure and chemical composition of the layered silicates are shown in Table 1.1 and Figure 1.1.

Table 1.1 Formulae of commonly used 2:1 phylosilicates

2:1 phylosilicate	General formula	CEC / mequiv/100 g	Particle length / nm
Montmorillonite	$Mx(Al_{4-x}Mg_x)Si_8O_{20}(OH)_4$	110	100-150
Hectorite	$Mx(Mg_{6-x}Li_x)Si_8O_{20}(OH)_4$	120	200-300
Saponite	$MxMg_6(Si_{8-x}Al_x)Si_8O_{20}(OH)_4$	87	50-60

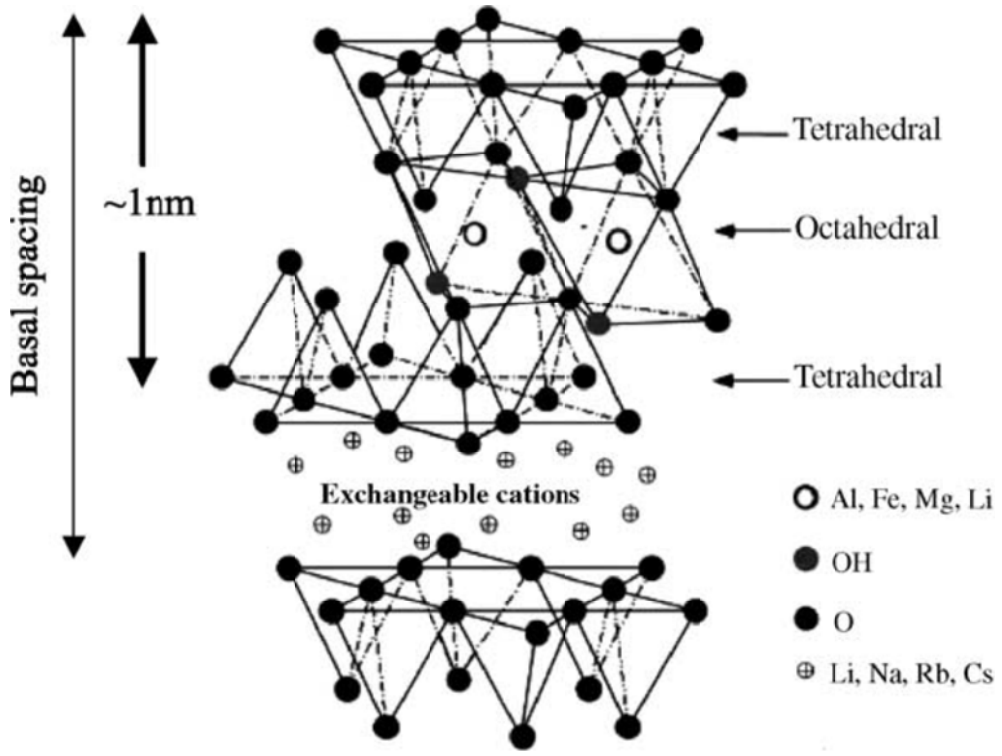

Figure 1.1 Structure of 2:1 phyllosilicates [25]

1.5 Methods used to prepare polymer-clay nanocomposites

There are three main preparative methods of polymer-clay nanocomposites according to the starting materials and processing techniques. The methods are solution mixing, *in situ* polymerization and melt mixing [22]. Solution mixing is based on a solvent system in which the polymer is soluble and the clay layers are swellable [19]. Clay is first swollen in a solvent and after mixing the polymer is added into the clay solution. The solvent separates the layers while allowing the polymer chains to be adsorbed onto the surface of individual silicate platelets. Clay layers can then exfoliate or the polymer chains intercalate into the clay galleries depending on the interaction between the polymer matrix and the clay. After mixing, the solvent is removed by evaporation and the nanocomposite maintains an intercalated or exfoliated structure [23,24].

During *in situ* polymerization, clay layers are swollen in a liquid monomer or a monomer solution such that polymerization occurs in between the clay layers. The process can be

initiated by heat, radiation or an organic initiator. The growing polymer chains have the ability to push the silicate layers apart leading to an exfoliated or intercalated structure [19, 25]. Melt blending involves mixing the layered silicates with the polymer above the softening point of the polymer. The applied shear causes the destruction of the clay stacking resulting in an intercalated or exfoliated structure [19,24].

Amongst the methods described above, melt blending is the most industrially valuable method to produce PCNs because of its low cost, high productivity, and environmental friendliness (due to the absence of organic solvents). Furthermore, it is compatible with current polymer processing techniques such as extrusion (co-extrusion twin-screw extruder) and injection moulding [24]. Although the use of solution mixing and *in situ* polymerization gives better results, their use is limited because of the unavailability of compatible solvents or suitable monomers, hence the preparation of nanocomposites via melt blending has been more explored [24,25].

1.6 Polymer-clay nanocomposite structures

The physical mixture of polymers and layered silicates does not necessarily form nanocomposites, because the compatibility and interaction between the two phases are very important [5]. The structures of PCNs are influenced by a number of factors which include (a) the nature of the components used (layered silicate, organic cation and polymer matrix), (b) the exchange capacity of the clay, (c) the chemical nature of the interlayer cations, (d) the polarity of the reaction medium, (e) the preparation method, (f) the clay loading, and (g) the interfacial adhesion between the polymer matrix and the clay layers [2,19,25].

Three structures of polymer clay nanocomposites can be achieved when nanoclays are dispersed into polymer matrices i.e. phase separated microcomposites, intercalated and exfoliated nanocomposites (Figure 1.2). Phase separated macrocomposites show no interaction between the polymer and clay layers and hence there is no separation of clay layers. In this case there is very little improvement in polymer properties [23, 26]. In intercalated nanocomposites one or more polymer chains penetrate the clay layers such that the interlayer spacing is expanded. However, the clay layers still retain their regular stacking arrangement and only certain polymer properties are improved. In exfoliated nanocomposites the clay layers are completely separated and individual layers are dispersed throughout the

polymer matrix. The individual clay platelets usually cause a significant improvement in the polymer properties due to their high aspect ratio and high interfacial interaction with the polymer matrix [12,19].

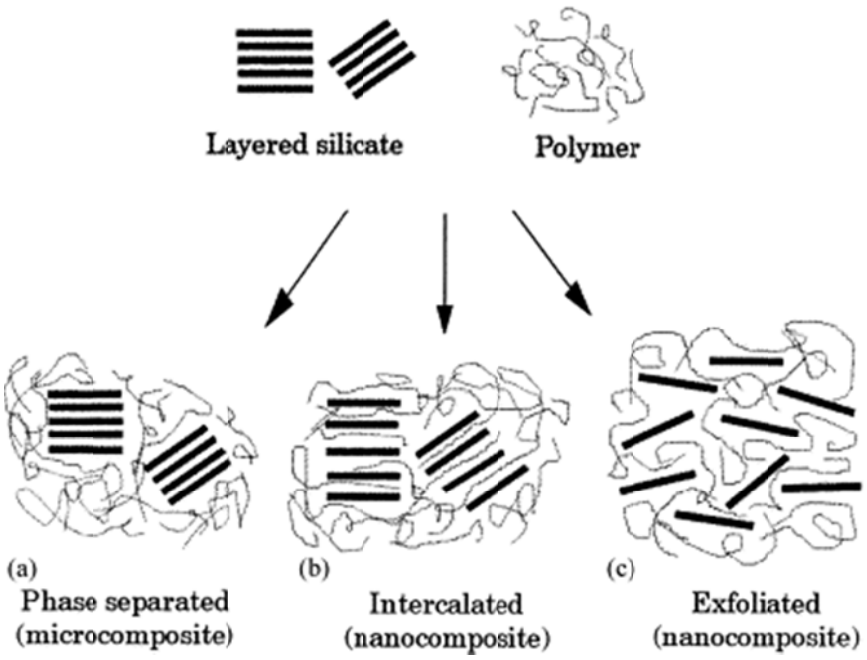

Figure 1.2 Scheme of different types of composite morphology which can arise from the interaction between layered silicates and polymers: (a) phase separated microcomposite, (b) intercalated nanocomposite, and (c) exfoliated nanocomposite [19]

1.7 Drawbacks and limitations of polymer-clay nanocomposites

Most polymers are hydrophobic while clays are naturally hydrophilic [5]. This makes them completely incompatible with each other and also difficult to intercalate/exfoliate clay into the polymer matrix. In most cases, the use of layered silicate as reinforcing agent is hindered because of the preferred face-to-face stacking of nanolayers. This normally results in agglomerated tactoids and incompatibility between the hydrophilic-layered silicate and hydrophobic polymer matrix [27]. The main drawbacks of using silicate layers include the difficulty of achieving good dispersion and strong interfacial adhesion between clay and the polymer matrix. However, in order to facilitate the uniform dispersion of clay into the polymer matrix it is necessary to chemically modify the clay [7,28]. Generally, this can be

done through ion-exchange reactions. Ion-exchange reactions involve the replacement of interlayer cations (Na^+, Ca^{2+}, K^+) with cationic surfactants. Typical cations used include primary, secondary, tertiary and quaternary alkyammonium or alkylphosphonium cations [19,23]. Cationic surfactants render the naturally hydrophilic silicate surface organophilic, thus expanding the basal spacing between the silicate layers [21,29]. They also lower the surface energy of the inorganic component and improve the wetting characteristics of the polymer. Furthermore, they can provide functional groups that can react with the polymer and even initiate polymerization [23]. A comprehensive discussion on clay modification will follow in section 2.2.2.

In its pristine state, layered silicates are only miscible with polar polymers and surface modification increases their interaction even further. However, organically modified clay do not disperse well in nonpolar polymers such as polypropylene (PP) and polyethylene (PE) because of their strong hydrophobicity [19,30]. In order to facilitate the interaction between organophilic layered silicates and non-polar polymers, the introduction of a polymer modified with maleic anhydride or hydroxyl group as a compatabilizer is often employed to mediate the polarity between the polymer and the modified montmorillonite [31]. Another alternative in improving the clay and polymer interaction is the use of vinylalkoxysilanes as coupling agents. The most widely used vinylsilanes are vinyltriethoxysilane (VTES) and vinyltrimethoxysilane (VTMS). Both the silane compounds contain two functional groups in their chemical structure: one is the C=C group that can be grafted onto the backbone of the polymer through the initiation of radicals from the decomposition of DCP; the other is the ≡Si-OR (R: CH_3 or CH_2CH_3) that can be hydrolysed to form silanols (Si-OH) [30,32].

1.8 Applications of polymer clay nanocomposites

Since the addition of clay improves the mechanical, thermal, barrier and decreases flammable properties of polymers, their applications have increased tremendously [10,16]. The most common use of PCNs has been in mechanical reinforcement of thermoplastics like nylon-6 and polypropylene. Toyota was the first company to commercialise these nanocomposites and use them in one of their popular models [12]. They produced polyamide-clay nanocomposites and used them to replace a metal component near the engine block that caused some weight savings. Clay in this application improved the heat distortion temperature of the material and allowed it to be used in high temperature applications.

Polypropylene-clay nanocomposites have also been used for automotive applications (fuel tanks, bumpers, interior and exterior panels) were the presence of the clay results in an increase in flexural and modulus while maintaining impact performance [33,34]. PCNs were found to improve the flame-retardancy of polymers without degrading their properties. In actual fact, in addition to acting as a flame retardant, it can also improve other properties of the polymer. Organoclays are also much cheaper than the flame retardants they are replacing. Another common application of clay nanocomposites is for gas-barrier materials. The clay nanoparticles create a complex network in the polymer matrix such that various gases either diffuse very slowly or not at all through the polymer chains. The success of clay nanocomposites for decreased diffusion of oxygen and water resulted in their application in food/liquid packaging in order to keep foods fresher for longer [34].

1.9 Aims and objectives

The overall objective of the study was to investigate the influence of organically modified nanoclay and pure Cloisite Ca^{2+}MMT on the morphology, as well as thermal and mechanical properties of low-density and high-density polyethylenes (LDPE and HDPE). In order to improve the interfacial adhesion and the dispersion of nanoclay into the polymer matrix, vinyltriethoxysilane (VTES) was used as a coupling agent. Various contents of clay (1, 3, and 5 wt. %) and VTES (1 and 3 phr) were used for both the PE matrices. The samples were characterized using transmission electron microscopy (TEM), X-ray diffractometry (XRD), thermogravimetric analysis (TGA), differential scanning calorimetry (DSC), tensile testing, dynamic mechanical analysis (DMA), Fourier-transform infrared spectroscopy (FTIR) and gel content analysis (to determine the extent of crosslinking or grafting in the nanocomposites).

1.10 Thesis outline

- Chapter 1. General introduction
- Chapter 2. Literature review
- Chapter 3. Materials and methods
- Chapter 4. Results and discussion
- Chapter 5. Conclusions

1.11 References

1. M.F. Hochella, Jr. There is plenty of room at the bottom: Nanoscience in geochemistry. Geochimica et Cosmochimica Acta 2002; 66:735-743.
   PII S0016-7037(01)00868-7
2. A. Nourbakhsh, A. Ashori. Influence of nanoclay and coupling agent on the physical and mechanical properties of polypropylene/bagasse nanocomposite. Journal of Applied Polymer Science 2009; 112:1386-1390.
   DOI:10.1002/app.29499
3. LU. Jiankun, KE Yucai, QI Zongneng, YI Xiao-Si. Study on intercalation and exfoliation behavior of organoclays in epoxy resin. Journal of Polymer Science: Part B: Polymer Physics 2001; 39:115-120.
   DOI:10.1002/1099-0488(20010101)
4. M. Tillekeratne, M. Jollands, F. Cser, S.N. Bhattacharya. Role of mixing parameters in the preparation of poly(ethylene vinyl acetate) nanocomposites by melt blending. Journal of Applied Polymer Science 2006; 100:2652-2658.
   DOI:10.1002/app.22755
5. R.K. Gupta, S.N. Bhattacharya. Polymer-clay nanocomposites; Current status and challenges. Indian Institute of Chemical Engineers 2008; 50:242-267.
6. E.M. Araujo, R. Barbosa, A.W.B. Rodrigues, T.J.A. Melo, E.N. Ito. Processing and characterization of polyethylene/Brazilian clay nanocomposites. Materials Science and Engineering A 2007; 445-446:141-147.
   DOI:10.1016/j.msea.2006.09.012
7. S.G. Lei, S.V. Hoa, M.-T. Ton-That. Effect of clay types on the processing and properties of polypropylene nanocomposites. Composites Science and Technology 2006; 66:1274-1279.
   DOI:10.1016/j.compscitech.2005.09.012
8. N.Tz. Dintcheva, F.P. La Mantia, V. Malatesta. Effect of different dispersing additives on the morphology and the properties of polyethylene-based nanocomposite films. eXPRESS Polymer Letters 2011; 5:923-935.
   DOI:10.3144/expresspolymlett.2011.90
9. M.J. Hato, S.S. Ray, A.S. Luyt. Nanocomposites based on polyethylene and polyhedral oligomeric silsesquioxanes, 1 - Microstructure, thermal and

thermomechanical properties. Macromolecular Materials and Engineering 2008; 293:752-762
DOI:10.1002/mame.200800146

10. H. Azizi, J. Morshedian, M. Barikani, M.H. Wagner. Effect of layered silicate nanoclay on the properties of silicate crosslinked linear low-density polyethylene (LLDPE). eXPRESS Polymer Letters 2010; 4:252-262.
DOI:10.3144/expresspolymlett.2010.32
11. D.W Jin, S.M Seol, G.H Kim. New compatibilizer for linear low density polyethylene (LLDPE)/clay nanocomposites. Journal of Applied Polymer Science 2009; 114:25-31.
DOI:10.1002/app.30544
12. L.B. de Paiva, A.R. Morales, T.R. Guimaraes.Structural and optical properties of polypropylene-montmorillonite nanocomposites. Materials Science and Engineering A 2007; 447:261-265.
DOI:10.1016/j.msea.2006.10.066
13. L. Liao, C. Zhang, S. Gong. Preparation of poly(Ɛ-caprolactone)/clay nanocomposites by microwave-assisted in-situ ring-opening polymerization. Marcomolecular Rapid Communications 2007; 28:1148-1154.
DOI:10.1002/marc.200700063
14. H.R. Dennis, D.L. Hunter, D. Chang, S. Kim, J.L. White, J.W. Cho, D.R Paul. Effect of melt processing conditions on the extent of exfoliation in organoclay-based nanocomposites. Polymer 2001; 42:9513-9522.
DOI: org.10.1016/S0032-3861(01)00473-6
15. H.W. Awad, W.J. Gilman, M. Nyde, R.H. Harris, Jr., T.E. Sutto, J. Callahan, P.C. Trulove, H.C. DeLong, D.M. Fox. Thermal degradation studies of alkyl-imidazolium salts and their application in nanocomposites. Thermochimica Acta 2004; 409:3-11.
DOI:10.1016/S0040-6031(03)00334-4
16. A.K. Barick, D.K. Tripathy. Effect of organoclay on the morphology, mechanical, thermal, and rheological properties of organophilic montmorillonite nanoclay based thermoplastic polyurethane nanocomposites prepared by melt blending. Polymer Engineering and Science 2010; 50:484-498.
DOI:10.1002/pen.21556
17. A. Durmus, A. Kasgoz, C.W. Macosko. Mechanical properties of linear low-density polyethylene (LLDPE)/clay nanocomposites: Estimation of aspect ratio and interfacial

strength by composite models. Journal of Macromolecular Science, Part B: Physics 2008: 47:608-619.
DOI:10.1080/00222340801957780

18. M. Du, B. Guo, D. Jia. Newly emerging applications of halloysite nanotubes: A review. Polymer International 2010; 59:574-582.
DOI:10.1002/pi.2754

19. M. Alexandre, P. Dubois. Polymer-layered silicate nanocomposites: Preparation, properties and uses of a new class of materials. Materials Science and Engineering 2000; 28:1-63.
PII:S0927-796X (00)00012-7

20. I.Y. Jeon, J.B. Baek. Nanocomposites derived from polymers and inorganic nanoparticles. Materials 2010; 3:3654-3674.
DOI:10.3390/ma3063654

21. G.I. Nakas, C. Kaynak. Use of different alkyammonium salts in clay surface modification for epoxy-based nanocomposites. Polymer Composites 2009; 30:357-363.
DOI:10.1002/pc.20667

22. S. Arunvisut, S. Phummanee, A. Somwangthanaroj. Effect of clay on mechanical and gas barrier properties of blown film LDPE/clay nanocomposites. Journal of Applied Polymer Science 2007; 106:2210-2217.
DOI:10.1002/app.26839

23. Q.T. Nguyen, D.G. Baird. Preparation of polymer-clay nanocomposites and their properties. Advances in Polymer Technology 2006; 25:270-285.
DOI:10.1002/adv.20079

24. J.M. Yeh, K.C. Chang. Polymer/layered silicate nanocomposite anticorrosive coatings. Journal of Industrial and Engineering Chemistry 2008; 14:275-291.
DOI:10.1016/j.jiec.2008.01.011

25. S.S. Ray, M. Okamoto. Polymer/layered silicate nanocomposites: A review from preparation to processing. Progress in Polymer Science 2003; 28:1539-1641.
DOI:10.1016/j.progpolymsci.2003.08.002

26. S. Xie, S. Zhang, B. Zhao, H. Qin, F. Wang, M. Yang. Tensile fracture morphologies of nylon-6/montmorillonite nanocomposites. Polymer International 2005; 54:1673-1980.
DOI:10.1002/pi.1901

27. P.C. LeBaron, Z. Wang, T.J. Pinnavaia. Polymer-layered silicate nanocomposites: An overview. Applied Clay Science 1999; 15:11-29.
PII: S0169-1317(99)00017-4

28. W.A.W.A. Rahman, N. Adenan, R.R. Ali, H. Sulaiman. Effect of silane crosslinker on the thermal properties of rice straw/HDPE biocomposite. Journal of Applied Sciences 2009; 17:3041-3047.
DOI:10.3923/jas.2009.3041.3047

29. C.D. Castel, T. Pelegrini, Jr., R.V. Barbosa, S.A. Liberman, R.S. Mauler. Properties of silane grafted polypropylene/montmorillonite nanocomposites. Composites: Part A 2010; 14:185-191
DOI:10.1016/j.compositesa.2009.09.017

30. H. Lu, Y. Hu, M. Li, Z. Chen, W. Fan. Structure characteristics and thermal properties of silane-grafted-polyethylene/clay nanocomposite prepared by reactive extrusion. Composites Science and Technology 2006; 66:3035-3039.
DOI:10.1016/j.compscitech.2006.01.018

31. R. Rezanavaz, M.K. Razavi Aghjeh, A.A. Babaluo. Rheology, morphology, and thermal behaviour of HDPE/clay nanocomposites. Polymer Composites 2010; 31:1028-1036.
DOI:10.1002/pc.20889

32. H. Lu, Y. Hu, L. Yang, Z. Wang, Z. Chen, W. Fan. Preparation and thermal characteristics of silane-grafted polyethylene/montmorillonite nanocomposites. Journal of Materials Science 2005; 40:43-46.
DOI:10.1007/s10853-005-5685-2

33. S. Ray, S.Y. Quek, A. Easteal, X.D. Chen. The potential use of polymer-clay nanocomposites in food packaging. International Journal of Food Engineering 2006; 2:1-11.
DOI.org/10.2202/1556-3758.1149

34. A.B. Morgan, R.H. Harris Jr., T. Kashiwagi. L.J. Chyall, J.W. Gilman. Flammability of polystyrene layered silicate (clay) nanocomposites: Carbonaceous char formation. Fire and Materials 2002; 26:247-253.
DOI:10.1002/fam.803

35. http://www.azom.com/article.aspx?ArticleID=921 (Accessed April 2012)

Chapter 2: Literature review

2.1 Introduction

Polymer layered silicates (PLS) nanocomposites have generated considerable interest over the past decade because of their improved properties at very low loading levels compared to conventional filler composites. Improved properties include mechanical, physical, thermal stability, gas barrier properties, and reduced flammability [1,2]. These improved properties cause PLS nanocomposites to be widely used in various fields such as food packaging, safety equipment, automotive, aerospace, electronics and optical devices [3,4]. PLS nanocomposites can be prepared by different methods i.e. melt mixing, solution mixing and *in situ* polymerization [5]. Melt mixing is the most industrially valuable method because of its high productivity, low cost, environmental friendliness (does not require the use of solvent), and compatibility with current polymer processing techniques such as extrusion and injection moulding. For most technologically important polymers, solution mixing and *in situ* polymerization are limited since neither a suitable monomer nor a solvent are available [5-7].

2.2 Layered silicate

Layered silicates are natural or synthetic minerals consisting of extremely thin layers that are generally bound together with counter ions [8]. There are different types of layered silicates i.e. montmorillonite, saponite, and hectorite. The most commonly used layered silicate for the preparation of PLS nanocomposites is montmorillonite which belongs to the general family of 2:1 phylosillicates. Montmorillonites are mostly preferred because of their high cation exchange capacity (CEC), the degree to which the clay can absorb and exchange cations, large surface area, surface reactivity, adsorptive properties, high aspect ratio, their platelets' morphology, as well as their low cost and natural availability [8,9].

2.2.1 Structure and properties of layered silicates

Layered silicates are built from tetrahedral sheets in which a silicon atom is surrounded by four oxygen atoms (Figure 2.1 (a)) and octahedral sheets in which a metal like aluminium or magnesium is surrounded by eight oxygen atoms (Figure 2.1(b)). The crystal structure of

MMT is made up of one octahedral sheet sandwiched between two layers of tetrahedral sheets. The thickness of the layers is around 1 nm, and the lateral dimensions of these layers may vary from 30 nm to several microns or larger, depending on the particular layered silicate. These layers organize themselves to form stacks with a regular Van der Waals gap in between them called the interlayer spacing or the gallery [10-12].

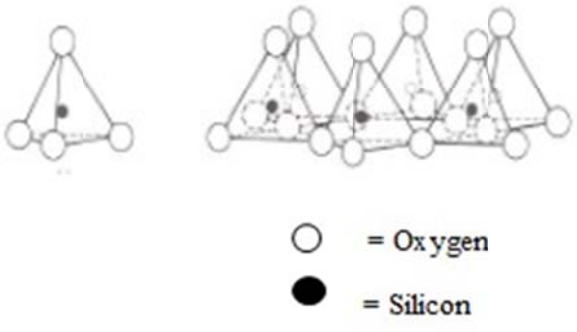

(a)

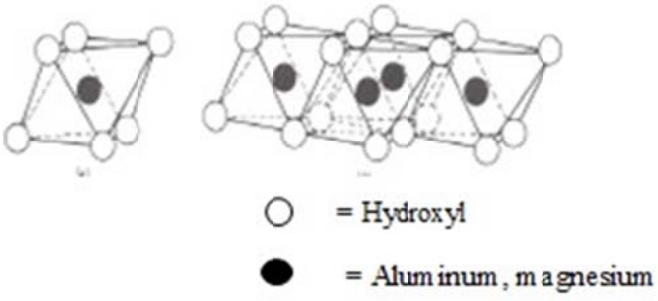

(b)

Figure 2.1 (a) Silica tetrahedron and tetrahedral units arranged in a hexagonal network, and (b) octahedron and octahedral units arranged in a sheet [13]

Naturally, layered silicates undergo isomorphous substitution within them, which involves the replacement of one ion by another with different or similar size without any change in the structure (e.g. Al^{3+} is replaced by Mg^{2+} or Fe^{2+}, or Mg^{2+} is replaced by Li^{+}). Isomorphous substitution generates negative charges on the surface of the clay which are counterbalanced by hydrated alkali or alkaline earth cations (such as Na^{+}, K^{+} and Ca^{2+}) residing in the interlayer space [13-15]. The presence of the cations in the galleries makes the silicate layers completely hydrophilic and compatible with only a few hydrophilic polymers, and poorly

compatible with hydrophobic polymers. Figure 2.2 shows the arrangement of charges on the surface of the silicate layers. The cations are attracted to the net negative charge within the clay platelets and can be shared by two neighbouring platelets, which forms stacks of platelets that are held tightly together. This makes the penetration of polymer or monomer(s) into the clay platelets more difficult. For these reasons, the clay surface must be modified before it can be used to prepare nanocomposites [16,17].

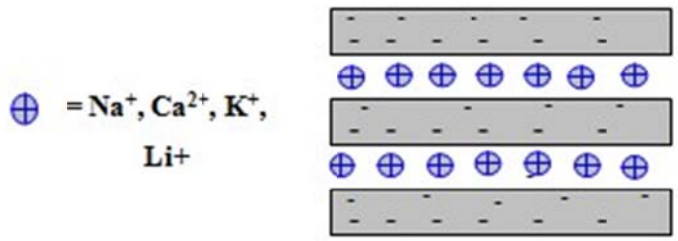

Figure 2.2 The arrangement of charges on the surface of silicate layers

2.2.2 Modification of layered silicates

A few authors found that the preparation of polymer-clay nanocomposites with good dispersion of clay layers in the polymer matrix is not possible by physical mixing. Although the high aspect ratio of silicate nanolayers is ideal for reinforcement, nanolayers are not easily dispersed in most polymers due to the preferred face-to-face stacking in agglomerated tactoids. The intrinsic incompatibility of the hydrophilic layered silicates and the hydrophobic polymer further hinders the dispersion of tactoids into discrete monolayers. Only a few hydrophilic polymers such as poly(ethylene oxide) and poly(vinyl alcohol) are miscible with clay nanolayers [9,18-21]. The importance of the surface modification of clay is to: (a) convert the normally hydrophilic silicate surface to organophilic; (b) weaken the polar interaction between adjacent clay layers and increase the interlayer spacing between them; and (c) reduce the surface energy of clay layers and improve its wettability with the polymer matrix. Generally, this can be done through ion exchange reactions. However, an ion exchange reaction has a number of limitations, and several authors explored an alternative method (silane modification) to modify the clay surface [9,22,23]. Both ion exchange and silane modifications will be discussed in the following sections.

2.2.2.1 Ion-exchange modification

Ion-exchange reactions have traditionally been exploited as an effective method to replace inorganic ions with organic cationic surfactant molecules which intercalate into the clay gallery [24]. An ion exchange reaction depends on the type of organic surfactants and the cationic exchange capacity (CEC) of the clay. This reaction simply replaces the sodium or calcium cations situated in the gallery with alkylammonium or alkylphosphonium cations. The clay is swelled in an aqueous alkylammonium solution which increases the interlayer gallery due to the hydration of the inorganic cations (Na^+, Ca^{2+}) situated in the gallery, allowing alkylammonium ions to intercalate between the clay platelets. Since the cations (Na^+ and Ca^{2+}) are not strongly bound to the clay surface, they can be easily replaced. The most common cationic surfactants used in ion-exchange reactions are primary, secondary and quaternary alkyammonium or alkyphosphonium cations. The insertion of alkylammonium or alkylphosphonium cations into the galleries increases the interlayer spacing and creates more room for the polymer chains to enter and also increases the hydrophobicity of the clay layers. Furthermore, they can provide functional groups which can interact with polymer chains or initiate polymerization. Figure 2.3 shows the surface modification of an MMT clay *via* ion-exchange reaction using alkylammonium cations [16,25-28].

The affinity of monovalent sodium cations to hydration promotes the ion exchange process and increases the efficiency of the organic modification. However, clays with divalent counter cations such as calcium cannot be easily hydrated and therefore their replacement by an ion exchange process is not efficient [26]. The efficiency of organic modification by ion exchange also depends on the surface charge density of the clay layers. When the charge density of the clay is as high as 1 equiv mol^{-1} for mica, the electrostatic force between the layers is also high. Therefore, the interlayer cations cannot be hydrated or swollen and as a result ion exchange cannot be carried out. The lower charge density (0.25-0.5 equiv mol^{-1}) in montmorillonite causes weak electrostatic forces between the clay layers which makes them swell more easily. A couple of studies showed that the structure of the organoclay and its basal spacing depends on the alkyl chain length and its configuration in the inter layer spacing after modification [9,29].

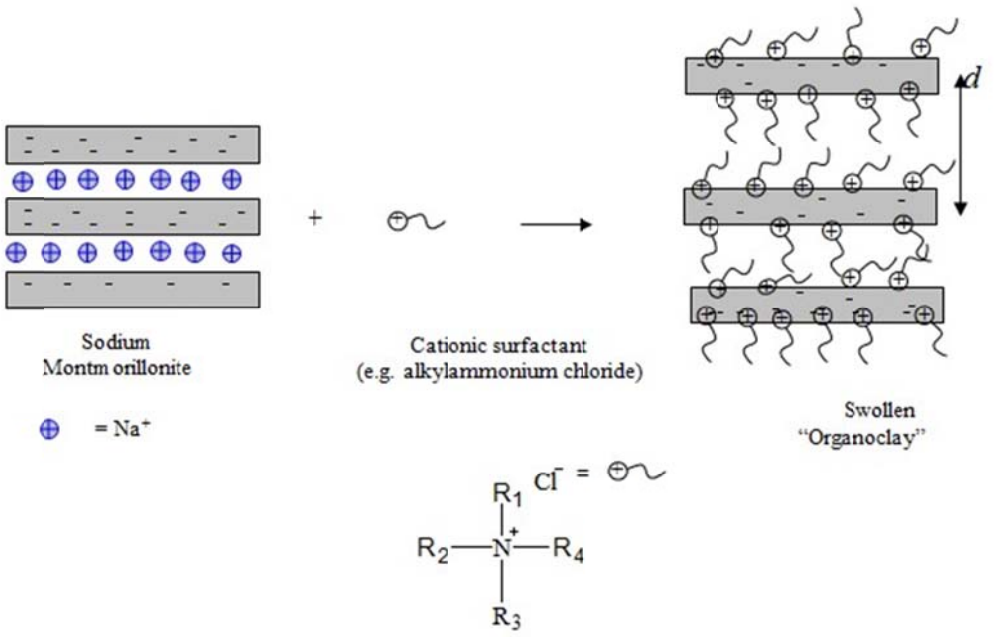

Figure 2.3 Schematic representation of clay surface treatment by ion-exchange reaction

Although ion exchange reactions gained significant success in the preparation of polymer-clay nanocomposites, there are a few drawbacks which limit their application: (a) they do not provide efficient linkage between the intercalating agent and the clay, and (b) they are thermally unstable above 200 °C. In fact, most alkylammonium surfactants are known to undergo degradation at temperatures were most plastics are commonly processed. When nanocomposites are prepared at high temperatures, the alkylammonium salt degrades through the well-known Hofmann degradation. Therefore, organoclays prepared using quaternary alkyl ammonium salts are not suitable for most engineering plastics with high processing temperatures. Researchers in the field of nanocomposites were, therefore, faced with the challenge to develop alternative method to modify clay minerals [30-32].

2.2.2.2 Modification of clay with a silane compound

The silylation approach has recently attracted more attention, and represents a viable method of making compatible inorganic platelets and organic matrices nanocomposites [31,33]. The process occurs through the reaction between a silane coupling agent and the reactive silanol group located at the broken edge of the clay platelets, interlayer or external surface. By using organosilane, it is possible to covalently bond the organic functional groups onto the silicate

layer. The functionalization of clay with organosilane can take place at three different sites: (1) at the interlayer spacing which results in a significant increase in the clay basal spacing, (2) at the external surface with no change in basal spacing, and (3) at the broken edges resulting in a less pronounced increase in basal spacing. Several organosilanes with different functionalities have been used to modify layered silicate such as MMT. Figure 2.4 shows the interaction between silane and the clay surface [30,31,34].

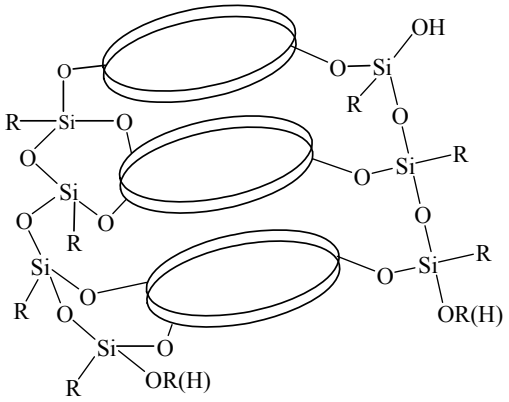

Figure 2.4 Schematic representation of the coupling reaction of trifunctional silane molecules on clay [33]

2.3 Techniques used to characterize polymer-clay nanocomposites (PCNs)

During the analysis of polymer-clay nanocomposites it is important to study the degree of dispersion of clay layers (intercalation/exfoliation), because it affect the final properties of the nanocomposites. Several techniques have been used to study the nanostructure of PCNs and clay, and they include neutron magnetic resonance (NMR) spectroscopy, neutron scattering methods, X-ray diffractometry (XRD) and transmission electron microscopy (TEM). However, XRD and TEM are the most commonly used techniques. Figure 2.5 shows the relation between different states of dispersion of organoclays in a polymer matrix and typical XRD and TEM results [35-37]. The darker lines in the brighter matrix in the TEM pictures show the clay layers in the polymer matrix. The description of the different states of dispersion is given in the next paragraph.

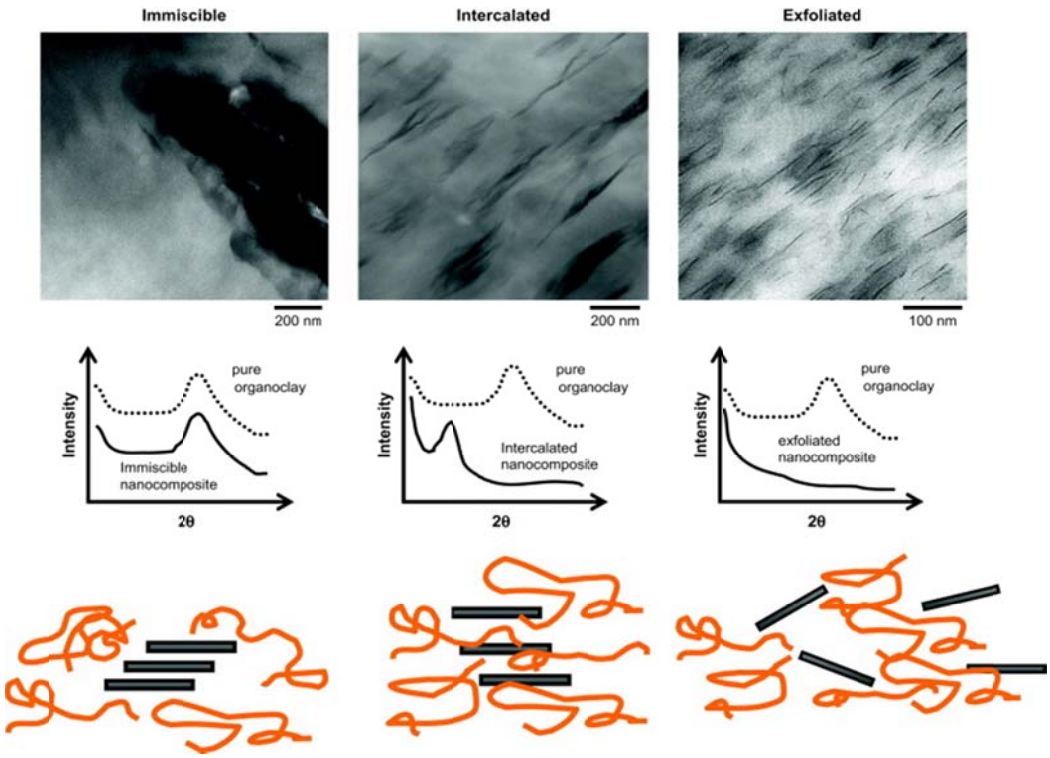

Figure 2.5 Illustration of the different states of dispersion of organoclays in a polymer matrix observed through XRD and TEM [37]

Clay and organoclays show a characteristic peak in XRD due to their regular layered structures. The peak is indicative of the platelet separation or d-spacing in the clay structure. The nanocomposite structure (intercalated and exfoliated) can be identified by monitoring the position, shape, and intensity of the characteristics peak in the XRD spectra. These changes can be caused by either organic modification of clay or penetration of the polymer chains into the clay gallery [9,29,35]. As shown in Figure 2.5, the polymer composite containing clay micro-particles shows a peak at the same position as that obtained for the organoclay powder. There is no increase in the *d*-spacing hence the polymer chains did not enter the clay gallery. The intercalated structure shows the characteristic peak of the organoclay, but the peak shifts towards lower angles because the d-spacing increased as a result of the polymer chains having entered the gallery. The exfoliated structure shows no peak, indicating that the interaction between the polymer chains and the clay platelets was so good that the clay platelets were completely separated and their crystalline structure destroyed, which is normally referred to as exfoliation [9,29,36,37].

A number of studies found that one cannot study the dispersion of clay in a polymer with only TEM or XRD, because the two techniques complement each other. In most studies TEM was found to be an excellent method to characterize the clay dispersion in PCNs. XRD is mostly used to measure the d-spacing of ordered immiscible and ordered intercalated PCNs. However, it may be insufficient for the confirmation of exfoliated structures, since the absence of a peak can be misinterpreted, especially where mixed intercalated and exfoliated structures exist, because XRD is not sensitive enough to measure low concentrations of clay crystallinity in a polymer matrix [29,35-38].

2.4 Factors affecting the extent of clay modification

The extent of ion exchange modification depends on a number of factors which needs to be taken into consideration when preparing PCNs, i.e. the type of surfactant, the length of the surfactant chain, the type of organic modifier, the concentration of the modifier, the charge density of clay and also the preparation method of PCNs. Several authors found that alkylammonium ions are easily intercalated between the clay layers and offer better interfacial interaction compared to amino acids. Clays have different cationic exchange capacities ranging from 80-125 meq/100 g of clay. A few studies showed that the longer the chain length of the surfactants, the further apart the clay layers will be forced. A number of authors studied the factors affecting the extent of clay modifications, and a few are discussed below. Modification of clay with silane compounds has also been studied by a number of authors and is discussed below.

Lei *et al.* [39] studied the effect of clay type on the processing and properties of polypropylene (PP) nanocomposites prepared using a Brabender Plasticorder. The nanocomposites were prepared using different types of commercial clays, i.e. Na (non-modified montmorillonite clay), Cloisite (modified with long-chain alkyl ammonium compounds), and Nanomer (modified with long alkyl amines) at a constant clay loading of 3 wt%. SEM images of the nanocomposites without modification showed aggregates and poor interfacial bonding between the matrix and the aggregates. However, modified clay nanocomposites showed a significant reduction in agglomerates size. The authors attributed this to the ability of surface treatment to reduce particle-particle attraction and promote the expansion of the gallery distance between the clay sheets. DMA analysis showed that all the nanocomposites had higher storage modulus than pure PP over the complete temperature

range of the analysis. Nanocomposites with alkyl ammonium salt had higher storage moduli than the alkyl amine nanocomposites.

Nakas *et al.* [40] studied the influence of alkyammonium salts on epoxy-clay nanocomposites prepared by *in situ* intercalative polymerization. Raw Na-montmorillonites was first purified and then the surface was modified with five alkylammonium salts: tetramethyl ammonium bromide (TMAB), dodecyl trimethyl ammonium bromide (DDTMAB), hexadecyl trimethyl ammonium bromide (HDTMAB), octadecyl trimethyl ammonium bromide (ODTMAB), to investigate the effect of increasing chain length, and benzyl triethyl ammonium bromide (BTEAB), to investigate the effect of the benzene ring. X-ray diffractograms showed that by increasing the chain length of the modifier the interlayer spacing also increases by pushing the layers further apart. The interlayer spacing of TMAB, BTEAB, DDTMAB, HDTMAB and ODTMAB modified clay was 13.9, 14.7, 16.1, 17.9, 20.3 Å respectively. The flexural strength and fracture toughness increased with an increase in chain length of the modifier. The flexural strength improved in the order TMAB < BTEAB < DDTMAB < HDTMAB < ODTMAB. However, the fracture toughness value of the BTEAB modified clay was lower than that of the clay modified with TMAB. The presence of the benzene ring in the BTEAB made it difficult for the clay layers to be thoroughly dispersed in polymer matrix.

Ryznarova *et al.* [41] studied the effect of four different clay surface modifiers on the structure of epoxy-clay nanocomposites. The nanocomposites were prepared by *in situ* intercalation polymerization. The Na^+ montmorillonites was modified with bis(2-hydroxyethy) methyloctadecyl ammonium chloride (A), dimethyloctadecylphenyl ammonium chloride (B), dimethyloctadecyloctyl ammonium chloride (C) and methyldioctadecyl ammonium chloride (D). The degree of clay surface coverage was 78, 87, 70, and 66 % for A, B, C, and D respectively. XRD showed an exfoliated structure for organoclay A nanocomposites, and the authors attributed this behaviour to the presence of the hydroxyl functionalities. Organoclay D nanocomposites showed an intercalated structure due to the high hydrophobicity of the modifier. TEM pictures of the organoclay A nanocomposites showed exfoliated individual clay platelets at higher magnifications, but the organoclay C nanocomposites showed poor dispersion. A slight decrease in the Young's modulus was observed for the organoclay 8A nanocomposites, which was attributed to the plasticizing effect of the modifier. This observation was consistent with the decrease in the T_g observed in the DMA results.

Greesh *et al.* [42,70] studied the effect of four different organic modifiers and different clay loadings on the properties of poly(styrene-co-butyl acrylate) (poly(S-co-BA))-clay nanocomposites prepared by *in situ* free-radical polymerization in emulsion. Na-MMT was modified with sodium 1-allyloxy-2-hydroxypropyl (Cops), 2-acrylamido-2-methyl-1-propanesulfonic acid (AMPS), *N*-isopropylacrylamide (NIPA) and sodium 11-methyacryloyxy-undecan-1-yl sulphate (MET). At 10% loading of clay the XRD and TEM results showed intercalated to partially exfoliated structures with Cops-, NIPS-, and MET-modified clay, while AMPS-modified clay showed fully exfoliated structures. This was because the sulphate and amino groups in the AMPS structure allowed it to interact easily with clay by forming hydrogen bonds between the sulphates and the amino groups of AMPS and the hydroxyl groups situated on the edges of the clay sheets. The XRD results of the AMPS modified clay nanocomposites showed intercalated structures with 1-5 % of clay and a partially exfoliated structure with 7 % of clay. The nanocomposites with 10% of clay showed an exfoliated structure, which was unusual since it is known that it becomes more difficult to obtain exfoliated structures at higher clay contents. This behaviour was attributed to thermodynamic factors. At high clay loadings the clay platelets were close to each other and as a result they generated energy by friction. This energy could lead to more free movement of platelets thus randomizing their orientation.

Wilson *et al.* [43] studied the influence of clay content and amount of organic modifier on the morphology of EVA-clay nanocomposites. The nanocomposites were prepared using Cloisite 15A and 20A with the same organic modifier but different modifier concentrations (125 and 90 meg/100gclay respectively) at varying loadings. The morphology of the nanocomposites was evaluated using small-angle X-ray diffraction spectroscopy (SAXS), TEM, and scanning electron microscopy (SEM). The SAXS results of the EVA-clay nanocomposites containing organo-modified clay showed an intercalated morphology at low loadings and an immiscible morphology at high loadings. The SEM images showed smooth surfaces at low loadings and rough surfaces at high loadings. This behaviour was attributed to the formation of agglomerates due to poor interfacial adhesion between the polymer and clay at high loadings. The TEM images showed the same trend as SEM, with homogenous dispersion of individual clay layers at low loadings and inhomogeneous dispersion due to agglomerates at higher loadings. The Cloisite 15A nanocomposites showed better dispersion than the Cloisite 20A nanocomposites, because more of the modifier was intercalated between the clay layers resulting in further expansion of the gallery and better interaction with the polymer chains.

Choi *et al.* [33] investigated the influence of ammonium salt functionalized MMT (O-MMT) and silane functionalized MMT (S-MMT) on the morphology, thermomechanical and mechanical properties of epoxy. Various concentrations (2, 6, and 10 wt%) of pure-MMT, O-MMT, and S-MMT were incorporated. XRD analysis showed the interlayer spacing of pure MMT, O-MMT, and S-MMT to be 12.8, 32.1, 20.8 Å respectively. After adding 6 wt% of P-MMT, O-MMT, S-MMT into epoxy, the (001) peak shifted to lower angles with interlayer spacings of 14.4, 38.3, and 28.0 Å respectively. TEM micrographs showed individual layers uniformly dispersed for the O-MMT nanocomposites, while few MMT stacks were observed for the S-MMT nanocomposites. The grafted silane between the platelets and the edges restricted the separation of the platelets, while in O-MMT the platelets could separate without restriction. However, the S-MMT nanocomposites showed better mechanical properties than the O-MMT nanocomposites due to the better chemical interaction between the amine group of the grafted silane on the MMT and the polymer matrix compared to the physical interactions between O-MMT and the polymer matrix. The DMA results showed that the chemical interactions in the S-MMT/epoxy nanocomposite restricted the molecular motion and increased T_g.

Park *et al.* [34] investigated the effect of silane treatment on the mechanical interfacial properties of MMT/epoxy nanocomposites. MMT was modified with various silane coupling agents (SCAs) i.e. γ-amino propyl triethoxy silane, γ-glycidoxy propyl methoxy silane, and γ-methacyloxy propyl trimethoxy silane. XRD showed that after modification with SCAs there were no diffraction peaks, which indicated that the silicate layers were totally dispersed or exfoliated in the polymer matrix. The exfoliation of the MMT layers was further conformed by TEM as individual silicate layers were seen to be well dispersed in the polymer matrix. The mechanical interfacial properties showed that the critical stress intensity of the surface modified MMT/epoxy composites was higher than those of the Na MMT/epoxy composites. This was due to the silane treatment which increased the interfacial adhesion between the MMT and the polymer matrix.

2.5 Polyethylenes

Polyethylenes are commodity plastics and account for more than 70% of the total plastics market [44]. Polyethylenes are mostly used because of their light weight, low cost, high chemical resistance, and good processability. It is the most versatile thermoplastic and is used

in a variety of applications such as packaging, household items, flexible lids, bottles, net ropes, pipes, and wires. Due to their easy processability PE is used in the insulation and sheathing of both telecommunication and power cable systems [44-46]. All these applications are important, but the fact that LDPE is a thermoplastic polymer with low melting temperature, limits its service temperature [47]. It also has a low resistance to tensile and creep forces, low strength, low stiffness, highly flammability, poor UV resistance and high gas permeability, particularly for CO_2. In order to overcome these limitations and improve the quality of PE for high temperature applications, modification is necessary [48,49].

2.5.1 Modification of polyethylene

The method mostly used to modify PE is crosslinking. Crosslinking leads to the formation of insoluble and infusible polymers in which the polymer chains are joined together to form a three-dimensional network structure. Crosslinking of polyethylene has been used commercially since the 1950s [44,50,51]. During crosslinking, molecules are joined together chemically by covalent bonds. Generally, crosslinking increases the maximum operating temperature and improves the environmental stress cracking resistance of polymers. It also reduces their flow, and enhances their chemical resistance, mechanical properties, and to a certain extent retards their flammability [44,52,53]. Currently there are three commercial methods used for crosslinking low density polyethylene: (a) peroxide crosslinking; (b) radiation crosslinking; and (c) crosslinking through silane grafting followed by moisture crosslinking [50,52,54,55].

Peroxide crosslinking is initiated by heating a peroxide above its decomposition temperature. The decomposition of the peroxide initiates free radicals capable of extracting hydrogen atoms from the polyethylene backbone, thus transferring a free radical site to the polyethylene backbone. Crosslinking can occur thorough the combination of two radicals [44,46]. During radiation crosslinking the free radicals are generated in the polymer backbone by using high energy radiation. The free radicals can also recombine to form crosslinks. Crosslinking by radiation depends upon the photon energy of the radiation source. The higher the photon energy, the more the penetration takes place and more effective crosslinking is obtained [44].

Silane crosslinking has gained much attention in recent years because of various advantages such as easy processing and low cost. Silane crosslinking was first patented in the late 1960s by Dow Corning. The most commonly used silane to make silane crosslinkable polyethylene is vinyl trimethoxysilane [52-54]. Crosslinking *via* silane is a thermochemical reaction in which the peroxide decomposes at an elevated temperature which results in the formation of oxy-radicals. These oxy radicals have the potential to abstract hydrogen from the PE molecule and can attack the vinyl group of a molecule and convert it into free radicals [47]. The vinyl part of the silane becomes grafted to the polymer backbone *via* the initiated free radical. In the crosslinking process by VTES two reaction steps are involved i.e. hydrolysis and condensation (Scheme 1). During hydrolysis, the silane methoxy group is hydrated by moisture to form a silanol. During the second step, two of the silanols condense with each other forming crosslinks as shown in Scheme 1. The silanol bridges are less rigid than the C-C bonds formed *via* peroxide or radiation initiated crosslinking, which gives more flexibility to the crosslinked polymer [51,53,54].

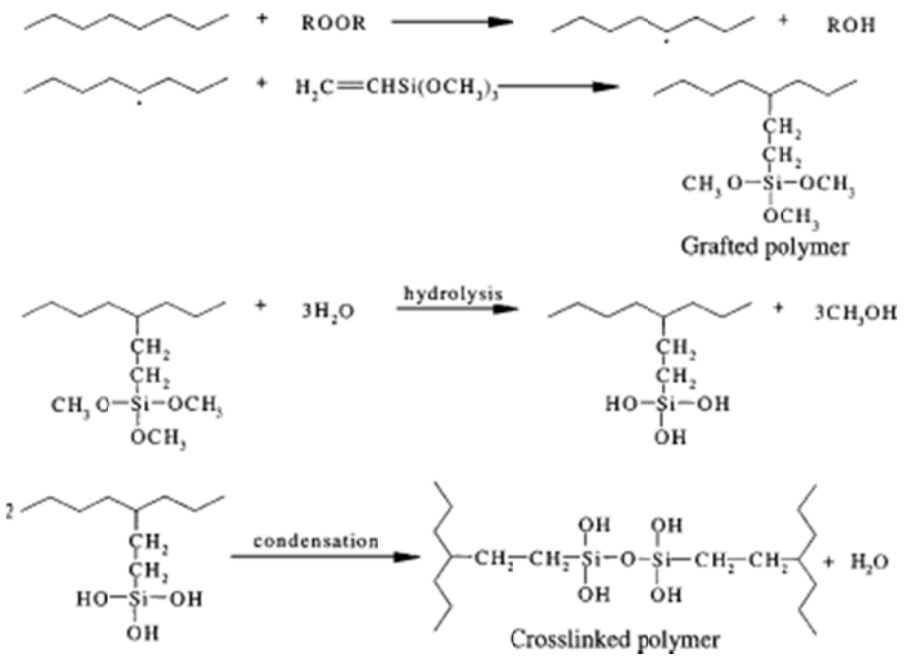

Scheme 1 Mechanism of the silane–grafting and water–crosslinking processes [51]

Shah *et al*. [47] studied the different aspects of the crosslinking of polyethylene with vinyl silane. The silane used was vinyl triethoxysilane (0-27.33 phr) and (0-1.25 phr) of benzyl peroxide. The grafting process was performed in a Brabender mixer, followed by curing. Gel

content analysis showed that by increasing the silane concentration, crosslinking also increased. The elongation at break decreased while the tensile strength showed an initial increase and then decreased. Increases in silane content above 4.56 phr caused further crosslinking, which reduced the average length segment between the crosslinking nodes to such an extent that the chains did not have enough capacity for orientation during extension, and hence the ability to sustain external stress failed. Crosslinking of PE with silane is believed to perform two functions. First, it ties the chains to one another through covalent bonds; this causes tightness of the polymer network and so that the performance of PE increases at higher temperatures. Secondly, it results in the formation of Si-O-Si bonds and gives rise to flame retardancy of the polymer network.

Shieh *et al*. [53] studied the effect of silane grafting reactions on the thermal properties of low-density polyethylene. The reagents used for the grafting reactions were vinyl trimethoxysilane (VTMS) and dicumyl peroxide (DCP) at contents of 7 phr and 0.2 phr respectively. The thermal stability of pure LDPE, LDPE grafted with silane and LDPE grafted with silane followed by crosslinking with boiling water were studied. The thermal stability of LDPE increased after silane grafting and crosslinking reactions. However, the thermal stability of crosslinked LDPE was higher than that of grafted LDPE. This suggested that crosslinking reactions of LDPE can increase its upper temperature limit.

2.5.2 Polyethylene reinforced nanocomposites

Apart from crosslinking, the properties of polyethylene can be improved with the addition of nanofillers. Nano-filled polymer composites have received considerable attention in the past few years [1]. The potential of this new class of materials is outstanding. Even small filler contents (<6 wt %) result in effective enhancement of several properties, which is unique and quite different from conventional composites. Conventional fillers like talc, calcium carbonate, and fibres require high loadings in order to improve polymer properties, which results in undesirable properties like brittleness or loss of opacity [2,6]. It has been observed that the addition of small quantities of nano-sized layered silicates greatly improved the properties of virgin polymers without affecting their processability. One of the challenges faced when working with polyethylene is their incompatibility with most fillers due to their high hydrophobicity. In order to improve the compatibility between the organic and inorganic components the addition of compatibilizers is necessary [1,5,10,36,40].

2.6 Properties of polymer-clay nanocomposites

A number of studies showed that in order to obtain optimal properties for polymer-clay nanocomposites, the clay layers should be thoroughly dispersed as single platelets throughout the polymer matrix, i.e. exfoliation, in order for the clay to have a larger contact area with the polymer matrix [41,43]. To attain such dispersion, the polymer chains should first penetrate the clay layers (intercalation). Intercalation is possible if both the polymer and the clay layers have polar groups and are compatible with each other. If the polymer and clay are incompatible, the clay platelets remain as large stacks without any polymer chains entering the gallery of the clay platelets, resulting in little improvement in polymer properties [8,43,56].

2.6.1 Morphology

The most commonly used techniques to study the dispersion of clay layers within the polymer matrix are X-ray diffraction (XRD) and transmission electron microscopy (TEM) [40-41]. These techniques were earlier discussed in section 2.3. The interfacial adhesion between the clay and polymer matrix can be studied by using scanning electron microscopy (SEM).

Zhang *et al.* [57] studied the morphology of PE/clay and PP/clay nanocomposites prepared by direct melt blending. The nanocomposites were prepared using a novel oligomerically-modified clay that contained styrene, lauryl acrylate and vinylbenzyl chloride. XRD showed a strong peak for all the nanocomposites at 2.4° corresponding to the clay. The lack of change in peak position was due to no insertion of polymer chains into the gallery (immiscible morphology), and the clay layers were already well-expanded by the oligomeric surfactant. TEM images at low magnification for 5% inorganic clay loading showed less uniform distribution of the clay layers for PE, while for PP they only showed tactoids. The poor dispersion of the clay in the PP and PE matrices was due to a lack of compatibility between the polymers and the clay.

Castel *et al*. [58] studied the influence of interfacial agent on the morphology of PP/MMT nanocomposites. The nanocomposites were prepared by an intermesh screw extruder with ethylene-vinyl acetate (EVA) and ethylene-vinyl alcohol (EVOH) copolymers as

compatibilizers. XRD showed the interlayer spacing of Cloisite 15A to be 3.3 nm before compounding. The uncompatibilized system exhibited no increase in interlayer spacing. This was due to the immiscibility between the clay and the polymer matrix, even after modification of the MMT with alkylammonium ions. The addition of 3 wt. % of EVA or EVOH increased the interlayer spacing to 3.7 and 4.5 nm respectively. This was due to the intercalation of polymer chains into the clay galleries through the interaction between the polar groups of the functionalized polymer and the clay. TEM micrographs of all the compatibilized samples showed some degree of intercalation and exfoliation. Surprisingly, the EVOH-compatibilized samples, which showed larger interlayer spacings, presented poor dispersion in the polymer matrix. The EVA-compatibilized samples showed a more homogenous morphology.

Kar *et al*. [59] studied the morphology of chlorinated polyethylene nanocomposites (CPE) prepared with natural and organically treated montmorillonite through solution mixing with varying clay contents (5,10, and 20wt. %). The XRD results of Na^+ MMT showed a strong peak at $2\theta = 7.2°$ which corresponded to a basal spacing $d_{001} = 1.2$ nm. When mixed with CPE, the peak moved to lower angles and the basal spacing increased due to the penetration of the polymer chains in between the clay layers. The basal spacings at 5, 10, and 20 wt% clay loadings were 3.5, 2.5, and 1.8 nm respectively. The authors attributed this behaviour to the lack of polymer penetration into the clay layers due to the formation of agglomerates at high clay loadings. The clay peak of CPE/Cloisite 30B broadened and shifted towards a slightly lower angle of $2\theta = 1.8°$ (4.8 nm) compared to that of pure Cloisite 30B (1.90 nm). However, CPE/Cloisite 15A showed no peak due to the total exfoliation of the clay layers in the polymer matrix. The TEM micrographs of the nanocomposites with 5 and 10 wt% of Na^+ MMT clay showed an intercalated morphology, and with 20 wt% clay loading the clay layers were almost stacked together. However, 5 wt% loading of Cloisite 30B and Cloisite 15A respectively showed highly intercalated and fully exfoliated structures. This was due to better compatibilities of these clays with CPE, with Cloisite 15A being the best because it is modified with an excess amount of onium.

Mohaddespour *et al*. [60] studied the morphology of HDPE/clay nanocomposites with and without a compatibilizer using XRD and SEM. Polyethylene glycol was used as compatibilizer. The XRD results showed intercalated structures in the absence of compatibilizer, and exfoliated structures in the presence of compatibilizer. SEM images

showed poor dispersion with agglomerates without compatibilizer, but in the presence of compatibilizer it showed a homogenous dispersion of the clay layers.

2.6.2 Mechanical and thermomechanical properties

Generally, the incorporation of nanoclay into a polymer matrix may cause improvement in the mechanical properties of the nanocomposites such as tensile strength, modulus or stiffness [4]. Fillers, including nanoclays, are commonly called reinforcing agents. The reinforcing effect of clay depends on its interfacial interaction and its dispersion in the polymer matrix. Most authors found that at low loadings, clay layers are exfoliated and well dispersed in the polymer matrix, resulting in improved mechanical properties. However, at high clay loadings the mechanical properties decrease due to poor dispersion and the formation of agglomerates [3,61,62]. Non-polar polymers like PE and PP normally give poor dispersion and interfacial adhesion, even with organically modified clay. The introduction of a compatibilizer is necessary, but a few studies showed that large contents of compatibilizer can decrease the mechanical properties of the nanocomposites. The authors attributed this behaviour to the plasticizing effect of the compatibilizer due to its low molecular weight [60,63].

A number of authors reported that the addition of clay into a polymer improves the tensile strength and increases the tensile modulus. However, the tensile strength and tensile modulus are influenced by the final morphology of the nanocomposites. Some studies found that high clay loadings (>5 wt %) reduces the tensile strength and tensile modulus due to the formation of agglomerates [9,10,23,56,60]. The effect of clay on the stress at break in PCNs depends on the interfacial interaction between the polymer and the clay layers. Stronger interfacial interaction causes an increase in stress at break, while weak interfacial interaction decreases stress at break due to the lack of stress transfer between the polymer and the clay [34,63]. Elongation at break similarly depends on the interfacial interactions of the polymer/clay system, with both increasing and decreasing values reported for PCNs [63]. Dynamic mechanical analysis studies on PCNs have shown that storage modulus and glass transition temperature (T_g) increases with the addition of nanoclay due to its reinforcing effect and its restricting effect on the mobility of polymer chains [10,42,64,65].

Supri *et al.* [66] studied the mechanical properties of LDPE-clay nanocomposites with and without poly(acrylic acid) (PAA) as a compatibilizer. Nanocomposites were prepared by a melt compounding technique in an internal Z-blade mixer with different contents of clay (2.5, 5, 7, and 10 phr). The tensile strength increased at 2.5 and 5 phr clay loading, while at higher contents (7 and 10 phr) it showed a gradual decrease. This behaviour was observed for both treated and untreated nanocomposites, but the tensile strength was higher for the treated nanocomposites. The authors attributed this behaviour to the fact that the modified nanocomposites had good interfacial interaction between the filler and the matrix. The modulus of elasticity of the treated nanocomposites increased at all compositions compared to the untreated nanocomposites and pure LDPE due to the reinforcing effect of the clay. Elongation at break decreased with an increase in clay loading for both the treated and untreated nanocomposites. This was attributed to the increasing stiffness of the nanocomposites with the addition of clay which is in agreement with the increasing tensile modulus.

Ha e*t al.* [67] studied the mechanical properties of epoxy-clay nanocomposites. The nanocomposites were fabricated by mixing 2, 6, and 10 wt. % of unmodified and silane modified MMT with epoxy resins. The results showed that the tensile strength increased with increasing concentration of clay for the silane modified MMT, while in the case of the un-modified MMT the tensile strength was almost unaffected by the clay concentration. The elastic modulus increased with the concentration of MMT in both cases, but was higher for the silane modified MMT. The difference in the mechanical properties was attributed to the interfacial strength between the clay and the epoxy due to silane modification. The hardness of the nanocomposites increased with the addition of clay in both cases, but the silane modified MMT nanocomposites were harder. This was due to the adhesion strength and the good dispersion of the clay in the epoxy matrix in the presence of silane.

Ansari *et al*. [68] studied the mechanical properties of polypropylene composites filled with silane treated and untreated feldspar. The tensile strength of the composites with untreated feldspar was reduced as the loading increased from 10 to 40 wt%. However, at similar filler loadings the treated feldspar showed an increase in tensile strength. Silane treatment improved the adhesion and interfacial strength between the PP and feldspar, causing the stress to be transferred from PP to feldspar. The elongation at break of the composites decreased with the addition of untreated feldspar, but the composites with silane treated

feldspar showed a slight improvement. At similar filler loadings the silane treated feldspar/PP composites also showed higher Young's modulus values than the untreated feldspar/PP composites. This was also attributed to good interfacial adhesion between the silane treated feldspar and the matrix.

Rezanejad *et al.* [69] investigated the thermomechanical properties of crosslinked polyethylene-clay nanocomposites. The nanocomposites were prepared by melt blending with varying clay loadings. The storage modulus, loss modulus, and loss factor were determined by dynamic mechanical analysis (DMA). The storage and loss modulus increased with about 300% with the incorporation of clay. The authors attributed this behaviour to an increase in both the elasticity and plasticity characteristics of the nanocomposites. Further increase in clay loading showed slight increases in storage and loss modulus due to the reinforcing effect of the clay. The T_g decreased with the addition of clay.

Greesh *et al.* [42,70] also studied the thermomechanical properties of poly(S-co-BA)-clay nanocomposites prepared with four different organic modifiers and different clay contents. With different organic modifiers, nanocomposites with exfoliated and partially exfoliated structures showed higher storage modulus values and glass transition temperatures compared to the intercalated nanocomposites. The authors ascribed this to the fact that the highly dispersed clay layers had reinforcing effect and inhibited the mobility of the polymer chains. The DMA results of the AMPS modified clay nanocomposites with different clay loadings showed that below the glass transition temperature the nanocomposites had higher storage modulus values compared to the pure copolymer. The storage modulus increased slightly with increasing clay loading. This was due to the reinforcing effect of the clay and the interfacial interaction between the copolymer and silicate layers. The exfoliated nanocomposites showed higher storage modulus values than the intercalated nanocomposites. The nanocomposites also showed higher T_g than the pure copolymer, and it increased linearly with clay loading due to the restriction of the molecular chain motions of the polymer.

Dong *et al.* [71] studied the thermomechanical properties of polypropylene/organoclay nanocomposites. The nanocomposites were prepared by melt compounding in a Brabender co-rotating intermesh twin screw extruder with varying content of clay (1,3,5 and 10 wt%, respectively indicated by NCI, NC3, NC5 and NC10) with maleated polypropylene as compatibilizer. The T_g of the neat polymer and NC1 remained almost the same at about 22

°C, but increased to 27.9 and 31.4 °C for NC3 and NC5, respectively. It was slightly lower at 30.7 °C for N10. The decrease in T_g was attributed to the formation of agglomerates due to poor dispersion. Furthermore, the addition of organoclay showed an increase in elastic modulus below T_g due to the reinforcing effect of the organoclay. The storage modulus of the nanocomposites was higher than that of pure PP over the whole temperature range. Since the polymer chains are intercalated into the interlayer galleries of the clay platelets, the chain mobility of the PP was restricted by the layered structure of the organoclay, which resulted in higher T_g and E' values for the nanocomposites.

2.6.3 Thermal properties

Generally, it has been reported that polymer-clay nanocomposites are more thermally stable than pure polymers. The improvement in thermal stability is attributed to the formation of char that acts as a mass transport barrier and an insulator between the bulk polymer and the surface where combustion takes place [33,72]. Clay also hinders the diffusion of volatile products within the nanocomposites during decomposition. Some authors attributed the enhancement in thermal stability to the restricted thermal motion of polymer chains inside the clay galleries [30,70,72]. A number of studies showed that the improvement in thermal stability is not simply a function of clay loading. In some cases polymers with low clay loadings showed better thermal stability than those with higher clay loadings [73,74]. The thermal stability of PCNs is normally studied by thermogravimetric analysis (TGA), while differential scanning calorimetry (DSC) is used to study the influence of fillers on the thermal transitions of the polymers in the nanocomposites.

Lepoittevin *et al*. [75] studied the thermal properties of poly(ε-caprolactone) (PCL)-clay nanocomposites prepared by melt intercalation. TGA was performed under air flow at a heating rate of 20 K min^{-1}. The PCL nanocomposites showed better thermal stability than neat PCL. The authors attributed this behaviour to the decrease in the diffusion of oxygen and volatile products through the composites. Furthermore, the temperature at 50% weight loss increased by 60 °C with the addition of 1 wt% of clay compared to that for pure PCL. However, at 10 wt% clay loading the temperature increased by only 30 °C. A number of other studies found the same behaviour, which was attributed to the fact that exfoliated structures restricted the thermal motions of the polymer chains near the clay surface [2,70,74]. Greesh *et al.* [42], on the other hand, observed that intercalated nanocomposites

had higher thermal stabilities than exfoliated and partially exfoliated nanocomposites. They concluded that intercalated structures have several closely parked layers of clay, which provide a more efficient barrier between the burning zone and the underlying flammable material that is being gasified. DSC measurements showed that the clay had no effect on the T_g of PCL, which was observed at -60 °C. Similarly, the melting temperature of the nanocomposite was very close to that of the neat PCL at 57 °C. However, the melting enthalpy (ΔH_m) was clearly affected by the presence of clay. ΔH_m and the degree of crystallinity decreased with the addition of clay and with increasing clay content. ΔH_m decreased from 71.2 to 40.6 J g^{-1} and the crystallinity decreased from 52.4 to 35.5%.

Teymouri *et al.* [76] studied the thermal properties of LDPE/organo-montmorillonite clay nanocomposites. The nanocomposites were prepared by a melt intercalation method using polypropylene-g-maleic anhydride (PP-g-MA) as a compatibilizer with varying content of org-MMT (2.5 and 5% denoted as LDCN 2.5 and LDCN 5 respectively). There was no significant difference in the melting temperature and amount of crystallinity between LDCN 2.5, LDCN 5 and neat LDPE. The behaviour indicated no nucleation activity of org-MMT in LDPE based system. Zhou *et al.* [77] also studied the thermal properties of LDPE-clay nanocomposites with maleic anhydride-styrene cografted polyethylene (PE-g-MAH-St) used as a compatibilizer. The addition of compatibilizer increased the crystallization peak temperature of LDPE from 117 to 119 °C. The grafted chains on PE can act as nucleating agent and promote nucleation of PE. This behaviour increases the crystallisation rate and make crystallization occur at a higher temperature. The addition of clay (1, 3, and 5 %), however, had no effect on the crystallization temperature of LDPE.

Greesh *et al.* [70] studied the thermal properties of poly(styrene-co-butyl acrylate)-clay nanocomposites prepared by batch emulsion polymerization at different clay loadings (1, 3, 5, 7 and 10%). All the nanocomposites were found to be thermally more stable than the neat polymer, but the improvement was not a function of clay loading. The increase in thermal stability was attributed to the formation of char that acts as a mass transport barrier and an insulator between the bulk polymer and the surface where combustion takes place. The nanocomposites with 3 and 5 clay loading showed the best thermal stability. The nanocomposites with 10% clay loading showed poor thermal stability due to the highly dispersed state of the clay layers.

Lu *et al.* [78] studied the thermal properties of linear low-density polyethylene (LLDPE)-clay nanocomposites. The addition of vinyltrimethoxysilane (VTMS) increased the thermal stability of LLDPE. Mixing of the clay into the grafted LLDPE even further improved the thermal stability. The authors attributed the improvement in thermal-oxidative stability to the chemical bonds formed between the polymer matrix and the clay surface during both the extrusion process and the thermal-oxidation degradation process. Minkova *et al*. [79] studied the thermal properties of HDPE/Cloisite 15A (C15A) nanocomposites. The nanocomposites were compatibilized by different functionalized polyethylenes i.e. ethylene-acrylic acid copolymer (EAA), acrylic acid grafted HDPE (HDAA), and maleic anhydride grafted HDPE (HDMA). TGA was performed in air atmosphere and showed an increase in thermal stability for the HDPE/HDAA/C15A and HDPE/HDMA/C15A nanocomposites. However, the thermal stability of the HDPE/EAA/15A nanocomposites showed only a small increase compared to neat HDPE. The increase in thermal stability was due to the improved barrier to diffusion of oxygen in the material. The dispersion of the residue in the HDAA and HDMA nanocomposites led to larger improvement in barrier properties, but the residue in the EAA nanocomposites could not provide sufficient barrier to hinder the diffusion of oxygen.

2.7 Properties of other polyethylene reinforced nanocomposites

2.7.1 Morphology

Kontou *et al.* [80] studied the properties of an LLDPE matrix and nanocomposites containing 2, 4, 6, 8, and 10 wt% of SiO_2. Two types of commercial LLDPE, one prepared by traditional Ziegler-Natta catalysis (zLLDPE) and the other by metallocene catalysis (mLLDPE) were used. The surfaces of the silica nanoparticles were treated with dimethyldichlorosilane. Scanning electron microscopy (SEM) was used to study the morphology of the nanocomposites. The SEM images showed agglomerates in all the samples, which varied in size with the silica content. At silica contents higher than 4% the agglomerates formed in mLLDPE were smaller than those formed in zLLDPE, and increases in silica content resulted in larger agglomerates.

Jeziorska *et al*. [81] studied the properties of LDPE/spherical silica nanocomposites containing 1, 2, and 6 wt% of neat and modified silica particles. The nanocomposites were prepared by melt mixing, and to improve the degree of dispersion, glicydyl methacrylate

grafted ethylene/n-octene copolymer (EOR-g-GMA) was used as a compatibilizer. The fractured surface was examined using SEM. The SEM images of pure LDPE showed a relatively smooth surface. In the case of the nanocomposite with neat silica and without EOR-g-GMA, a rougher surface was observed at all silica contents. In contrast, the nanocomposites with modified silica and 2 wt% of EOR-g-GMA showed smoother surfaces. This was due to better interfacial adhesion between the silica and LDPE which reduced the nanoparticle agglomeration. However, the tendency to form agglomerates increased with increasing silica content.

2.7.2 Thermal properties

Beta *et al*. [82] studied the thermal properties of polystyrene (PS)/silica nanocomposites containing 2, 5, 10, 15 and 30 wt% of SiO_2. The surface of the silica nanoparticles were treated with hexamethyldisilazane. The thermal stability of the polystyrene was improved with the addition of clay. This improvement was attributed to the restricted thermal motions of PS and the hindered diffusion of the volatile decomposition products due to the finely dispersed silica particles. The best thermal stability was achieved at 15 wt% of silica – higher contents decreased the thermal stability. This was due to the formation of agglomerates at higher filler loadings.

Kontou *et al*. [80] also studied the thermal properties of LLDPE/silica nanocomposites. Their DSC results showed that T_gs of the LLDPE/SiO_2 composites were higher than the T_g of the corresponding LLDPE. This was due to the silica nanoparticles restricting the segmental and long-range chain mobility of the LLDPE phase. However, there was no relationship between the T_g and the silica content. Furthermore, the melting peak of both types of composites, mentioned in section 2.6.1, was not affected by the changes in silica content. Moreover, the melting enthalpy of mLLDPE/SiO_2 increased up to a silica content 4%, and then decreased. A similar but less pronounced trend was observed for the zLLDPE/SiO_2 composites.

2.7.3 Mechanical and thermomechanical properties

Jeziorska *et al*. [81] also studied the mechanical properties of LDPE/spherical silica nanocomposites. The tensile and impact strengths increased with the addition of modified silica and compatibilizer, but at high silica loadings the strength decreased due the formation

of agglomerates. The addition of both modified silica and compatibilizer increased the elongation at break, but only at lower silica contents. This behaviour was attributed to the good dispersion of the nanoparticles and the strong adhesion between the filler and the matrix, thus transferring the applied stress between the two materials. Young's modulus increased with the addition of modified silica and EOR-g-GMA, so the silica acted as a reinforcing agent. The authors concluded that the addition of modified silica and compatibilizer resulted in a finer dispersion of the individual silica nanoparticles in the LDPE matrix, as was verified by SEM, which enhanced the mechanical properties.

In their analysis of LLDPE/SiO_2 nanocomposites, Kontou *et al*. [80] observed that the storage moduli of the composites were higher than that of the corresponding LLDPE, particularly at lower loadings. Moreover, the storage modulus of the composites increased with increasing silicate content and at 8% SiO_2 this trend was reversed above the main transition temperature around -40 °C. The loss moduli of the composites were higher than those of the corresponding LLDPE. All the LLDPE-based materials exhibited a γ-transition in the temperature range of -145 to -135 °C. The position of the γ-transition peak was not affected by changes in silica content, but its intensity increased with silica content and reached its maximum at 4% silica content. All the samples exhibited a β-transition in the temperature range -40 to -20 °C. The β-transition of the mLLDPE /SiO_2 nanocomposites shifted to higher temperatures and increased in intensity with increasing silica content, and its intensity reached a maximum at 4% silica. This behaviour was due to the increase in the size of the interphase and a decrease in the polymer chain mobility at loadings smaller than or equal to 4%. However, the β-transition of the zLLDPE/SiO_2 nanocomposites was not affected by the filler content. The addition of nanofiller resulted in an increase in the elastic modulus and in the tensile strength of the LLDPE, accompanied by a slight increase in elongation at break.

2.8 References

1. C. Zhao, H. Qin, F. Gong, M. Feng, S. Zhang, M. Yang. Mechanical, thermal and flammability properties of polyethylene/clay nanocomposites. Polymer Degradation and Stability 2005; 87:183-189. DOI:10.1016/j.polymdegradstab.2004.08.005
2. Kusmono, Z.A. Mohd Ishak, W.S. Chow, T. Takeichi, Rochmadi. Effect of clay modification on the morphological, mechanical, and thermal properties of polyamide

6/polypropylene/montmorillonite nanocomposites. Polymer Composites 2010; 31:1156-1167.
DOI:10.1002/pc.20902

3. H.M.C. de Azeredo. Nanocomposites for food packaging applications. Food Research International 2009; 42:1240-1253.
DOI:10.1016/j.foodres.2009.03.019
4. I.Y. Jeon, J.B. Baek. Nanocomposites derived from polymers and inorganic nanoparticles. Materials 2010; 3:3654-3674.
DOI: 10.3390/ma3063654
5. N. Greesh, R. Sanderson, P. Hartmann. Preparation of polystyrene-clay nanocomposites via dispersion polymerization using oligomeric styrene-montmorillonites as stabilizer. Polymer International 2012; 61:834-843.
DOI:10.1002/pi.4151
6. R. Rezanavaz, M.K.R Aghjeh, A.A. Babaluo. Rheology, morphology, and thermal behaviour of HDPE/clay nanocomposites. Polymer Composites 2010; 31:1028-1036.
DOI:10.1002/pc.20889
7. M.P. Villanueva, L. Cabedo, E. Gimenez, J.M. Lagaron, P.D. Coates, A.L. Kelly. Study of the dispersion of nanoclays in a LDPE matrix using microscopy and in-process ultrasonic monitoring. Polymer Testing 2009; 28:277-287.
DOI:10.1016/j.polymertesting.2008.12.009
8. P.P. Sambarkar, S.L. Patwekar, B.M. Dudhgaonkar. Polymer Composites: An overview. International Journal of Pharmacy and Pharmaceutical Sciences 2012; 4:60-65.
9. S.S. Ray, M. Okamoto. Polymer/layered silicate nanocomposites: A review from preparation to processing. Progress in Polymer Science 2003; 28:1539-1641.
DOI:10.1016/j.progpolymsci.2003.08.002
10. H. Wang, P. Fang, Z. Chen, S. Wang, Y. Xu, Z. Fang. Effect of silane grafting on the microstructure of high-density polyethylene/organically modified montmorillonite nanocomposites. Polymer International 2008; 57:50-58.
DOI: 10.1002/pi.2310
11. J.K. Kim, H.S. Park, D.K. Rhee, S.J. Ham, K.J. Lee, P.J. Yoo, J.H. Park. Ultrathin nanoclay film with tunable thickness as barrier layers in organic light emitting devices. Journal of Materials Chemistry 2012; 22:7718-7723.
DOI: 10.1039/c2jm00047d

12. S.H. Bahrami, Z. Mirzaie. Polypropylene/modified nanoclay composite-processing and dyeability properties. World Applied Sciences Journal 2011; 13:493-501.
13. http://www.groundwaterresearch.com.au/reference/clayliners/clay%20liners.htm (Accessed April 2012).
14. B. Ryznarova, J. Zelenka, F. Lednicky, J. Baldrian. Epoxy-clay nanocomposites: Influence of the clay surface modification on structure. Journal of Applied Polymer Science 2008; 109:1492-1497.
DOI: 10.1002/app.28219
15. Y. Park, G.A. Ayoko, J. Kristof, E. Horvath, R.L. Frost. A thermoanalytical assessment of an organoclay. Journal of Thermal Analysis and Calorimetry 2012; 107:1137-1142.
DOI 10.1007/s10973-011-1568-8
16. P. Singla, R. Mehta, S.N. Upadhyay. Clay modification by the use of organic cations. Green and Sustainable Chemistry 2012; 2:21-25.
DOI:10.4236/gsc.2012.21004
17. N.N. Herrera, J.L. Putaux, E.B. Lami. Synthesis of polymer/laponite nanocomposite latex particles via emulsion polymerization using silylated and cationic-exchanged laponite clay platelets. Progress in Solid State Chemistry 2006; 34:121-137.
DOI:10.1016/j.progsolidstchem.2005.11.040
18. http://www.pslc.ws/macrog/mpm/composit/nano/modify1.htm(Accessed May2012)
19. S. Praveen, P.K. Chattopadhyay, S. Jayendran, B.C. Chakraborty, S. Chattopadhyay. Effect of rubber matrix on the morphology and reinforcement effects in carbon black-nanoclay hybrid composites – A comprehensive assessment. Polymer Composites 2010; 31:97-104.
DOI:10.1002/pc.20772
20. J. Gaume, A. Rivaton, S. Therias, J.L. Gardette. Influence of nanoclays on the photochemical behaviour of poly(vinyl alcohol). Polymer Degradation and Stability 2012; 97:488-495.
DOI:10.1016/j.polymdegradstab.2012.01.022
21. M. Okamoto. Recent advances in polymer/layered silicate nanocomposites: An overview from science to technology. Materials Science and Technology 2006; 22: 756-779.
DOI: 10.1179/174328406X101319

22. S. Pavlidou, C.D. Papaspyrides. A review on polymer-layered silicate nanocomposites. Progress in Polymer Science 2008; 33:1119-1198.
DOI:10.1016/j.progpolymsci.2008.07.008

23. Kusmono, Z.A. Mohd Ishak, W.S. Chow, T. Takeichi, Rochmadi. Enhancement of properties of PA6/PP nanocomposites via organic modification and compatibilization. eXPRESS Polymer Letters 2008; 2:655-664.
DOI:10.3144/expresspolymlett.2008.78

24. R.R. Tiwari, K.C. Khilar, U. Natarajan. Synthesis and characterization of novel organo-montmorillonites. Applied Clay Science 2008; 38:203-208.
DOI:10.1016/j.clay.2007.05.008

25. A. Vazquez, M. Lopez, G. Kortberria, L. Martin, I. Mondragon. Modification of montmorillonite with cationic surfactants. Thermal and chemical analyses including CEC determination. Applied Clay Science 2008; 41:24-36.
DOI:10.1016/j.clay.2007.10.001

26. L.L. Pluart, J. Duchet, H. Sautereau, J.F. Gerard. Surface modifications of montmorillonite for tailored interfaces in nanocomposites. The Journal of Adhesion 2002; 78:645-662.
DOI: 10.1080/00218460290010359

27. Z. Narratilova, P. Wojtowicz, L. Vaculikova, V. Sugarkova. Sorption of alkylammonium cations on montmorillonites. Acta Geodynamica et Geomaterialia 2007; 147:59-65.

28. P. Jash, C.A. Wilkie. Effect of surfactants on the thermal and fire properties of poly(methyl methacrylate)/clay nanocomposites. Polymer Degradation and Stability 2005; 88:401-406.
DOI:10.1016/j.polymdegradstab.2004.12.004

29. J.M. Yeh, K.C. Chang. Polymer/layered silicate nanocomposite anticorrosive coatings. Journal of Industrial and Engineering Chemistry 2008; 14:275-291.
DOI:10.1016/j.jiec.2008.01.011

30. A.A. Silva, K. Dahmouche, B.G. Soares. Nanostructure and dynamic mechanical properties of silane-functionalized montmorillonite/epoxy nanocomposites. Applied Clay Science 2011; 54:151-158.
DOI.org/10.1016/j.clay.2011.08.002

31. F. Piscitelli, P. Posocco, R. Toth, M. Fermeglia, S. Pricl, G. Mensitieri, M. Lavorgna. Sodium montmorillonite silylation: Unexpected effect of the aminosilane chain length. Journal of Colloid and Interface Science 2010; 351:108-115.
DOI:10.1016/j.jcis.2010.07.059

32. H.A. Patel, R.S. Somani, H.C. Bajaj, R.V. Jasra. Preparation and characterization of phosphonium montmorillonite with enhanced thermal stability. Applied Clay Science 2007; 35:194-200.
DOI:10.1016/j.clay.2006.09.012

33. Y.Y. Choi, S.H. Lee, S.H. Ryu. Effect of silane functionalization of montmorillonite on epoxy/montmorillonite nanocomposite. Polymer Bulletin 2009; 63:47-55.
DOI: 10.1007/s00289-009-0068-5

34. S.J. Park, B.J. Kim, D.I. Seo, K.Y. Rhee, Y.Y. Lyu. Effects of a silane treatment on the mechanical interfacial properties of montmorillonite/epoxy nanocomposites. Materials Science and Engineering A 2009; 526:74-78.
DOI:10.1016/j.msea.2009.07.023

35. Q.T. Nguyen, D.G. Baird. Preparation of polymer-clay nanocomposites and their properties. Advances in Polymer Technology 2006; 25:270-285.
DOI: 10.1002/adv.20079

36. A.B. Morgan, J.W. Gilman. Characterization of polymer-layered silicate (clay) nanocomposites by transmission electron microscopy and X-ray diffraction: A comprehensive study. Journal of Applied Polymer Science 2003; 87:1329-1338.
DOI:10.1002/app.11884

37. D.R. Paul, L.M. Robeson. Polymer nanotechnology: Nanocomposites. Polymer 2008; 49:3187-3204.
DOI:10.1016/j.polymer.2008.04.017

38. X. Fu, S. Qutubuddin. Polymer-clay nanocomposites: Exfoliation of organophilic montmorillonite nanolayers in polystyrene. Polymer 2001; 42:807-813.
DOI.org/10.1016/S0032-3861(00)00385-2

39. S.G. Lei, S.V. Hoa, M.T.T. That. Effect of clay types on the processing and properties of polypropylene nanocomposites. Composites Science and Technology 2006; 66:1274-1279.
DOI: 10.1016/j.compscitech.2005.09.012

40. G.I. Nakas, C. Kaynak. Use of different alkylammonium salts in clay surface modification for epoxy-based nanocomposites. Polymer Composites 2009; 30:357-363.
DOI: 10.1002/pc.20667

41. B. Ryznarova, J. Zelenka, F. Lednicky, J. Baldrian. Epoxy-clay nanocomposites: Influence of clay surface modification on structure. Journal of Applied Science 2008; 109:1492-1497.
DOI: 10.1002/app.28219

42. N. Greesh, P.C. Hartmann, V. Cloete, R.D. Sanderson. Impact of the clay organic modifier on the morphology of polymer-clay nanocomposites prepared by in-situ free-radical polymerization in emulsion. Journal of Polymer Science 2008; 46:3619-3628.
DOI: 10.1002/pola.22701

43. R. Wilson, T.S. Plivetic, C. Ranganathaiah, M.Y. Kariduraganavar, A.K. Sivasankarapillar, S. Thomas. Influence of clay content and amount of organic modifiers on morphology and pervaporation performance of EVA/clay nanocomposites. Industrial and Engineering Chemistry Research 2011; 50:3986-3993.
DOI.org/10.1021/ie102259s

44. S.M. Tamboli, S.T. Mhaske, D.D. Kale. Crosslinked polyethylene. Indian Journal of Chemical Technology 2004; 11:853-864.

45. J. Barzin, H. Azizi, J. Morshedian. Preparation of silane-grafted and moisture crosslinked low density polyethylene. Part II: Electrical, thermal and mechanical properties. Polymer-Plastics Technology and Engineering 2007; 46:305-310.
DOI: 10.1080/03602550601155815

46. R. Anbarasan, O. Babot, B. Maillard. Crosslinking of high-density polyethylene in the presence of organic peroxides. Journal of Applied Polymer Science 2004; 93:75-81.
DOI: 10.1002/app.20390

47. G.B. Shah, M. Fuzail, J. Anwar. Aspects of the crosslinking of polyethylene with vinyl silane. Journal of Applied Polymer Science 2004; 92:3796-3803.
DOI: 10.1002/app.20381

48. T.M. Shukri, J. Mosnacek, A.A. Basfar, M.A. Bahattab, P. Noireaux, A. Courdreuse. Flammability of blends of low-density polyethylene and ethylene vinyl acetate crosslinked by both dicumyl peroxide and ionizing radiation for wire and cable applications. Journal of Applied Polymer Science 2008; 109:167-173.
DOI:10.1002/app.28080

49. F.W. Fabris, F.C. Stedile, R.S. Mauler, S.M.B. Nachtigall. Free radical modification of LDPE with vinyltriethoxysilane. European Polymer Journal 2004; 40:1119-1126. DOI:10.1016/j.eurpolymj.2004.01.008

50. M. Palmlof, T. Hjertberg. Catalysis of the crosslinking reactions of ethylene vinyl silane copolymers using carboxylic acids and DBTDL. Journal of Applied Polymer Science 1999; 72:521-528. DOI: 10.1002/(SICI)1097-4628(19990425)

51. K. Sirisinha, D. Meksawat. Preparation and properties of metallocene ethylene copolymer crosslinked by vinyltrimethoxysilane. Polymer International 2005; 54:1014-1020. DOI: 10.1002/pi.1800

52. H. Azizi, J. Barzin, J. Morshedian. Silane crosslinking of polyethylene: The effects of EVA, ATH and Sb_2O_3 on properties of the production in continuous grafting of LDPE. eXPRESS Polymer Letters 2007; 1:378-384. DOI: 10.3144/expresspolymlett.2007.53

53. Y.T. Shieh, T.H. Tsai. Silane grafting reactions of low-density polyethylene. Journal of Applied Polymer Science. 1998; 69:255-261 DOI: 10.1002/(SICI)1097-4628(19980711)

54. Z. Wang, Y. Hu, Z. Gui, R. Zong. Halogen-free flame retardation and silane crosslinking of polyethylenes. Polymer Testing 2003; 22:533-538. DOI:10.1016/S0142-9418(02)00149-6

55. H. Azizi, J. Morshedian, M. Barikani. Silane grafting and moisture crosslinking of polyethylene: The effect of molecular structure. Journal of Vinyl and Additive Technology 2009; 15:184-190. DOI:10.1002/vnl.20194

56. T.P. Mohan, K. Kanny. Effect of synthesis and processing methods on dispersion characteristics of nanoclay in polypropylene polymer matrix composites. Materials Sciences and Application 2011; 2:785-800. DOI: 10.423/msa.2011.27108

57. J. Zhang, D.D. Jiang, C.A. Wilkie. Polyethylene and polypropylene nanocomposites based on a three component oligomerically-modified clay. Polymer Degradation and Stability 2006; 91:641-648. DOI:10.1016/j.polymdegradstab.2005.02.004

58. C.D Castel, O. Bianchi, M.A.S. Oviedo, S.A. Liberman, R.S. Mauler, R.V.B. Oliveira. The influence of interfacial agents on the morphology and viscoelasticity of PP/MMT nanocomposites. Materials Science and Engineering C 2009; 29:602-606. DOI:10.1016/j.msec.2008.10.012

59. S. Kar, P.K. Maji. A.K. Bhowmick. Chlorinated polyethylene nanocomposites: Thermal and mechanical behaviour. Journal of Materials Science 2010; 45:64-73. DOI: 10.1007/s10853.009-3891-z

60. A. Mohaddespour, S.J. Ahmadi, H. Abolghasemi, S. Jafarinejad. Investigation of mechanical, thermal and chemical properties of HDPE/PEG/OMT nanocomposites. Journal of Applied Sciences 2007; 7:2591-2597. DOI: 10.3923/jas.2007.2591.2597

61. S.M. Shirazi. Study of processing and mechanical behaviour of PP/clay nanocomposites prepared by melt blending. International Journal of Modern Physics: Conference Series 2012; 5:536-544. DOI: 10.1142/S2010194512002449

62. A. Alipour. Fabrication and characterization of nanostructured polymer composites prepared by melt compounding. International Journal of Bioscience, Biochemistry and Bioinformatics 2012; 2:79-84.

63. M.W. Spencer, L. Cui, Y. Yoo, D.R. Paul. Morphology and properties of nanocomposites based on HDPE/HDPE-g-MA blends. Polymer 2010; 51:1056-1070. DOI:10.1016/j.polymer.2009.12.047

64. C. Wan, B. Chen. Reinforcement and interphase of polymer/grapheme oxide nanocomposites. Journal of Materials Chemistry 2012; 22:3637-3646. DOI: 10.1039/c2jm15062j

65. Z. Martin, I. Jimenez, M.A. Gomez-Fatou, M. West, A.P. Hitchcock. Interfacial interactions in polypropylene-organoclay-elastomer nanocomposites: Influence of polar modifications on the location of the clay. Macromolecules 2011; 44:2179-2189. DOI.org/10.1021/ma102707f

66. A.G. Supri, H. Salmah, K. Hazwan. Low density polyethylene-nanoclay composites: The effect of poly(acrylic acid) on mechanical properties, XRD, morphology properties and water absorption. Malaysian Polymer Journal 2008; 3:39-53.

67. S.R. Ha, S.H Ryu, S.J. Park, K.Y. Rhee. Effect of clay surface modification and concentration on tensile performance of clay/epoxy nanocomposites. Materials Science and Engineering A 2007; 448:264-268.

DOI:10.1016/j.msea.2006.10.052

68. M.N.M. Ansari, H. Ismail. The effect of silane coupling agent on mechanical properties of feldspar filled polypropylene composites. Journal of Reinforced Plastics and Composites 2009; 28:3049-3060.
DOI: 10.1177/0731684408095197

69. S. Rezanejad, M. Kokabi. Shape memory and mechanical properties of cross-linked polyethylene/clay nanocomposites. European Polymer Journal 2007; 43:2856-2865.
DOI:10.1016/j.eurpolymj.2007.04.031

70. N. Greesh, P.C. Hartmann, R.D. Sanderson. The effect of clay loading on the morphology and properties of poly(styrene-co-butyl acrylate)/clay nanocomposites. Macromolecular Materials and Engineering 2009; 294:206-212.
DOI: 10.1002/mame.200800285

71. Y. Dong, D. Bhattacharyya, P.J. Hunter. Experimental characterisation and object-oriented finite element modelling of polypropylene/organoclay nanocomposites. Composites Science and Technology 2008; 68:2864-2875.
DOI:10.1016/j.compscitech.2007.10.026

72. N. Greesh, P.C. Hartmann, R.D. Sanderson. Preparation of polystyrene/clay nanocomposites by free-radical polymerization in dispersion. Macromolecular Materials and Engineering 2009; 294:787-794.
DOI: 10.1002/mame.200900129

73. M.A. Perez, B.L. Rivas, S.M. Rodriguez, A. Maldonado. Polypropylene/clay nanocomposites. Synthesis and characterization. Journal of the Chilean Chemical Society 2010; 55:440-444.
DOI: 10.4067/S0717-97072010000400006

74. A. Nese, S. Sen, M.A. Tasdelen, N. Nugay, Y. Yagci. Clay-PMMA nanocomposites by photoinitiated radical polymerization using intercalated phenacyl pyridinium salt initiators. Macromolecular Chemistry and Physics 2006; 207:820-826.
DOI: 10.1002/macp.200500511

75. B. Lepoittevin, M. Devalckenaere, N. Pantoustier, M. Alexandre, D. Kubies, C. Calberg, R. Jerome, P. Dubois. Poly(ε-caprolactone)/clay nanocomposites prepared by melt intercalation: Mechanical, thermal and rheological properties. Polymer 2002; 43:4017-4023.
PII: S0032-3861(02)00229-X

76. Y. Teymouri. H. Nazockdast. The effect of process parameter on physical and mechanical properties of commercial low density polyethylene/ORG-MMT nanocomposites. Journal of Materials Science 2011; 46:6642-6647.
DOI: 10.1007/s10853-011-5616-3

77. Z. Zhou, H. Zhai, W. Xu, H. Guo, C. Liu, W.P. Pan. Preparation and characterization of polyethylene-g-maleic anhydride-styrene/montmorillonite nanocomposites. Journal of Applied Polymer Science 2006; 101:805-809.
DOI: 10.1002/app.22107

78. H. Lu, Y. Hu, M. Li, Z. Chen, W. Fan. Structure characteristics and thermal properties of silane-grafted-polyethylene/clay nanocomposite prepared by reactive extrusion. Composites Science and Technology 2006; 66:3035-3039.
DOI:10.1016/j.compscitech.2006.01.018

79. L. Minkova, Y. Peneva, E. Tashev, S. Filippi, M. Pracella, P. Magagnini. Thermal properties and microhardness of HDPE/clay nanocomposites compatibilized by different functionalized polyethylenes. Polymer Testing 2009; 28:528-533.
DOI:10.1016/j.polymertesting.2009.04.001

80. E. Kontou, M. Niaounakis, Thermo-mechanical properties of LLDPE/SiO_2 nanocomposites. Polymer 2006; 47:1267-1280.
DOI:10.1016/j.polymer.2005.12.039

81. R. Jeziorska, B.S Motysia, M. Zielecka, A. Szadkowska, M. Studzinski. Structure and mechanical properties of low density polyethylene/spherical silica nanocomposites prepared by melt mixing: The joint action of silica's size, functionality, and compatibilizer. Journal of Applied Polymer Science 2012; 125:4326-4337.
DOI: 10.1002/app.36579

82. O. Bera, B. Pilic, J. Pavlicevic, M. Jovicic, B. Hollo, K. M. Szecsenyi, M. Spirkova. Preparation and thermal properties of polystyrene/silica nanocomposites. Thermochimica Acta 2011; 515:1-5.
DOI:10.1016/j.tca.2010.12.006

Chapter 3: Materials and methods

3.1 Materials

3.1.1 High-density polyethylene (HDPE)

HDPE was supplied in powder form by Safripol, Sasolburg, South Africa. It has a melt flow index of 3 g/10 min (ISO 1133), a molecular weight of 230489 g mol^{-1}, a melting point of 130 °C, and a density of 0.949 g cm^{-3}.

3.1.2 Low-density polyethylene (LDPE)

LDPE was supplied in pellet form by Sasol Polymers, Johannesburg, South Africa. It has a melt flow index of 7 g/10 min (ASTM D-1238) and a molecular weight of 96 000 g mol^{-1}. It has a density of 0.918 g cm^{-3} and the melting point of 108 °C. The granules were powderized before further use.

3.1.3 Nanoclays

Calcium montmorillonite (Ca^{2+}MMT) and Cloisite 15A (C15A) were supplied as cream white powders by Southern Clay Products Inc. (Taxes, USA). Their specifications are summarized in Table 3.1. The structure of the organic modifier used is shown in Figure 3.1, with HT a hydrogenated tallow (~65 wt. % C18; ~30 wt. % C16; ~5 wt. % C14).

Table 3.1 Properties of nanoclays

Nanoclays	Organic modifier	Modifier concentration (meg/100g clay)	XRD d-spacing (001) / Å
Cloisite 15A	Dimethyl, dehydrogenated tallow, quaternary ammonium chloride	125	33.7
Cloisite Ca^{2+}MMT	None	None	15.2

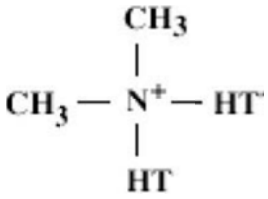

Figure 3.1 Structure of the organic modifier [1]

3.1.4 Other chemicals

3.1.4.1 Dicumyl peroxide (DCP)

Dicumyl peroxide was supplied by Sigma-Aldrich, Krugersdorp, South Africa as a white crystalline powder with an assay of 99%. It was used as a free radical initiator and has a melting point of 39 °C and a molar mass of 270 g mol^{-1}.

3.1.4.2 Vinyltriethoxysilane (VTES)

Vinyltriethoxysilane was supplied by Merck (Pty) Ltd, Germiston, South Africa as a liquid with an assay of 98%. It was used as a coupling agent with a density of 0.91 g cm^{-3} and a molar mass of 190 g mol^{-1}.

All the chemicals where used without further purification.

3.2 Methods

3.2.1 Preparation of polyethylene-g-vinyltriethoxysilane (PE-g-VTES)

VTES was grafted onto the polyethylene (PE) chains by a free radical reaction, initiated by DCP. In system A, 0.1 g of DCP was dissolved in respectively 1 and 3 ml of VTES to form a solution, and in system B the amount of DCP was 0.2 g with 1 and 3 ml of VTES, respectively. Each solution was added dropwise onto PE powder using a syringe at room temperature and physically stirred for 10 min. After mixing, the mixture was transferred into a Brabender Platostograph 50 ml internal mixer which was set at 170 °C, 60 r.p.m for 10 min.

To confirm whether grafting has actually taken place, Fourier-transform infrared analysis (FTIR) was performed. Figures 3.2 and 3.3 show the FTIR spectra of LDPE and silane grafted LDPE for systems A and B respectively, while Table 3.2 summarizes the new bands that developed in the 'grafted' LDPE.

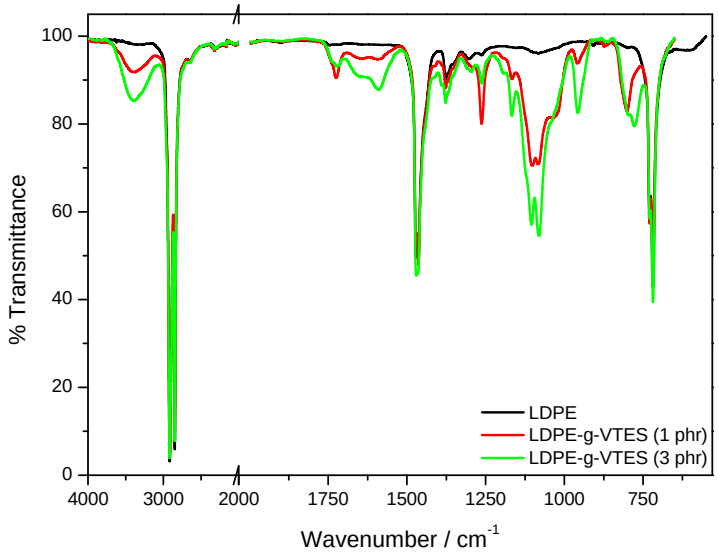

Figure 3.2 FTIR spectrum of pure LDPE and vinyltriethoxysilane grafted LDPE (System A)

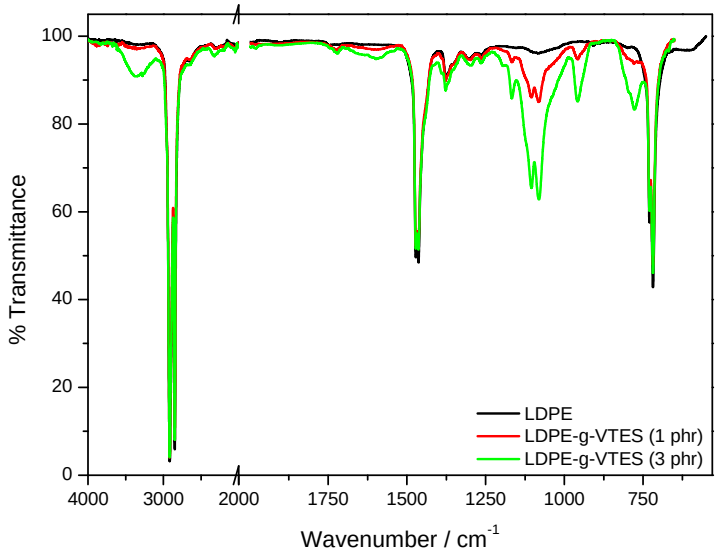

Figure 3.3 FTIR spectrum of pure LDPE and vinyltriethoxysilane grafted LDPE (System B)

Table 3.2 New peaks observed in the FTIR spectrum of vinyltriethoxysilane treated LDPE

Wavenumber / cm^{-1}	Assigned vibrations
776, 974	Si-C stretching
956	CH_2 wagging of vinyl group
1033	Stretching vibration of Si-O-Si
1079, 1106	Si-O out-of-plane stretching, in-plane stretching
1168	C-C stretching
1263	C-O stretching
1594-1653, 1723	C=C stretching
3392	Stretching vibration of -OH

In the silane grafted LDPE, the broad band at 989-1195 cm^{-1} is attributed to the Si-O-C stretching of silane. The intensity of this band increases with increase in silane concentration. The strong absorption bands at 1083 and 1107 cm^{-1} belong to Si-O out-of-plane stretching and in-plane stretching respectively of Si-O-C. The peak at 1168 cm^{-1} is attributed to the C-C stretching of $–CH_2-CH_3$. The peak observed at 1263 cm^{-1} belongs to the C-O stretching of Si-O-C, while the peak at 956 cm^{-1} is attributed to the CH_2 wagging vibration of the vinyl group. The peak at 794 cm^{-1} is attributed to the Si-C stretching and with increase in VTES it broadens and shifts towards lower wavenumber, with the development of a new peak at 777 cm^{-1}. The C=C stretching peak is observed in the range of 1590-1660 cm^{-1}, and the peak becomes more intense with an increase in VTES content, which is probably the result of the unreacted vinyl group of silane. In the presence of moisture Si-O-C can be hydrolysed to form silanols (Si-OH) with a broad band around 3388 cm^{-1}, which arises from the O-H stretching of the silanol group. The silanols can condense with each other and form the Si-O-Si peak at 1033 cm^{-1} which appears as a shoulder on the larger band of Si-O-C [15,16]. From these results it is clear that the grafting in system A was not very effective, and that the 'grafted' LDPE contained an appreciable amount of ungrafted (pure or hydrolysed) VTES. However, sufficient grafting was achieved in system B.

3.2.2 Preparation of PE-g-VTES /clay nanocomposites

The nanoclays were first dried in an oven at 80 °C for 12 hrs to remove any adsorbed moisture. Different amounts of nanoclay (1, 3 and 5 wt. %) were added to the molten PE-g-VTES in the Brabender after the initial 10 min. mixing, and the mixing continued for another 8 min. The samples were then melt pressed into 1 mm thick sheets between aluminium plates at 170 °C for 10 min at 50 bar, and samples were cut from these sheets for the various analyses.

3.2.3 Preparation of PE/clay nanocomposites

The PE was put into a Brabender Platostograph 50 ml internal mixer set at 170 °C and 60 r.p.m. After 10 min of mixing, different contents of the nanoclays as shown in Table 3.2 were added. The mixing process was continued for another 8 minutes. The samples were melt pressed into 1 mm thick sheets between aluminium plates at 170 °C for 10 min at 50 bar, and samples were cut from these sheets for various analyses.

Table 3.3 Sample ratios used to prepare the nanocomposites

LDPE-g-VTES (1phr)/C15A (w/w)	**LDPE-g-VTES (3phr)/C15A (w/w)**	**LDPE/C15A (w/w)**	**LDPE/Ca^{2+} MMT (w/w)**
100/0	100/0	100/0	100/0
99/1	99/1	99/1	99/1
97/3	97/3	97/3	97/3
95/5	95/5	95/5	95/5
LDPE-g-VTES (1 phr)/Ca^{2+}MMT (w/w)		**LDPE-g-VTES (3 phr)/Ca^{2+}MMT (w/w)**	
97/3		97/3	
HDPE-g-VTES (1 phr)/C15A (w/w)		**HDPE-g-VTES (3 phr)/C15A (w/w)**	
100/0		100/0	
99/1		99/1	
97/3		97/3	
95/5		95/5	

3.3 Characterization techniques

3.3.1 X-ray diffraction (XRD)

X-ray diffraction observes the scattered intensity of an X-ray beam hitting a sample as a function of incident and scattered angle, polarization and wavelength or energy. XRD provides detailed information about the crystallographic structure, chemical composition, and physical properties of materials and thin films. In the case of polymer-clay nanocomposites (PCNs) XRD is used to study the dispersion of layered silicates (immiscible, intercalated or exfoliated morphology) in a polymer matrix by monitoring the position, shape and intensity of the diffraction peak. The space between the layered silicates can be calculated by using Bragg's law (Equation 3.1).

$$n\lambda = 2d \sin \theta \qquad (3.1)$$

where λ is the wavelength of the X-ray radiation used in the diffraction experiment. Copper is the most common target material used for single-crystal diffraction with the wavelength of CuK_α radiation 1.5418 Å. The spacing between the diffraction lattice planes is denoted as d and θ is the measured diffraction angle [1,2].

XRD measurements were performed using a D8 Advance diffractometer. The diffractometer was equipped with Cu-K_α radiation at 40 kV and 40 mA. The scanning range in 2θ was 0.2 – 10° with a speed of 0.01 deg sec^{-1}.

3.3.2 Transmission electron microscopy (TEM)

Transmission electron microscopy allows a qualitative understanding of the internal structure, distribution of the various phases, and views of the defect structure through direct visualization. During the analysis a beam of electrons is transmitted through an ultra-thin specimen and interacts with the specimen as it passes through it. An image appears on a screen, and can be magnified from 100 to approximately 500 000 times. In the case of polymer-clay nanocomposites, TEM is used to study the dispersion of the layered silicate (immiscible, intercalated or exfoliated morphology) in the polymer matrices [2,3,4].

The transmission electron microscopy images were obtained using a 200 kV FEI Tecnai20 transmission electron microscope fitted with Gatan Tridiem. The LDPE samples were mounted oncryo-pins and frozen in liquid nitrogen. 100-150 nm sections were cut at -100 °C using a Reichert Ultracut S ultramicrotome chuck and collected on copper grids and viewed. The HDPE samples were trimmed and sectioned to fit the ultramicrotome, since they were hard enough to cut without cooling. 100-150 nm thin sections were also collected on copper grids and viewed.

3.3.3 Differential scanning calorimetry (DSC)

Differential scanning calorimetry is the most popular thermal analysis technique, the "workhorse" of thermal analysis. DSC measures the heat required to maintain the same temperature in the sample and an appropriate reference material (or an empty sample pan) during controlled heating. DSC can be used to study thermal transitions in polymers. These transitions include the glass transition, melting, crystallization, and degradation or decomposition [5,6].

DSC analyses were performed using a Perkin Elmer Pyris-1 differential scanning calorimeter under nitrogen atmosphere (flowing rate of 20 ml min^{-1}). The instrument was calibrated using the onset temperatures of zinc and indium standard and the enthalpy of indium. Samples with masses between 5 and 10 mg were sealed in aluminium pans and heated from 25 to 170 °C at a rate of 10 °C min^{-1} and cooled to 25 °C at the same rate. For the second scan, the samples were heated and cooled under the same conditions. The onset and peak temperatures of melting and crystallization, as well as the melting and crystallization enthalpies were determined from the second scans. The normalized enthalpy (ΔH_n) was determined using Equation 3.2.

$$\Delta H_m^{norm} = \frac{Measured\ \Delta H}{Mass\ fraction\ of\ polymer} \qquad (3.2)$$

3.3.4 Thermogravimetric analysis (TGA)

Thermogravimetric analysis is a technique where the mass of a sample is measured as a function of temperature or time while the sample is subjected to a controlled temperature program in a controlled atmosphere. The heart of the thermogravimetric analyser is the thermobalance, which is capable of measuring the sample mass as a function of temperature or time. A purge gas, such as nitrogen, flowing through the balance creates an inert atmosphere. TGA can directly record the changes in mass due to dehydration, decomposition, or oxidation of a sample as function of time and temperature. TGA is mostly used to study the decomposition, thermal stability and ash content of polymer-clay nanocomposites [2,5,6,8].

TGA analyses were performed using a Perkin Elmer TGA7 thermogravimetric analyser, under nitrogen atmosphere at a flow rate of 20 ml min^{-1}. Samples with masses ranging between 5 and 10 mg were heated from 30 to 600 °C at a rate of 10 °C min^{-1}.

3.3.5 Dynamic mechanical analysis (DMA)

Polymers are viscoelastic materials. Viscoelasticity describes the time-dependent mechanical properties which in limiting cases can behave as either elastic solids or viscous liquids. Dynamic mechanical techniques are used to characterize the viscoelastic properties of polymers, because they are readily adapted to study both polymeric solids and liquids. Dynamic mechanical analysis involves imposing a small cyclic strain on a sample and measuring the resulting stress response, or equivalently, imposing a cyclic stress on a sample and measuring the resulting strain response. DMA can be used to study elastic modulus (storage modulus, E'), viscous modulus (loss modulus, E''), and damping coefficient (tan δ) as a function of time, temperature or frequency [2,5,6,9].

The dynamic mechanical properties of the polymer-clay nanocomposites were studied using a Perkin Elmer Diamond DMA. The conditions for the analysis were as follows:

Frequency	1 Hz
Amplitude	20 μm
Temperature range	-100 to 100 °C
Temperature programme mode	Ramp
Measurement mode	Bending (dual cantilever)
Heating rate	3 °C min^{-1}
Preloading force	0.02 N
Sample length	20 mm
Sample width	12.0 – 12.5 mm
Sample thickness	1.0 – 1.3 mm

3.3.6 Tensile testing

Tensile testing is also known as a tension test. It is used to measure the force required to break a specimen and the extent to which the specimen can stretch or elongate until it reaches the breaking point. The parameters most generally considered are stress, strain, and Young's modulus. Stress is defined as the force applied per unit cross sectional area with the basic dimensions of N m^{-2} in SI units. Strain is the increase in length of the specimen per original length and is without any dimensions. Young's modulus is the ratio of stress to strain. Tensile strength (at yield and at break), tensile modulus, elongation and percent elongation at yield, elongation and percent elongation at break can be determined from a tensile test [10,11].

A Hounsfield H5KS universal testing machine was used for the tensile analysis of the samples. The dumbbell shaped samples (Figure 3.1) with a Gauge length of 20 mm, a thickness of about 1.0 – 1.3 mm and a width of 5 mm were tested at a speed of 50 mm min^{-1}. About five test specimens for each composition were analysed and the averages and standard deviations are reported.

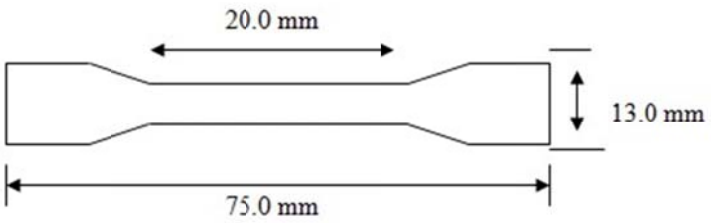

Figure 3.4 Dumbbell shaped tensile testing sample

3.3.7 Fourier-transform infrared (FTIR)spectroscopy

Fourier-transform infrared spectroscopy is a technique that is used to identify types of chemical bonds or functional groups in a molecule. During the analysis, IR radiation passes through a sample and produces an infrared absorption spectrum like a molecular 'fingerprint'. FTIR can be used to identify components of unknown mixtures including solids, liquids, gasses, semi-solids, powders, polymers, organics, inorganics and more. Advantages of an FTIR analysis include its high speed, sensitivity, mechanical simplicity and inexpensiveness [6,12,13].

FTIR spectroscopy was performed using a Perkin Elmer Spectrum 100 Fourier-transform infrared spectrophotometer. The polymer-clay nanocomposites were analysed in an attenuated total reflectance (ATR) detector in a 400 – 4000 cm^{-1} wavenumber range at a resolution of 4 cm^{-1}.

3.3.8 Gel content

Gel content analysis is a technique to determine the extent of crosslinking in the composites. The gel content in a crosslinked polyolefin can be determined by solvent extraction with toluene or xylene [14].

The gel content of the composites was determined through xylene extraction of the uncross-linked parts of the sample. Small samples of 10 x 10 mm were weighed and wrapped in stainless steel mesh with pore sizes of 43 microns, supplied by Meshcape Industries, Johannesburg, South Africa. The wrapped samples were tied with a string and then placed in a 250 ml round-bottom flask with 100 ml of xylene in the presence of an antioxidant, and refluxed for 24 hours. The samples were suspended just above the level of xylene throughout the experimental period. The solvent was changed after 12 hours of extraction. After the extraction, the wrapped samples were washed with acetone, air-dried at ambient temperature for 12 hours and then dried at 80 °C in a vacuum oven for 24 hours. The gel content was determined using the following equations [14].

$$w_{extracted} = w_{(sample+mesh)i} - w_{(sample+mesh)f} \quad (3.3)$$

$$w_{polymer} = w_{sample} \times m_1 \quad (3.4)$$

$$\% \text{ Extraction} = \frac{w_{extracted}}{w_{polymer}} \times 100\% \quad (3.5)$$

$$\% \text{ Gel} = 100 - \% \text{ Extraction} \quad (3.6)$$

where $w_{extracted}$ is the weight extracted, w_{sample} is the weight of nanocomposite, $w_{(sample+mesh)i}$ and $w_{(sample+mesh)f}$ are the weight of the nanocomposite and the mesh before and after extraction and $w_{polymer}$ is the weight of polymer without clay with m_1 is the mass fraction of polymer.

3.4 References

1. W.C. Chen, S.M. Lai, R.Y. Qiu, S.X. Tang. Role of silane crosslinking on the properties of melt blended metallocene polyethylene-g-silane/clay nanocomposites at various clay contents. Journal of Applied Polymer Science 2012; 124:2669:2681.
   DOI 10.1002/app.35261
2. D. Campbell, R.A Pethrick, J.R White. Polymer Characterization: Physical techniques, 2nd Ed. Stanley Thornes Ltd, London (2000).
   ISBN 0-7487-4005-8
3. S.L. Flegler. J.W. Heckman Jr, K.L. Klomparens. Scanning and Transmission Electron Microscopy: An Introduction. W. H. Freeman and Campany, New York (1993).
   ISBN 0-7167-7047-4
4. Q.T. Nguyen, D.G. Baird. Preparation of polymer-clay nanocomposites and their properties. Advances in Polymer Technology 2006; 25:270-285.
   DOI: 10.1002/adv.20079
5. J.D. Menczel, R.B. Prime. Thermal Analysis of Polymers: Fundamentals and Applications. John Wiley & Sons Inc, New Jersey (2009).
   ISBN 978-0-471-76917-0
6. S.R. Sandler, W. Karo, J.A. Bonesteel, E.M. Pearce. Polymer Synthesis and Characterization: A Laboratory Manual. Academic Press, New York (1998).

ISBN 0-12-618240-X

7. T.H. Mokhothu, B.R. Guduri, A.S. Luyt. Kenaf fiber-reinforced copolyester biocomposites. Polymers and Composites 2011; 32:2001-2009.
DOI:10.1002/pc.21233

8. V. Causin, C. Marega, A. Marigo, P. Carresi, V.D. Guardia, S. Schiavone. A method based on thermogravimetry/differential scanning calorimetry for the forensic differentiation of latex gloves. Forensic Science International 2009; 188:57-63.
DOI: 10.1016/j.forsciint.2009.03.014

9. R.K. Goyal, A.N. Tiwari, Y.S. Negi. Role of interface on dynamic modulus of high-performance poly(etherether ketone)/ceramic composites. Journal of Applied Polymer Science 2011; 121:436-444.
DOI: 10.1002/app.33684

10. J.W. Nicholson. The Chemistry of Polymers, 3rd Ed. The Royal Society of Chemistry, Cambridge (2006).
ISBN 0-854b04-684-4.

11. U. Bhaskar, V. Passi, S. Houri, E.E. Cousin, S.H. Olsen, T. Pardoen, J.P. Raskin. On-chip tensile of nanoscale silicon free-standing beams. Journal of Materials Research 2012; 27:571-579.
DOI:10.1557/jmr.2011.340

12. B.C. Smith. Fundamentals of Fourier Transform Infrared Spectroscopy, 2nd Ed. CRC Press Taylor and Francis group, New York (2011).
ISBN 978-1-4200-6929-7

13. http://www.wcaslab.com/tech/tbftir.htm (Accessed on 30 June)

14. K. Sirisinha, D. Meksawat. Preparation and properties of metallocene ethylene copolymer crosslinked by vinyltriethoxysilane. Polymer International 2005; 54:1014-1020.
DOI: 10.1002/pi.1800

15. F.W. Fabris, F.C. Stedile, R.S. Mauler, S.M.B. Nachtigall. Free radical modification of LDPE with vinyltriethoxysilane. European Polymer Journal 2004; 40:1119-1126.
DOI:10.1016/j.eurpolymj.2004.01.008

16. Y.S. Li, P.B. Wright, R. Puritt, T. Tran. Vibration spectroscopic studies of vinyltriethoxysilane sol-gel and its coating. Spectrochimica Acta Part A 2004; 60:2759-2766.
DOI:10.1016/j.saa.2003.12.047

Chapter 4: Results and discussion

4.1 Attenuated total reflectance Fourier-transform infrared (ATR-FTIR) spectroscopy

The ATR-FTIR spectra of calcium montmorillonite (Ca^{2+}MMT) and Cloisite 15A (C15A) are shown in Figure 4.1, while Figure 4.2 and Figure 4.3 show the spectra of LDPE-g-VTES/C15A and LDPE-g-VTES/Ca^{2+}MMT nanocomposites prepared using systems A and B respectively. Some band assignments are shown in Table 4.1.

Table 4.1 Some important peaks in the FTIR spectra of LDPE, LDPE-g-VTES, the two clays and the different nanocomposites

Wavenumber / cm^{-1}	Assigned vibrations	Visible in
623	Si-O-Al	C15A
718	CH_2 rocking	All composites
774	Si-O stretching	All samples except LDPE
788	Fe^{3+}-OH-Mg	C15A, Ca^{2+}MMT
845	Al-OH-Mg deformation	C15A, Ca^{2+}MMT
917	Al-O/Al-OH stretching	C15A, Ca^{2+}MMT
1116	Si-O in-plane stretching	All samples except LDPE
794, 999-1019	Si-O stretching	All samples except LDPE
1043	Si-O-Si stretching	C15A nanocomposites
1081	Si-O-C stretching	All sample except LDPE
1377	Weak C-H stretching	All samples exceptC15A, Ca^{2+}MMT
1472	Strong C-H stretching	All samples except Ca^{2+}MMT
3402, 1633	-OH stretching, bending of water molecule	Ca^{2+}MMT
2918, 2849	C-H asymmetric, symmetric stretching	All samples exceptCa^{2+}MMT
3628	-OH stretching	All samples exceptLDPE and LDPE-g-VTES (1 phr) (system B)

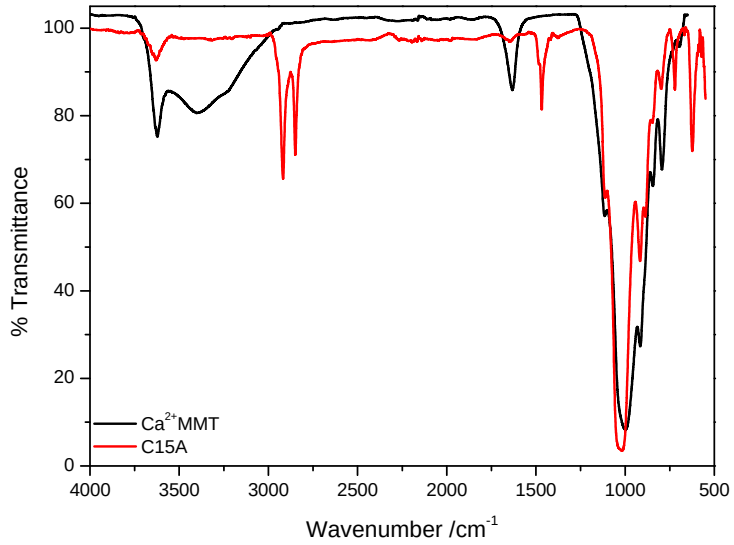

Figure 4.1 FTIR spectra of Ca^{2+}MMT and C15A

The FTIR spectra of Ca^{2+}MMT and C15A in Figure 4.1 are dominated by peaks at 3622, 1116, 999-1019, 915 and 841 cm^{-1}, that are respectively due to the O-H stretching, Si-O in-plane stretching, Si-O stretching, Al-Al-OH stretching vibrations and Al-Mg-OH deformation. The clay structure has an oxygen atom bonded to a hydrogen atom forming OH group. The two peaks observed at 3402 and 1632 cm^{-1} for Ca^{2+}MMT are respectively attributed to -OH stretching and bending of absorbed water molecules. However, after modification the two peaks disappear in C15A and this behaviour can be due to the effect of organophilic transformation of the Ca^{2+}MMT caused by the alkylammonium salt. This behaviour was also observed by Kusmono *et.al* [1]. The organic modifier can be intercalated between clay sheets through hydrogen bonds and ionic interaction generated by end functional groups of the organic modifier with oxygen on interlayer clay sheets [2]. Compared to Ca^{2+}MMT, C15A exhibits new peaks at 2917, 2849 and 1467 cm^{-1} that can be associated with the $–CH_3$, $–CH_2$ and C-H stretching, respectively. This indicates the organic groups of the modifier that are intercalated into the clay galleries [2-4].

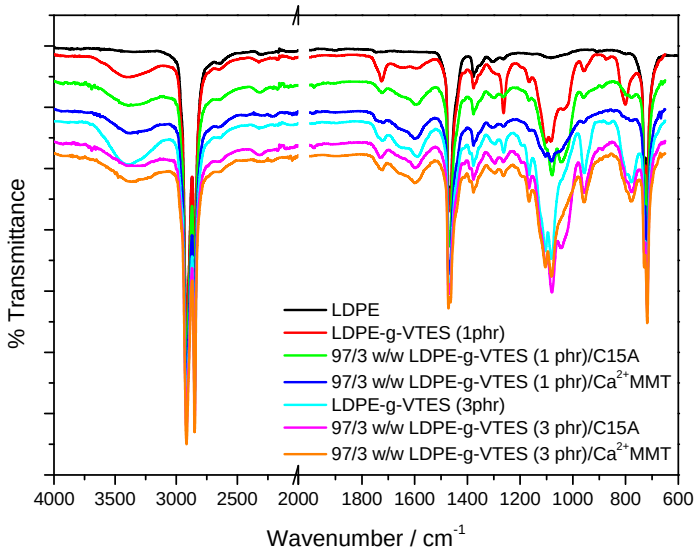

Figure 4.2 FTIR spectra of LDPE, VTES grafted LDPE (system A) and the different clay nanocomposites

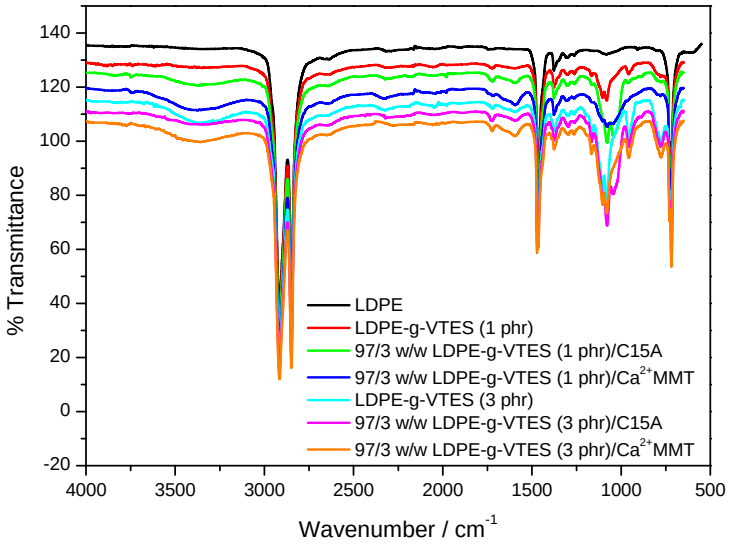

Figure 4.3 FTIR spectra of LDPE, VTES grafted LDPE (system B) and the different clay nanocomposites

The grafted LDPE shown in Figures 4.2 and 4.3 shows a broad peak at 3404 cm^{-1}. This peak is attributed to the -OH stretching of silanols formed by hydrolysis of the grafted VTES. The silanols (Si-OH) undergo a condensation reaction with the hydroxyl groups on the clay. Figure 4.4 shows the typical coupling mechanism between the clay surface and silane, which also includes the silane condensation mechanism [5]. In the presence of clay the -OH peak intensity is reduced due to the ability of the silanols to condense with the -OH group in the clay, forming stable covalent bonds in both systems. The interaction is more effective at high VTES content in both systems. The presence of the Si-O-Si peak at 1042 cm^{-1} shows that silane was successfully adsorbed on the clay surface. However, the Ca^{2+}MMT nanocomposites show a less intense Si-O-Si peak in both systems. Figure 4.3 shows a better improvement in the interaction between the clay and LDPE, hence VTES was successfully grafted onto the polymer and through hydrolysis and condensation the clay was chemically bonded with the polymer through VTES. This behaviour can improve the interaction between the polymer and clay and can also result in a good dispersion of the clay layers in the polymer matrix. Lu *et al.* [6] studied the effect of vinyltrimethoxysilane (VTMS) on the interfacial properties of LLDPE-clay nanocomposites. They observed that the LLDPE was chemically bonded with the clay surface through VTMS and this interaction enhanced the interfacial adhesion between the two dissimilar components.

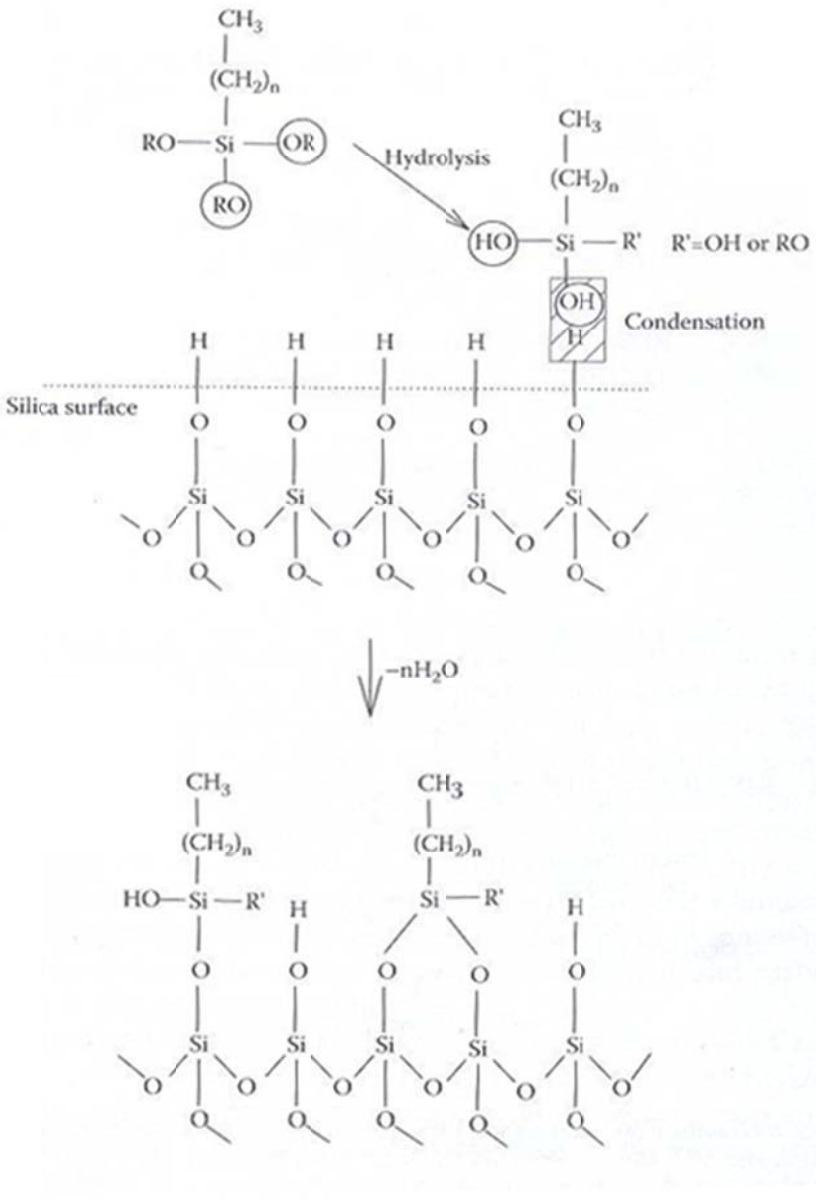

Figure 4.4 Coupling mechanism between the silica surface and silane [5]

4.2 X-ray diffraction (XRD) and transmission electron microscopy (TEM)

The degree of dispersion (intercalation and/or exfoliation) of the nanoclays in the LDPE and HDPE nanocomposites was studied using X-ray diffractometry (XRD) and transmission electron microscopy (TEM). The distance between the clay platelets in both the clay powder and nanocomposites was determined from the 2θ position of the diffraction peak of each sample using Bragg's law given in Equation 4.1.

$$n\lambda = 2d \sin \theta \qquad (4.1)$$

where n = 1 and λ = 1.5418 Å or 0.15418 nm

Clay and organoclays show a characteristic peak in XRD due to their regular layered structures. The peak is indicative of the platelet separation or d-spacing in the clay structure and the nanocomposite structure (intercalated and exfoliated) can be identified by monitoring the position, shape, and intensity of the characteristic peaks in the XRD spectra. These changes can be caused by either organic modification of the clay or penetration of the polymer chains into the clay gallery [7]. Table 4.2 summarizes the peak positions and the calculated d-spacing for the pure clays and the clays in the LDPE and HDPE nanocomposites. TEM was used to visually observe the morphology of the clay in the nanocomposites.

Figure 4.5 shows the XRD diffractograms of pure clay, organically modified clay and their untreated nanocomposites. Ca^{2+}MMT has a characteristic diffraction peak at 2θ = 5.8° with an interlayer spacing of 1.5 nm. The diffraction peak of the modified clay appears at a lower angle of 2θ = 2.6°, indicating a larger basal spacing of 3.4 nm (Table 4.2). The larger basal spacing indicates that alkylammonium chains are successfully intercalated between the clay layers. The same results were observed by Xie *et al.* [8] who investigated the influence of montmorillonite modification on the morphology of LDPE/clay nanocomposites. MMT was modified with octadecyl trimethyl ammonium (OTA) salt and dodecyl dimethylbenzyl ammonium (DDA). OTA-MMT and DDA-MMT showed a larger interlayer spacing than MMT. The increase in interlayer spacing indicated that the DDA and OTA had intercalated in

the MMT layers. OTA showed a larger gallery spacing than DDA due to its longer molecular chains. The same were observed by other authors [9,10].

Table 4.2 The basal spacings of the clays determined from the d_{001} peaks and 2θ in the XRD spectra

Sample	2θ	d_{001}/ nm
System A		
C15A	2.6	3.4
97/3 w/w LDPE/C15A	2.5	3.5
97/3 w/w LDPE-g-VTES (1 phr)/C15A	2.4	3.7
95/5 w/w LDPE-g-VTES (1 phr)/C15A	2.4	3.7
97/3 w/w LDPE-g-VTES (3 phr)/C15A	2.3	3.8
97/3 w/w HDPE-g-VTES (1 phr)/C15A	2.3	3.8
97/3 w/w HDPE-g-VTES (3 phr)/C15A	2.4	3.7
Ca^{2+}MMT	5.8	1.5
97/3 w/w LDPE/Ca^{2+}MMT	5.8	1.5
97/3 w/w LDPE-g-VTES (1 phr)/Ca^{2+}MMT	5.8	1.5
97/3 w/w LDPE-g-VTES (3 phr)/Ca^{2+}MMT	5.8	1.5
System B		
97/3 w/w LDPE-g-VTES (1 phr)/C15A	2.2	4.0
97/3 w/w LDPE-g-VTES (3 phr)/C15A	2.1	4.3
97/3 w/w LDPE-g-VTES (1 phr)/Ca^{2+}MMT	5.8	1.5
97/3 w/w LDPE-g-VTES (3 phr)/Ca^{2+}MMT	5.8	1.5

The dispersion of C15A into LDPE increased the interlayer spacing of clay and the diffraction peak slightly shifted towards lower angle. It seems as if very little intercalation and no exfoliation took place. Figure 4.6(a) confirms this observation, where the clay tactoids are clearly visible in the matrix (arrows A). The poor clay dispersion is due to the lack of interaction between the hydrophobic LDPE and the hydrophilic clay, and the clay modification did not seem to make much difference. Similar results were also observed by Xia *et al* [8]. The XRD diffractogram of the LDPE/Ca^{2+}MMT nanocomposite in Figure 4.5 shows a weak diffraction peak at the same position as that of the pure clay, which indicates the absence of intercalation or exfoliation in this case. Figure 4.6(b) also shows mostly clay

tactoids, which is in line with the XRD results (Figure 4.5, Table 4.2). In contrast to our observations, Dun *et.al* [11], in their study of the effect of Na^{+}-MMT and Ca^{2+}-MMT on the morphology of poly(ethylene-co-acrylic acid) ionomer/MMT nanocomposites, saw no diffraction peak for the nanocomposites. This indicated an exfoliated structure, which was due to the hydrophilic and polyanionic nature of PEAA which provides it with excellent miscibility with the Na^{+}-MMT and Ca^{2+}-MMT clays. The nature of the polymer seems to play a significant role in the dispersion of clay.

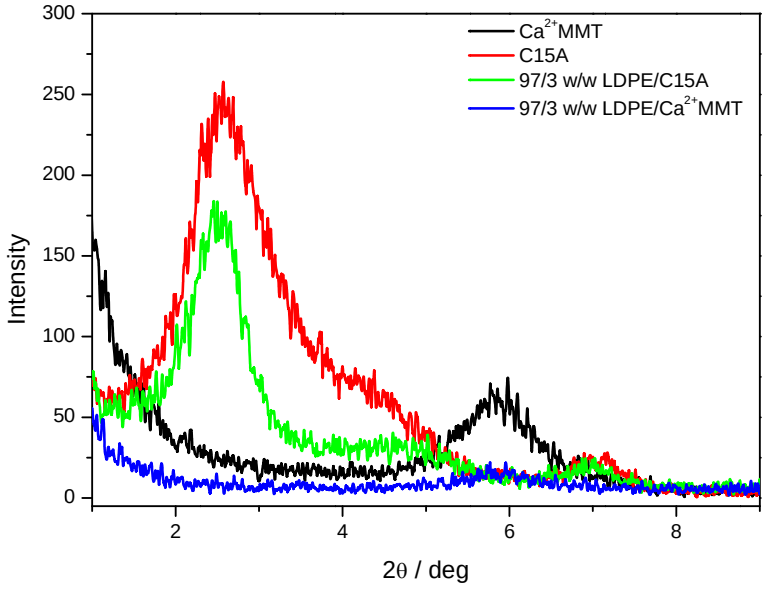

Figure 4.5 XRD diffractograms of the clays and their nanocomposites

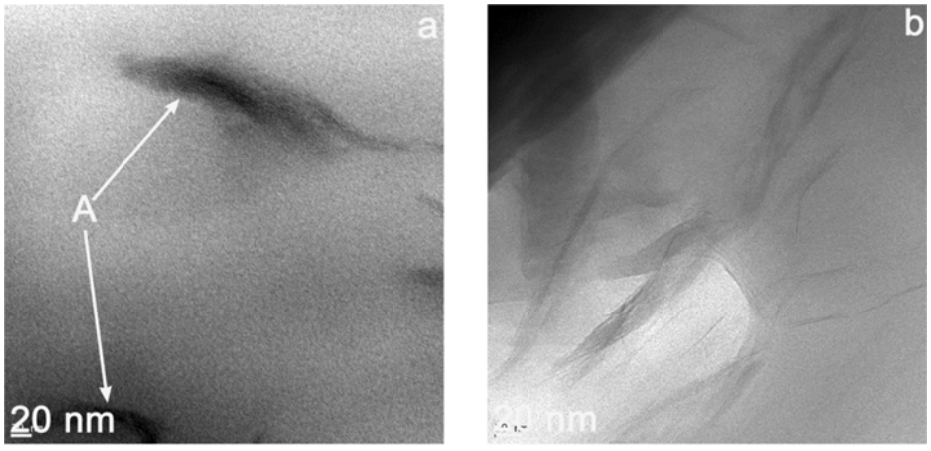

Figure 4.6 TEM images of (a) 97/3 w/w LDPE/C15A and (b) 97/3 w/w LDPE/Ca^{2+}MMT nanocomposites

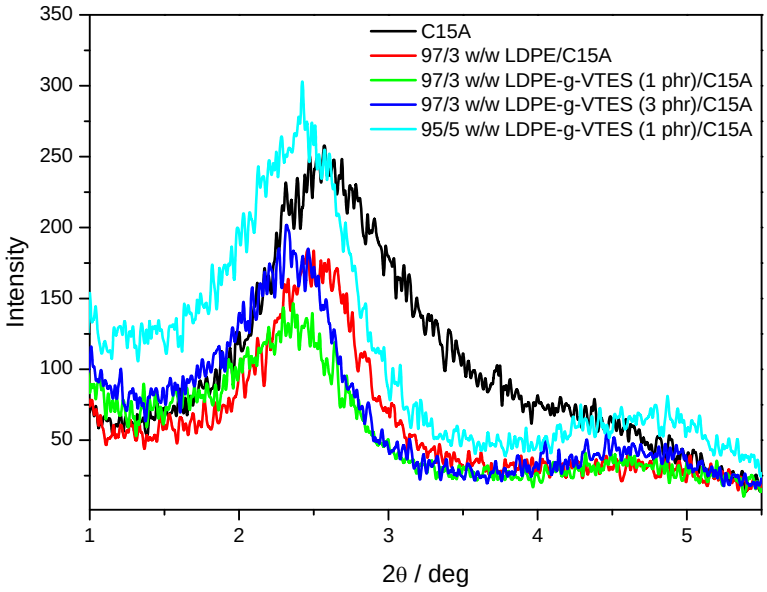

Figure 4.7 XRD diffractograms of C15A and its VTES treated LDPE nanocomposites (System A)

Figure 4.7 shows the XRD diffractograms of LDPE/C15A, treated with different VTES contents and having different clay loadings, using System A. The presence of VTES had very little influence on the interlayer spacing of the clay (Table 4.2). VTES (which in System A was not completely grafted onto the polymer) did not significantly improve the interaction between the polymer and C15A, and only a small extent of intercalation is visible in Figure 4.8(a,b). The observed intercalation may also be due to the free vinyl silane molecules (observed in FTIR) that are mobile and short enough to penetrate the clay layers. The increase in clay loading did not change the observed interlayer spacing (Figure 4.7), which was expected because of the preferred face to face stacking of clay layers at high loadings [12]. Figures 4.9 and Table 4.2 (for System B samples) show a more significant increase in interlayer spacing. This is due to more polymer chains intercalating into the clay layers. The diffraction peak also broadens and the intensity is reduced, which can be due to partially exfoliated clay layers. This is to some extent supported by the images in Figure 4.8 (c,d), which show evidence of single clay platelets. Choi *et al.* [13] studied the effect of MMT modification with silane on the morphology of epoxy nanocomposites. They observed that when silane is grafted onto the edges of the clay, the separation of the clay platelets can be

restricted (Figure 4.10). System A forms intercalated structures while system B forms partially exfoliated structures.

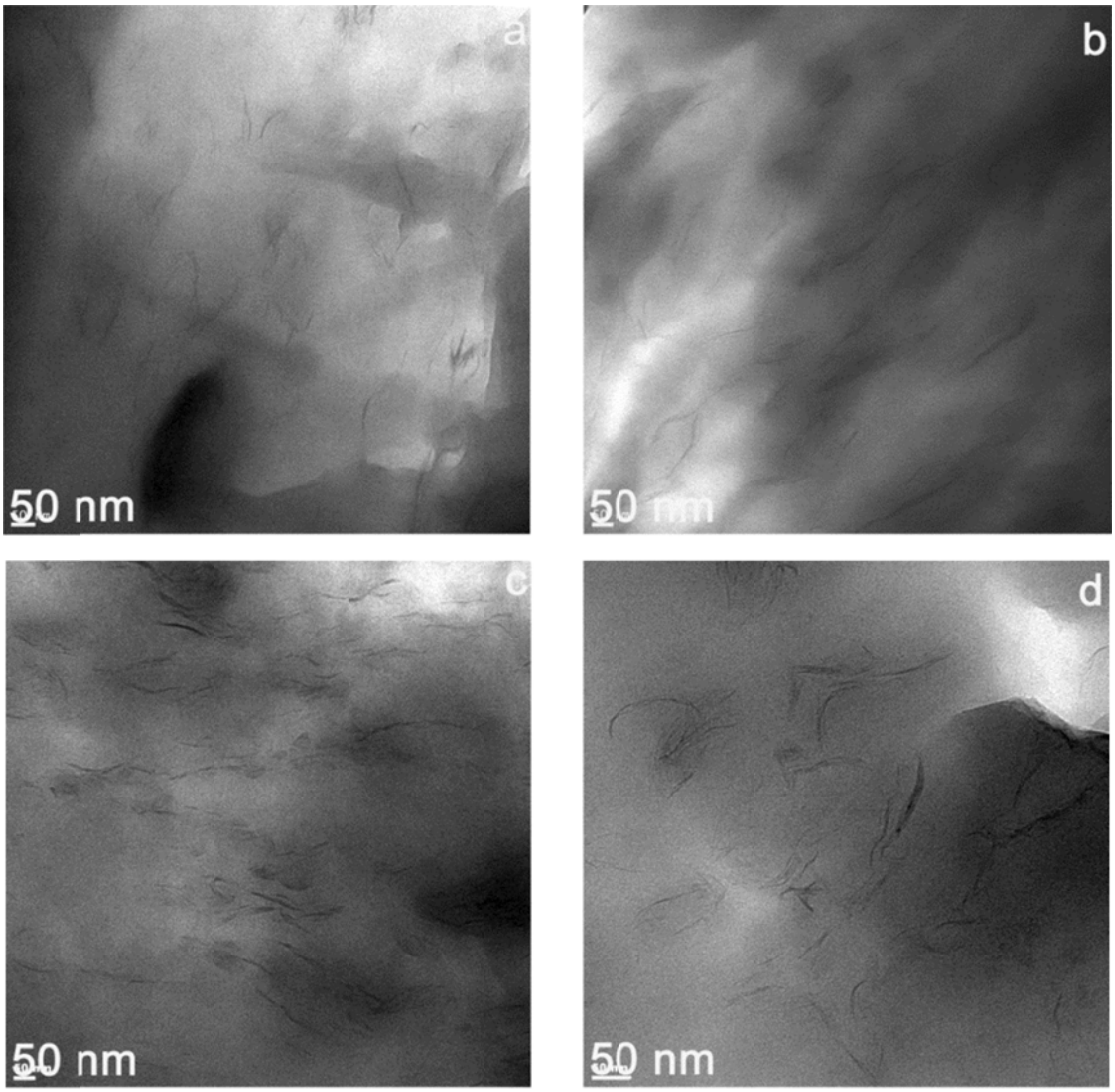

Figure 4.8 TEM micrographs of (a) 97/3 w/w LDPE-g-VTES (1 phr)/C15A and (b) 97/3 w/w LDPE-g-VTES (3 phr)/C15A (System A), (c) 97/3 w/w LDPE-g-VTES (1 phr)/C15A and (d) 97/3 w/w LDPE-g-VTES (3 phr)/C15A (System B)

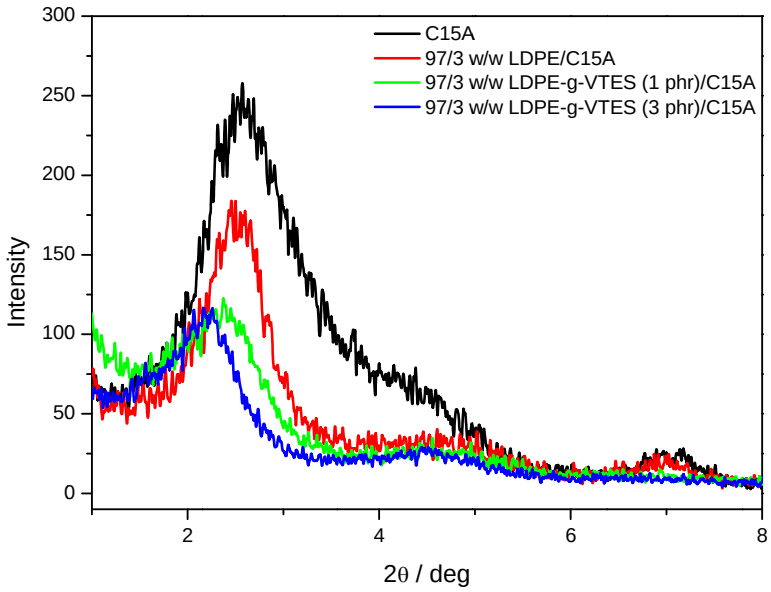

Figure 4.9 XRD diffractograms of C15A and its VTES treated LDPE nanocomposites (System B)

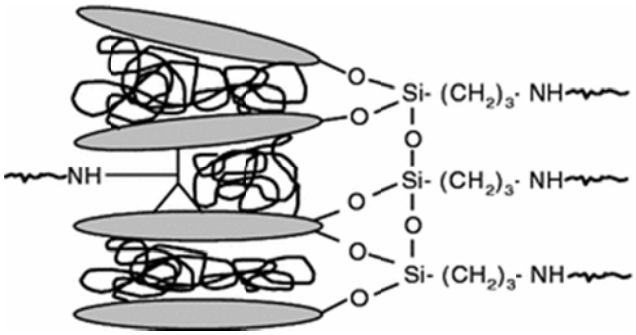

Figure 4.10 A proposed diagram of the interaction of an epoxy molecule with silane functionalized MMT [7]

Figures 4.11 to 4.13 show the TEM micrographs and X-ray diffractograms of the LDPE/Ca^{2+}MMT nanocomposites, prepared with Systems A and B, in the presence of different VTES contents. The addition of VTES does not have any influence on the position of the diffraction peak of Ca^{2+}MMT in the nanocomposites in both systems, and the TEM micrographs clearly show clay tactoids dispersed in the matrix (indicated with arrows A in

Figure 4.11a). This is probably due to the lack of interaction between the VTES and Ca^{2+}MMT (observed in FTIR).

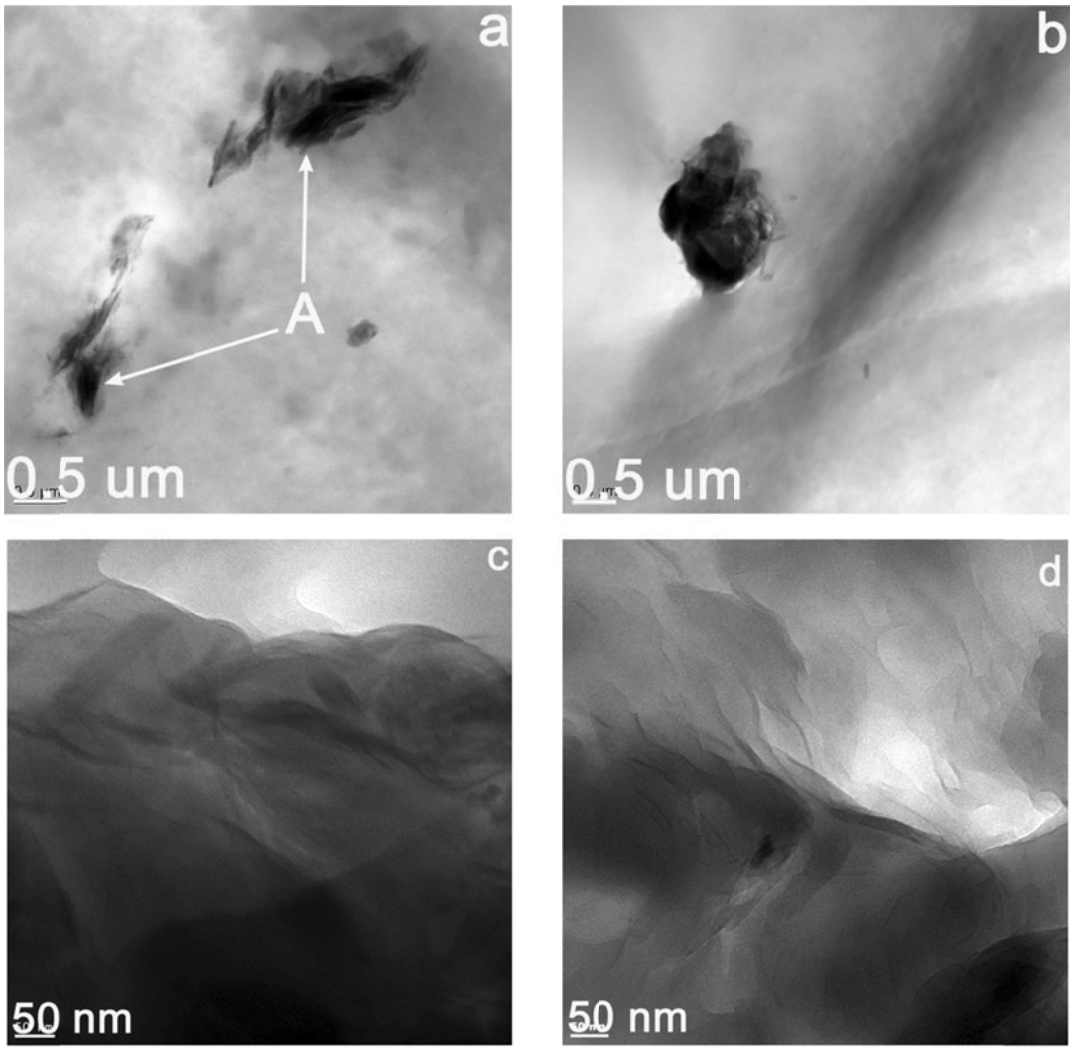

Figure 4.11 TEM micrographs of low magnification (a) 97/3 w/w LDPE-g-VTES (1 phr)/C15A and (b) 97/3 w/w LDPE-g-VTES (3 phr)/Ca^{2+}MMT (System B), 93/3 w/w LDPE-g-VTES (1 phr)/Ca^{2+}MMT (c) System A (d) System B

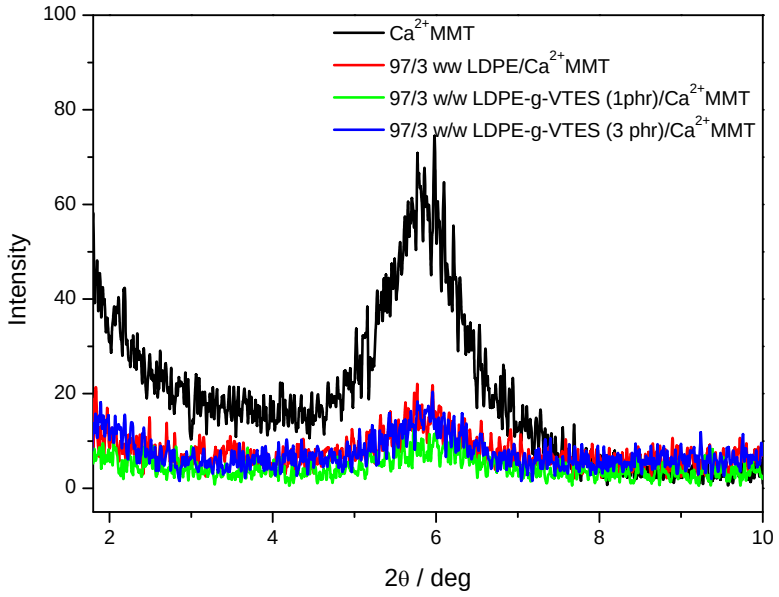

Figure 4.12 XRD diffractograms of Ca^{2+}MMT and its VTES treated LDPE nanocomposites (System A)

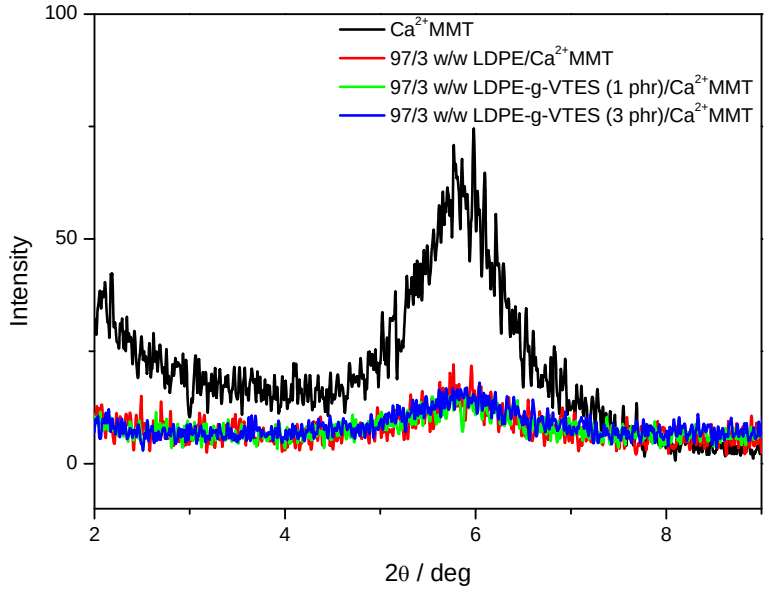

Figure 4.13 XRD diffractograms of Ca^{2+}MMT and its VTES treated LDPE nanocomposites (System B)

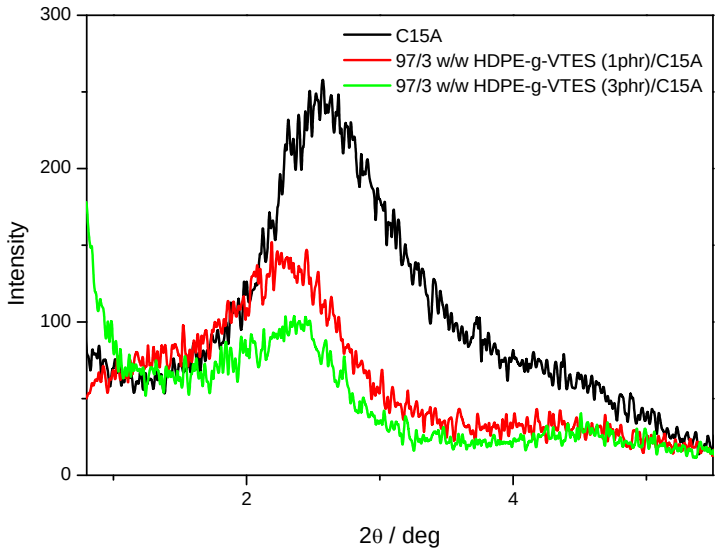

Figure 4.14 XRD diffractograms of Cloisite 15A, 97/3 HDPE-g-VTES (1 phr)/C15A and HDPE-g-VTES (3 phr)/C15A (System A)

Figure 4.14 shows the XRD diffractograms of the HDPE/clay treated nanocomposites (System A). The addition of C15A into the silane treated HDPE shifted the diffraction peak towards lower angles and the interlayer spacing increased (Table 4.2). The increase in interlayer spacing indicates that the polymer chains are intercalated in between the clay layers. Figure 4.15 shows some evidence of exfoliated clay platelets, which is an indication that this system may exhibit a mixed morphology. There is no difference in the d-spacing of LDPE-g-VTES/C15A and HDPE-g-VTES/C15A nanocomposites prepared with system A.

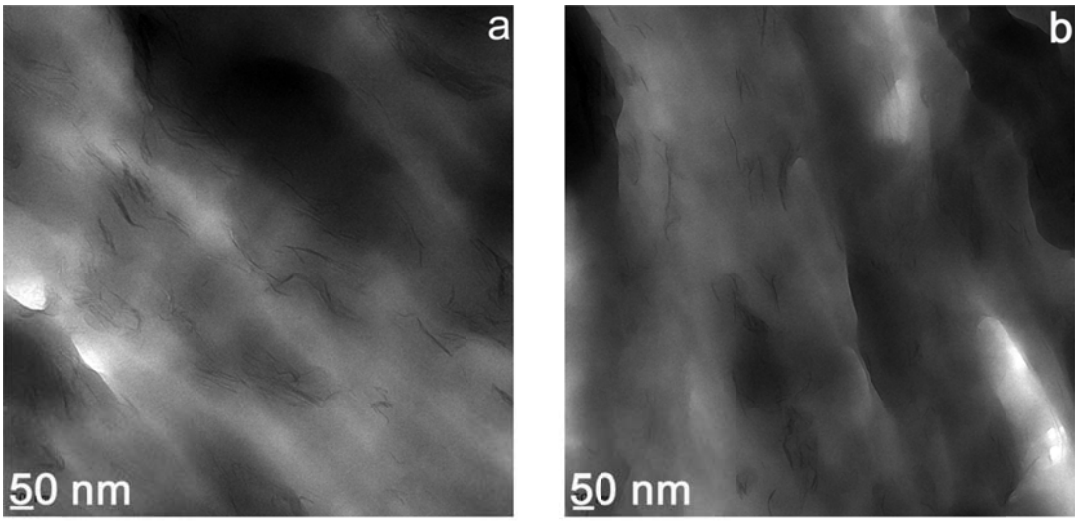

Figure 4.15 TEM micrographs of (a) HDPE-g-VTES (1 phr)/C15A (b) HDPE-g-VTES (3 phr)/C15A nanocomposites

4.3 Thermogravimetric analysis

The TGA curves of all the samples are shown in Figures 4.16 to 4.24. All the derivative curves are presented in the Appendix. The thermal stability of the samples were characterized in terms of the onset temperature of degradation and the maximum degradation temperature determined from the derivative curves. A summary of the TGA results is presented in Tables 4.3 and 4.4.

The TGA curves of Ca^{2+}MMT and C15A are shown in Figure 4.16. Below 100 ^{o}C, Ca^{2+}MMT shows an approximately 10% mass loss which is not visible in the C15A curve. This is probably the result of the removal of water. Cloisite 15A shows a mass loss of almost 40% at temperature range 200 – 400 °C. This is attributed to the decomposition of the intercalated ammonium salts by a Hofmann elimination reaction [1,14]. The non-volatile fraction for the modified clay at 600 °C is 63 %, which indicates the inorganic content.

Table 4.3 Summary of the TGA results for the LDPE, LDPE-g-VTES and the different nanocomposites (System A and System B)

Sample	T_{onset} / ^{o}C	T_{max} / ^{o}C
LDPE	444.3	474.6
LDPE/C15A (w/w)		
99/1	446.7	479.4
97/3	448.0	483.4
95/5	450.1	485.4
LDPE/Ca^{2+}MMT (w/w)		
99/1	445.2	475.4
97/3	442.3	480.4
95/5	444.2	480.7
System A		
LDPE-g-VTES (1 phr)	450.3	475.5
LDPE-g-VTES (1 phr)/C15A (w/w)		
99/1	455.7	483.4
97/3	456.1	483.4
95/5	457.2	473.4
97/3 (w/w) LDPE-g-VTES (1 phr)/Ca^{2+}MMT	449.5	475.3
LDPE-g-VTES (3 phr)	441.2	465.4
LDPE-g-VTES (3 phr)/C15A (w/w)		
99/1	449.9	478.4
97/3	451.8	478.4
95/5	460.3	478.4
97/3 (w/w) LDPE-g-VTES (3 phr)/Ca^{2+}MMT	447.6	469.1
System B		
LDPE-g-VTES (1 phr)	450.7	456.1
97/3 w/w LDPE-g-VTES (1 phr)/C15A	457.3	481.5
97/3 w/w LDPE-g-VTES (1 phr)/Ca^{2+}MMT	447.4	472.6
LDPE-g-VTES (3 phr)	443.0	463.7
97/3 w/w LDPE-g-VTES (3 phr)/C15A	455.4	480.0
97/3 w/w LDPE-g-VTES (3 phr)/Ca^{2+}MMT	449.5	468.7

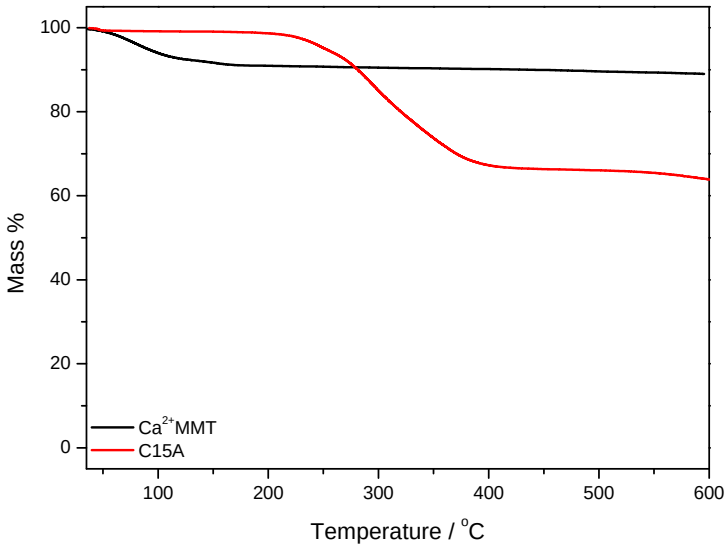

Figure 4.16 TGA curves of Ca^{2+}MMT and Cloisite 15A

Figures 4.17 and 4.18 show the TGA curves of the LDPE/C15A and LDPE/Ca^{2+}MMT nanocomposites. Thermal degradation of polymers is simply the molecular deterioration as a result of overheating. At high temperatures, the long chain backbone of the polymer begins to break up (molecular scission) and form free radicals. The free radicals react with each other and with other polymer chains and release volatile products causing a mass loss of the LDPE starting around 400 °C (Table 4.3) [15]. Figure 4.17 shows that all the nanocomposites are more thermally stable than the neat LDPE. The onset temperature of decomposition shifts towards higher temperatures as the clay loading increases. This is because the presence of the clay either immobilizes the polymer chains and free radicals formed during the degradation process, thus slowing down this process, or hinders the diffusion of volatile products through the nanocomposites, thus retarding the mass loss from the nanocomposites during degradation [16]. The increase in thermal stability can also be attributed to the restricted thermal motions of polymer chains inside the clay galleries [17]. The correlation between the % residue observed in Figure 4.17 and the amounts of clay initially mixed into the samples is not too good, which is an indication of a lack of homogeneity in the nanocomposites. Figure 4.18 shows that Ca^{2+}MMT had very little effect on the thermal stability of LDPE. This is probably due to the lack of interaction between LDPE and Ca^{2+}MMT. The same behaviour was observed by Dun *et al.* [11].

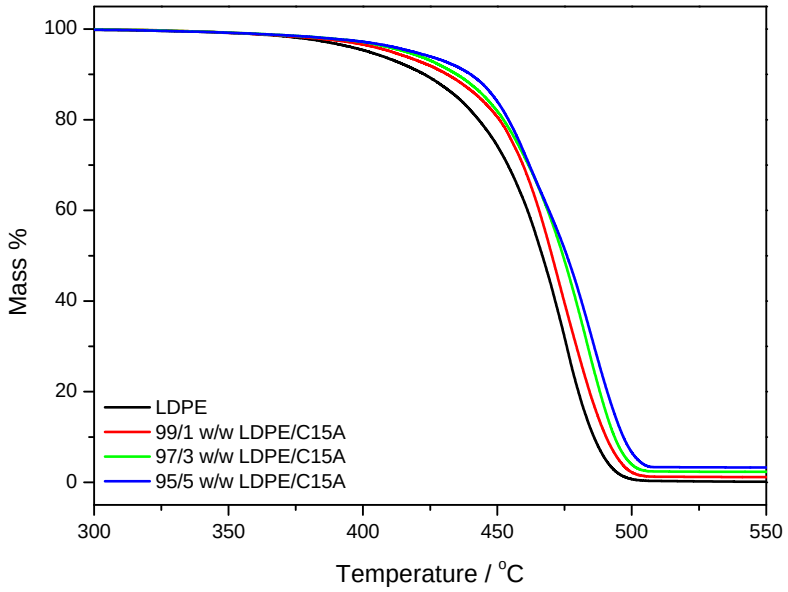

Figure 4.17 TGA curves of LDPE and the LDPE/C15A nanocomposites

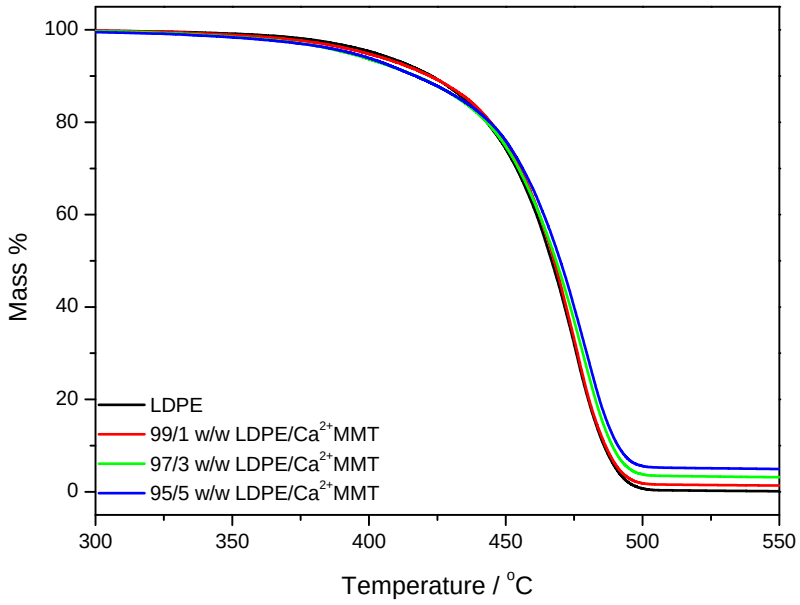

Figure 4.18 TGA curves of LDPE and the LDPE/Ca^{2+}MMT nanocomposites

The TGA curves of LDPE, VTES grafted LDPE, and the LDPE-g-VTES/C15A nanocomposites with different VTES content are shown in Figures 4.19 and 4.20. LDPE (Figure 4.19, Table 4.3) shows a significant increase in thermal stability with VTES treatment. This behaviour can be attributed to the crosslinking reaction due to the silane grafts. The thermal stability of treated LDPE also increases with the addition of clay, for the same reasons discussed in the previous paragraph. The presence of clay in polymers can have two effects: (i) it can catalyse the degradation of a polymer and decreases its thermal stability, or (ii) it can act as a barrier and increase the thermal stability [18,19]. At the highest clay loading the rate of degradation was higher than those of the other samples. Zhao *et al.* [18] observed that at low loading the clay layers were well dispersed in the polymer matrix and the barrier effect was dominant, but with increasing clay loading the catalysing effect was more dominant and decreased the thermal stability of the nanocomposites. This explanation fits our own observation. Figure 4.20 shows a decrease in thermal stability of LDPE when treated with a higher VTES content. This behaviour can be due to ungrafted VTES which forms free radicals at high temperatures and attack the polymer chains, initiating chain scission. This is possible, because Onischuk *et al.* [20] observed the formation of silyl radicals during silane decomposition. However, the addition of clay and increase in clay loading increased the thermal stability of LDPE. The reasons for this have already been discussed.

System B (Figures 4.21 and 4.22, Table 4.3) shows that the treated LDPE and nanocomposites have better thermal stabilities than the pure LDPE. However, the LDPE-g-VTES/Ca^{2+}MMT nanocomposites have worse thermal stabilities than the LDPE-g-VTES/C15A nanocomposites at the same clay loading. This behaviour is due to the poor interaction between the grafted LDPE and Ca^{2+}MMT. The thermal stabilities of the System B samples, with their partially exfoliated structures, did not differ much from those of System A with their intercalated structures. Nese *et al.* [21] observed that exfoliated PMMA nanocomposites had better thermal stability than the intercalated nanocomposites. This behaviour was attributed to the stronger interaction between the clay and polymer in the exfoliated samples. However, contradictory results were reported by Rezanavaz *et al.* [22], who observed that the intercalated LDPE nanocomposites had better thermal stabilities than the exfoliated and partially exfoliated nanocomposites.

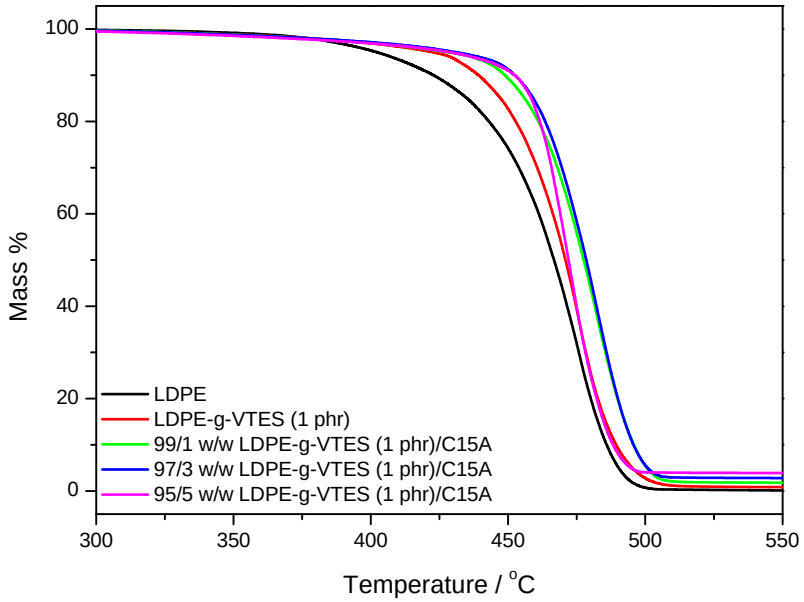

Figure 4.19 TGA curves of LDPE, VTES grafted LDPE (1 phr, System A) and the different nanocomposites

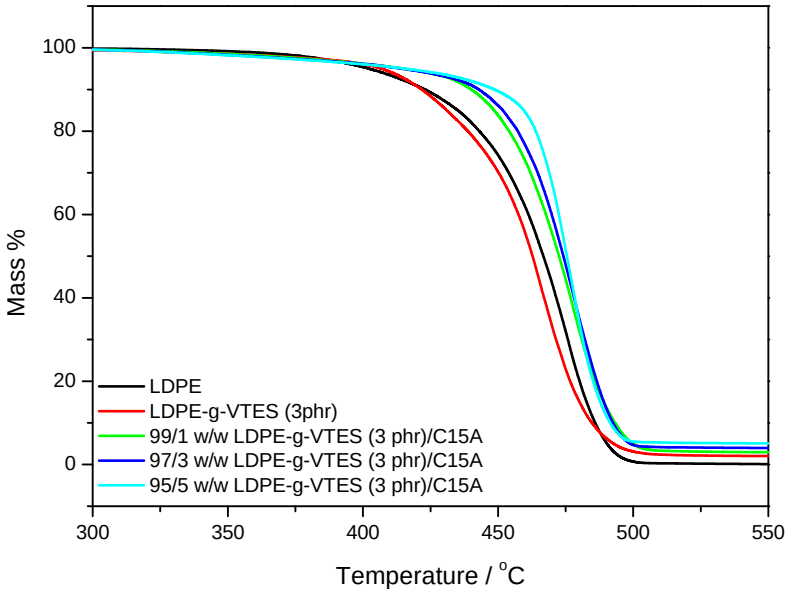

Figure 4.20 TGA curves of LDPE, VTES grafted LDPE (3 phr, System A) and the different nanocomposites

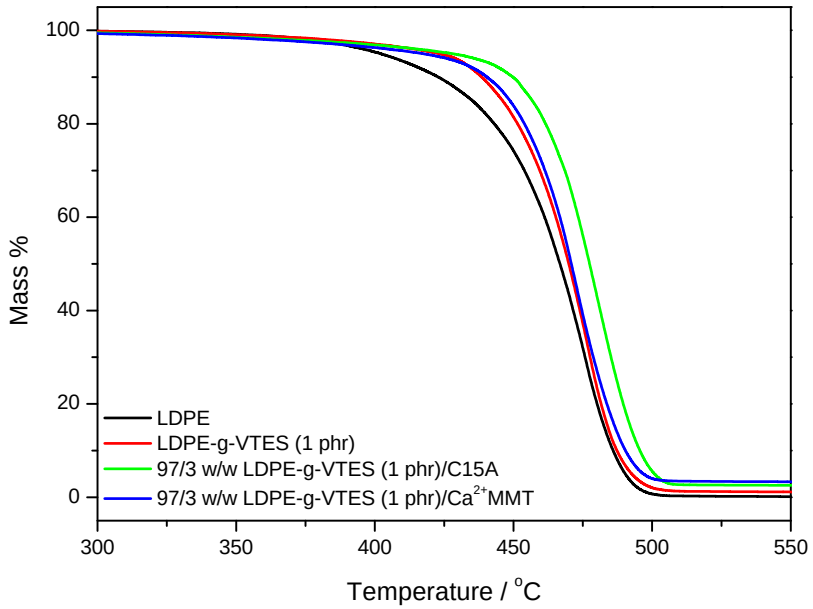

Figure 4.21 TGA curves of LDPE, VTES grafted LDPE (1 phr, System B) and the different nanocomposites

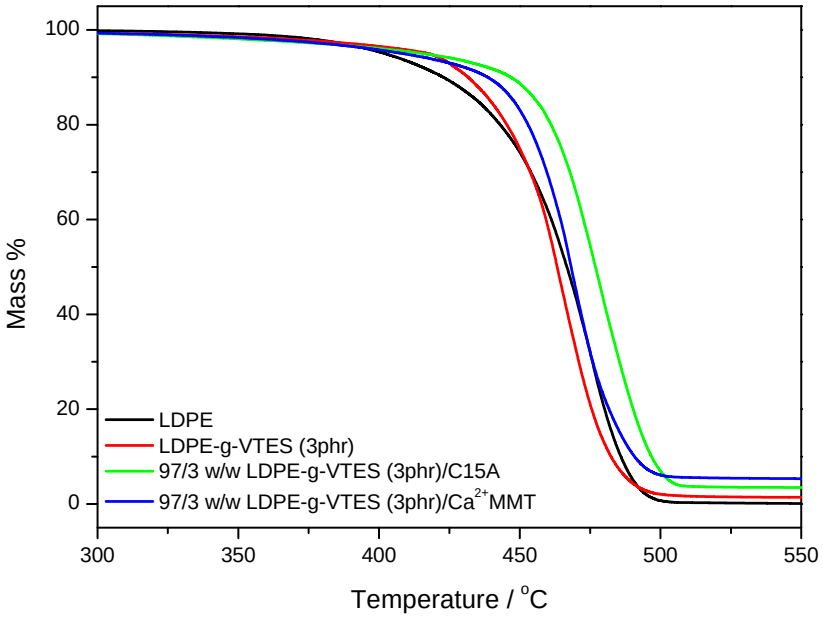

Figure 4.22 TGA curves of LDPE, VTES grafted LDPE (3 phr, System B) and the different nanocomposites

Table 4.4 Summary of the TGA results for the HDPE, HDPE-g-VTES and the different nanocomposites (Systems A)

Sample	T_{onset} / ^{o}C	T_{max} / ^{o}C
System A		
HDPE	445.8	478.6
HDPE/C15A (w/w)		
97/3	450.4	487.9
95/5	450.8	485.6
HDPE-g-VTES (1 phr)	452.4	474.3
HDPE-g-VTES (1 phr)/C15A (w/w)		
99/1	454.5	484.7
97/3	457.9	456.2
95/5	458.2	478.2
HDPE-g-VTES (3 phr)	450.6	471.6
HDPE-g-VTES (3 phr)/C15A (w/w)		
99/1	452.7	479.3
97/3	451.9	489.9

The TGA curves of HDPE, VTES grafted HDPE, and HDPE-g-VTES/C15A nanocomposites with different VTES content are shown in Figures 4.23 and 4.24. These figures show a mass loss of the VTES treated samples in the temperature range 200-400 °C. This can be due to the side-group elimination of VTES that was grafted onto the backbone of HDPE. The thermal stability of HDPE increased with increasing clay content at low VTES content, but it was lower at high VTES content (Table 4.4). This behaviour has been explained earlier in this section. The addition of clay in the treated HDPE results in a mass loss of the nanocomposites in the temperature range 200-418 °C. This mass loss may have been due to the degradation of the organic modifier in the clay combined with side-group elimination of the VTES [1,18,19]. Olad *et al.* [23] studied the thermal stability of polystyrene/Cloisite 30B nanocomposites. They attributed the mass loss around 220-312 °C to the decomposition of the modifying agent of Cloisite 30B. In our case the thermal stability of the nanocomposites increased at temperatures above 420 °C, and the explanation for this should be the same as that given for the LDPE degradation. The thermal stability of modified HDPE increased with an increase in clay loading (Table 4.4), which is probably due to the improved interaction

between HDPE and clay after VTES treatment. The well dispersed silicate layers in HDPE seem to be effective in immobilizing the free radicals formed during the initial stages of the degradation, and in hindering the diffusion of volatile decomposition products. There is very little difference between the thermal stabilities of the comparable nanocomposites of LDPE and HDPE.

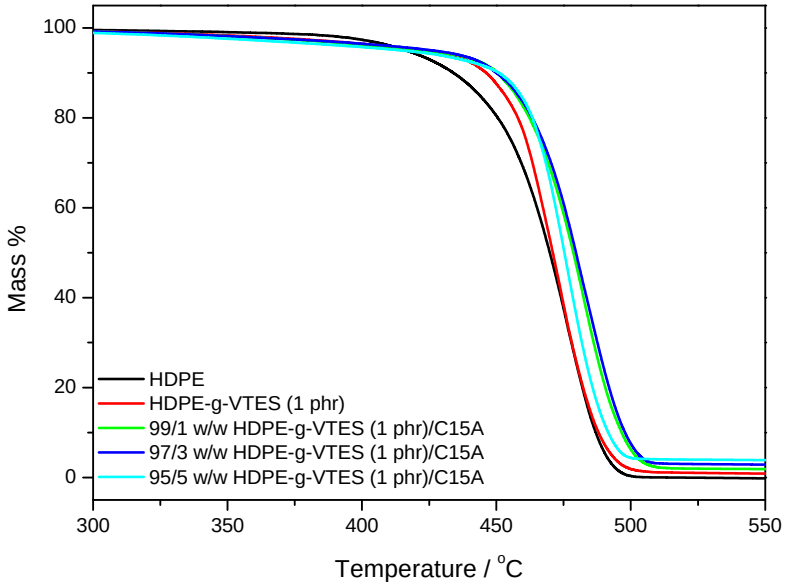

Figure 4.23 TGA curves of HDPE, VTES grafted HDPE (1 phr, System A) and the different nanocomposites

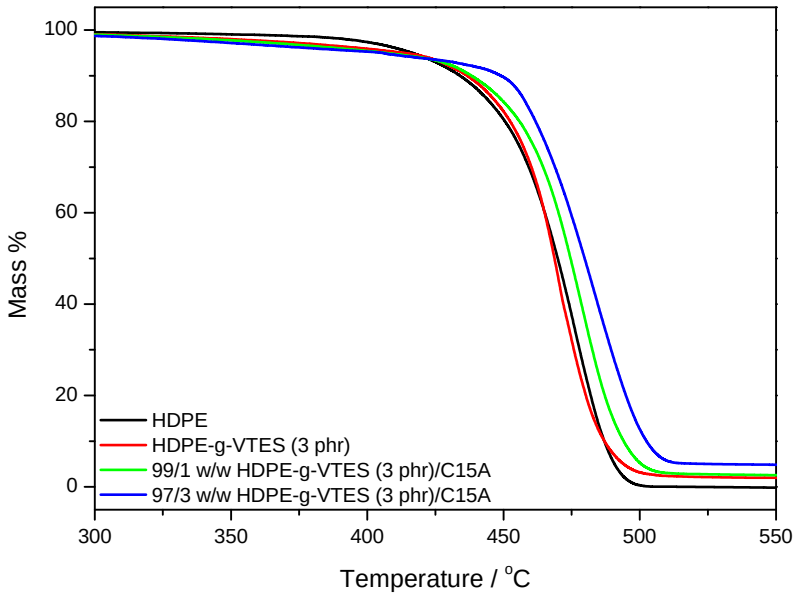

Figure 4.24 TGA curves of HDPE, VTES grafted HDPE (3 phr, System A) and the different nanocomposites

4.4 Gel content

Gel content is an important parameter indicating the extent of crosslinking in polyethylene, because many properties of the material will be affected by the extent of crosslinking. Figures 4.25 and 4.26 show the variation in gel content with different clay loadings in VTES treated LDPE and HDPE nanocomposites prepared with System A. The silane and peroxide concentrations can have a significant influence on the gel content. A few authors found that, besides external parameters such as processing conditions and grafting additives, there are number of factors that influence the receptiveness of polyethylene to grafting and crosslinking. These factors include the molecular weight, the presence of vinyl groups, as well as the branch content and branch length [24-27]. The gel contents of the different polyethylene samples differ considerably. The silane treated LDPE and HDPE in the absence of clay show high gel content values, indicating the presence of crosslinking. Generally the gel content increases with an increase in VTES content in both polyethylenes (Table 4.5). The grafting reaction can be accompanied by side reactions such as direct crosslinking of macroradicals and chain scissions. In this case the most probable side reaction is crosslinking.

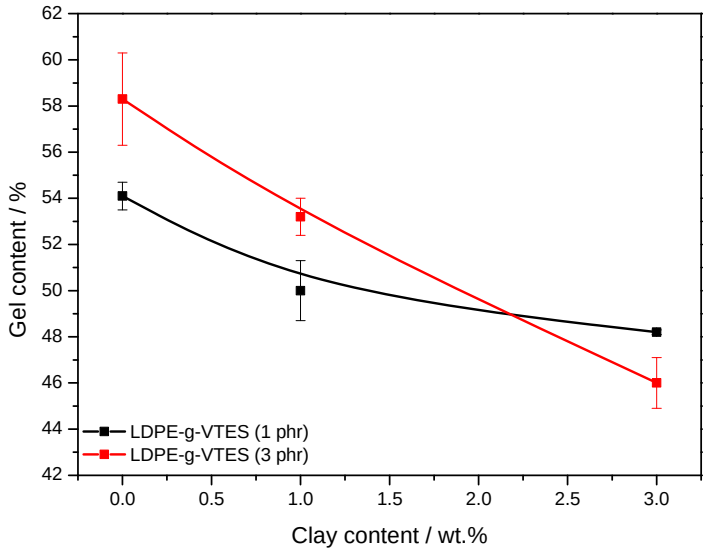

Figure 4.25 Gel content of VTES treated LDPE/C15A and its different nanocomposites (System A)

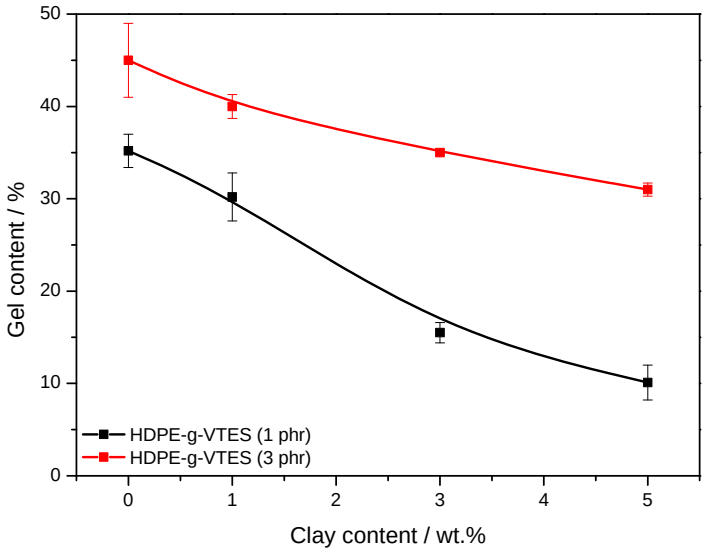

7

Figure 4.26 Gel content of VTES treated HDPE/C15A and its different nanocomposites (System A)

Table 4.5 Gel content of all the samples

Sample	Gel content / %
System A	
LDPE	
LDPE-g-VTES (1 phr)	54.1 ± 0.6
99/1 w/w LDPE-g-VTES (1 phr)/C15A	50.0 ± 1.3
97/3 w/w LDPE-g-VTES (1 phr)/C15A	48.2 ± 0.1
97/3 w/w LDPE-g-VTES (1 phr)/Ca^{2+}MMT	40.0 ± 0.3
LDPE-g-VTES (3 phr)	58.3 ± 2.0
99/1 w/w LDPE-g-VTES (3 phr)/C15A	53.2 ± 0.8
97/3 w/w LDPE-g-VTES (3 phr)/C15A	46.0 ± 1.1
97/3 w/w LDPE-g-VTES (3 phr)/ Ca^{2+}MMT	31.1 ± 3.4
HDPE	
HDPE-g-VTES (1 phr)	35.2 ± 1.8
99/1 w/w HDPE-g-VTES (1 phr)/C15A	30.2 ± 2.6
97/3 w/w HDPE-g-VTES (1 phr)/C15A	15.5 ± 1.1
95/5 w/w HDPE-g-VTES (1 phr)/C15A	10.1 ± 1.9
HDPE-g-VTES (3 phr)	45.0 ± 4.0
99/1 w/w HDPE-g-VTES (3 phr)/C15A	40.0 ± 1.3
97/3 w/w HDPE-g-VTES (3 phr)/C15A	35.0 ± 0.3
95/5 w/w HDPE-g-VTES (3 phr)/C15A	31.0 ± 0.7
System B	
LDPE-g-VTES (1 phr)	67.0 ± 0.5
97/3 w/w LDPE-g-VTES (1 phr)/C15A	54.0 ± 2.3
97/3 w/w LDPE-g-VTES (1 phr)/Ca^{2+}MMT	64.0 ± 0.7
LDPE-g-VTES (3 phr)	70.0 ± 0.9
97/3 w/w LDPE-g-VTES (3 phr)/C15A	67.0 ± 0.7
97/3 w/w LDPE-g-VTES (3 phr)/Ca^{2+}MMT	66.1 ± 0.5

Generally the addition of clay reduced the gel content in both polymers. The decrease in the gel content for the clay nanocomposites might have been due to the interaction of grafted silane with clay, which probably inhibited the crosslinking efficiency of the silane. System B shows the same trend as system A with the increase in VTES content and the addition of clay,

but the addition of clay does not have much influence on the gel content. It seems as if the higher DCP content causes more crosslinking (direct and through silane links), maybe in addition to silane grafting. The grafted silane groups will still interact with the clay, but it will have no influence on the already crosslinked polymer. When comparing the samples prepared with System A and System B at the same VTES content, System B samples show significantly higher gel contents (Table 4.5). This behaviour is probably due to the higher DCP contents which resulted in more free radicals that favoured direct crosslinking reactions.

4.5 Differential scanning calorimetry

The DSC results for the LDPE/clay and HDPE/clay nanocomposites are summarized in Figures 4.27 to 4.40. The peak temperatures of melting and crystallization together with the melting and crystallization enthalpies of all the samples are shown in Tables 4.6 to 4.10. All the reported DSC heating results were obtained from the second scan to eliminate the effect of thermal history. The normalized melting enthalpy (ΔH_m^{norm}) of all the samples was determined using Equation 4.2.

$$\Delta H_m^{norm} = \frac{Measured\ \Delta H}{Mass\ fraction\ of\ polymer} \qquad (4.2)$$

The DSC curves of pure LDPE, as well as the LDPE/C15A and LDPE/Ca^{2+}MMT nanocomposites, are shown in Figure 4.27. One endotherm is observed for the pure LDPE and the nanocomposites. Figure 4.27 shows a slight decrease in the melting peak temperature of LDPE after the addition of C15A and Ca^{2+}MMT. The clay might have influenced the crystal packing structure of LDPE, changing the crystallite size and/or lamellar thickness. The increase in clay content and the nature of clay had no effect on the melting temperature. D'Amico *et al*. [28] explained this behaviour as being the result of the clay predominately confined to the amorphous phase, without significantly affecting the development of crystals in the polymer matrix. They observed decreasing melting enthalpies with increasing clay content. This behaviour was related to a decrease in the quality of the LDPE matrix. The addition of clay had no significant influence on the melting enthalpy of LDPE. Figure 4.28 shows the DSC cooling curves of pure LDPE, and the LDPE/C15A and LDPE/Ca^{2+}MMT nanocomposites. The crystallization peak temperature of LDPE was not significantly affected by the addition of C15A and Ca^{2+}MMT (Table 4.8). This is probably because of the fairly

weak interaction between LDPE and the two clays in the absence of a compatibilizer. This lack in interaction was observed and discussed in Section 4.2. The nature of the clay also did not influence the crystallization peak temperature of LDPE.

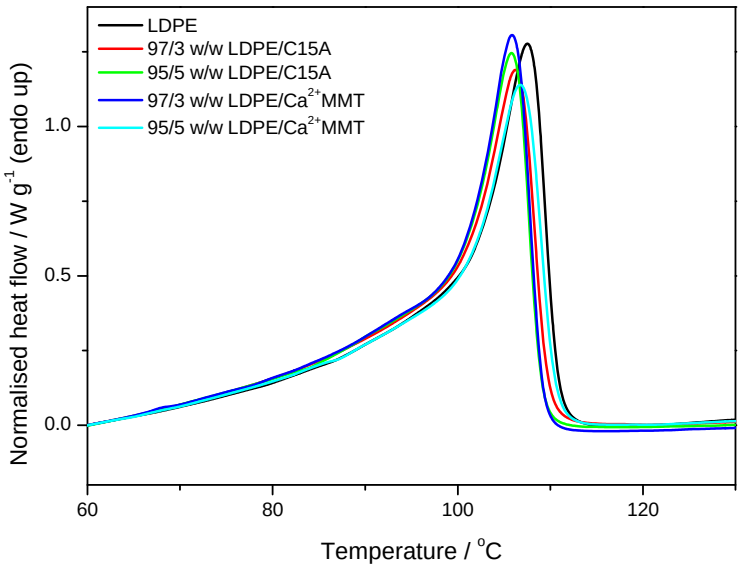

Figure 4.27 DSC heating curves of LDPE and its clay nanocomposites

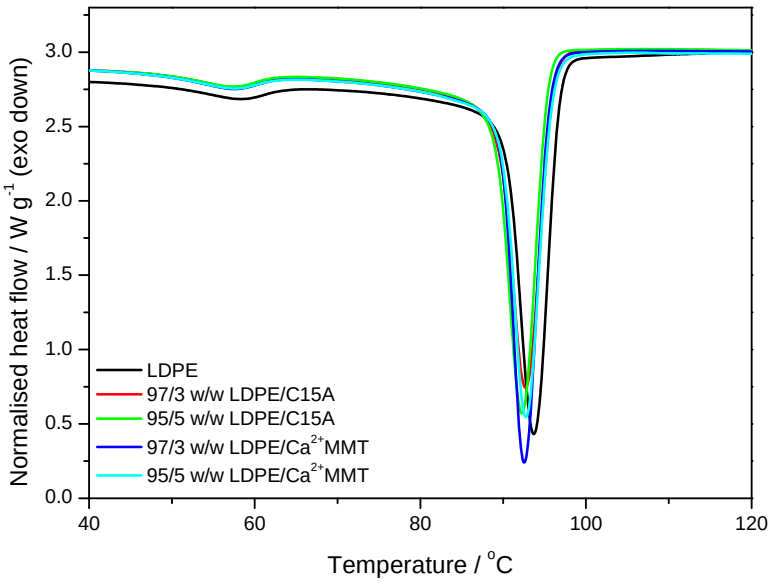

Figure 4.28 DSC cooling curves of LDPE and its clay nanocomposites

Table 4.6 Summary of the DSC heating results for all the investigated LDPE-based samples

Composition	$T_{p,m}$ / °C	ΔH_m^{obs} / J g^{-1}	ΔH_m^{norm} / J g^{-1}
LDPE	107.7 ± 0.4	81.9 ± 0.5	81.9
LDPE/C15A (w/w)			
97/3	105.9 ± 0.4	79.1 ± 0.8	81.5
95/5	105.8 ± 0.2	79.3 ± 1.8	83.4
LDPE/Ca^{2+}MMT (w/w)			
97/3	105.8 ± 0.3	81.8 ± 0.8	84.3
95/5	106.0 ± 0.7	78.0 ± 1.1	82.1
System A			
LDPE-g-VTES (1phr)	104.9 ± 0.5	74.7 ± 5.8	74.7
LDPE-g-VTES (1 phr)/C15A (w/w)			
99/1	104.5 ± 0.5	73.0 ± 1.6	74.0
97/3	104.1 ± 0.3	71.5 ± 0.9	73.7
95/5	103.9 ± 0.6	69.1 ± 0.8	72.7
97/3 w/w LDPE-g-VTES (1 phr)/ Ca^{2+}MMT	104.1 ± 0.4	72.7 ± 3.4	74.9
LDPE-g-VTES (3 phr)	103.4 ± 0.4	67.0 ± 0.4	67.0
LDPE-g-VTES (3 phr)/C15A (w/w)			
99/1	103.3 ± 0.9	67.8 ± 1.8	68.5
97/3	105.2 ± 0.2	68.6 ± 1.1	70.7
95/5	104.0 ± 0.2	63.1 ± 0.3	66.4
97/3 w/w LDPE-g-VTES (3 phr)/ Ca^{2+}MMT	103.8 ± 0.4	69.1 ± 1.9	71.2

$T_{p,m}$, ΔH_m^{obs}, and ΔH_n^{norm} are respectively the peak temperature of melting, observed melting enthalpy, and the normalised melting enthalpy

Figure 4.29 shows the DSC curves of LDPE and LDPE treated with different contents of VTES, and the melting temperatures and enthalpies are summarized in Table 4.6. The melting temperature and enthalpy of LDPE decreased when treated with VTES and with an increase in VTES content. Treatment of LDPE with VTES and DCP obviously gave rise to crosslinking in addition to VTES grafting onto the polymer chains. This crosslinking is clear

from the already discussed gel content results. The decrease in melting temperature shows that the VTES/DCP initiated crosslinking did not only reduce the total crystallinity, but also the crystallite size and/or lamellar thickness. Figure 4.30 shows that the presence of different amounts of C15A had very little influence on the melting temperature and enthalpy of the 1 phr VTES treated LDPE. It is clear that the effect of crosslinking on the polymer crystallization is much more significant than that of the presence of C15A clay. The nature of the clay also has very little influence on the thermal behaviour of the VTES treated LDPE (Table 4.6). Figure 4.31 and Table 4.6 show no significant change in the melting temperature and melting enthalpy of VTES treated LDPE with increasing clay loading, and there is no real trend.

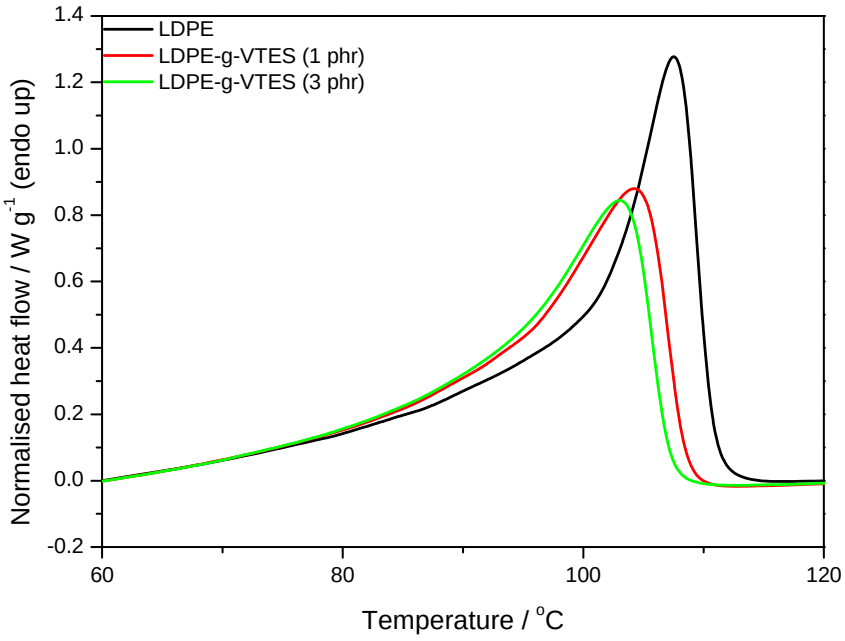

Figure 4.29 DSC heating curves of LDPE and LDPE treated different VTES contents (System A)

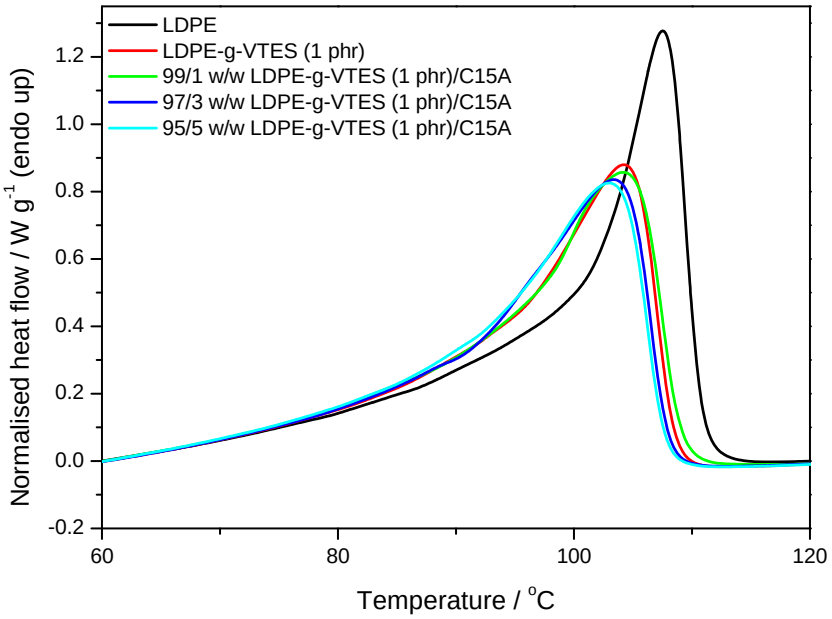

Figure 4.30 DSC heating curves of LDPE, VTES (1 phr) treated LDPE and the different nanocomposites (System A)

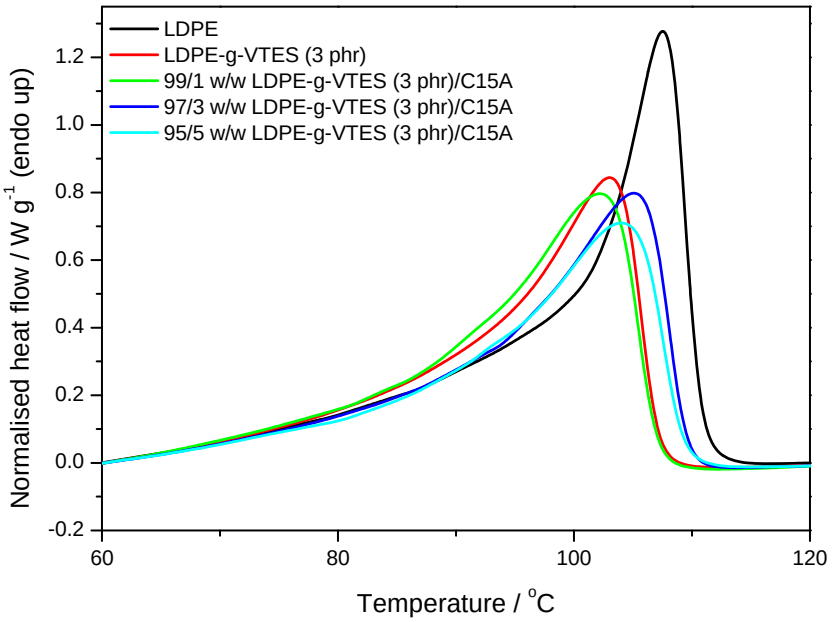

Figure 4.31 DSC heating curves of LDPE, VTES (3 phr) treated LDPE and the different nanocomposites (System A)

Table 4.7 Summary of the DSC heating results for all the investigated LDPE-based samples (System B)

Composition	$T_{p,m}$ / °C	ΔH_m^{obs} / J g^{-1}	ΔH_m^{norm} / J g^{-1}
LDPE	107.7 ± 0.4	81.9 ± 0.5	81.9
LDPE-g-VTES (1 phr)	105.2 ± 0.6	71.5 ± 1.0	71.5
97/3 w/w LDPE-g-VTES (1 phr)/C15A	104.1 ± 0.1	70.1 ± 1.9	72.3
97/3 w/w LDPE-g-VTES (1 phr)/Ca^{2+}MMT	104.2 ± 0.7	67.4 ± 1.2	69.5
LDPE-g-VTES (3 phr)	103.6 ± 0.5	62.8 ± 2.5	64.7
97/3 w/w LDPE-g-VTES (3 phr)/C15A	103.1 ± 0.6	62.6 ± 0.7	64.5
97/3 w/w LDPE-g-VTES (3 phr)/Ca^{2+}MMT	103.8 ± 0.5	63.7 ± 0.1	65.7

$T_{p,m}$, ΔH_m^{obs}, and ΔH_n^{norm} are respectively the peak temperature of melting, observed melting enthalpy, and the normalised melting enthalpy

Figure 4.32 shows the DSC heating curves of LDPE, and LDPE treated with different contents of VTES, prepared using System B. The melting temperatures and enthalpies are summarized in Table 4.7. As was the case with System A, the melting peak temperature of LDPE observably decreased for samples treated with VTES and with increasing VTES content. The explanation is the same as that given for System A earlier in this section. However, the melting enthalpies of similar samples of System B are lower than those of System A. This is probably due to more crosslinking as a result of the higher DCP content which reduced the total crystallinity of the polymer. The addition of clay had no significant influence on the melting temperature and melting enthalpy of LDPE treated with VTES in System B.

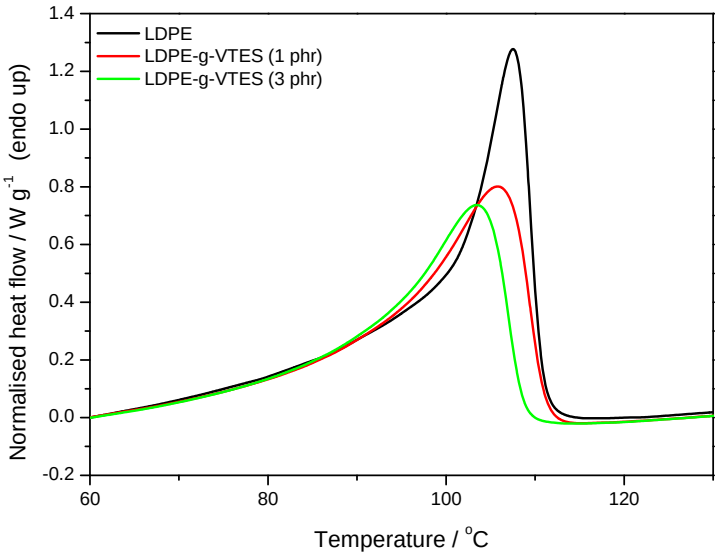

Figure 4.32 DSC heating curves of LDPE, and LDPE treated with different VTES contents (System B)

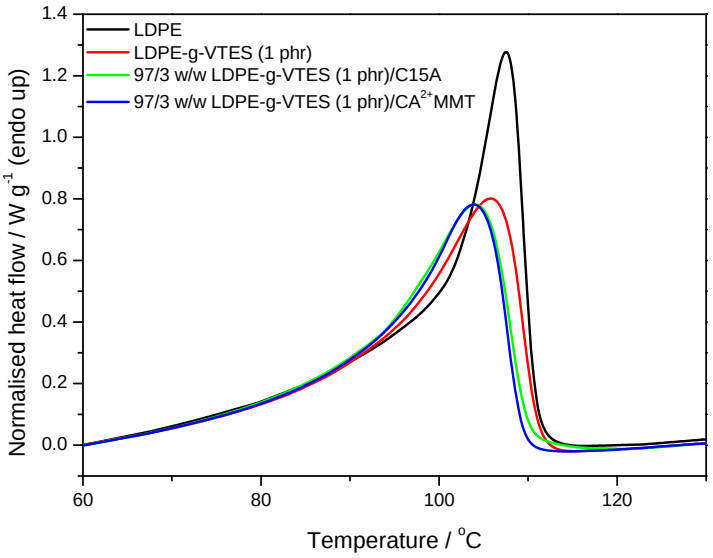

Figure 4.33 DSC heating curves of LDPE, VTES (1 phr) treated LDPE and the different nanocomposites (System B)

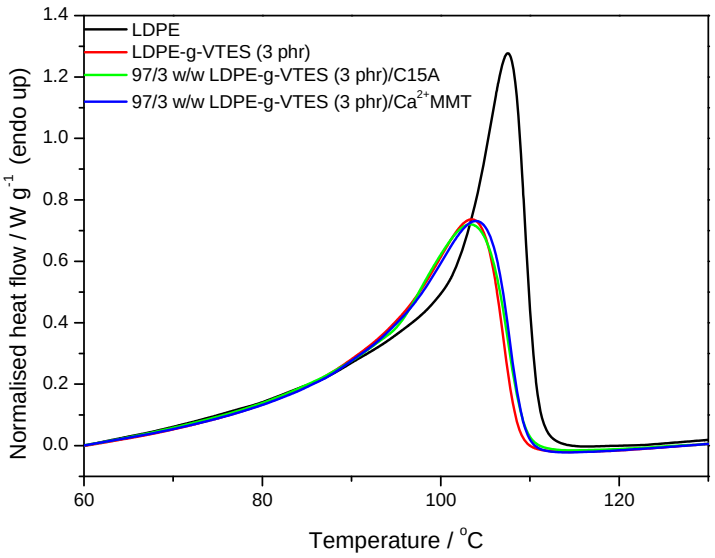

Figure 4.34 DSC heating curves of LDPE, VTES (3 phr) treated LDPE and the different nanocomposites (System B)

Figures 4.35 and 4.36 show the DSC cooling results for the LDPE/C15A nanocomposites treated with different VTES contents. The corresponding crystallization temperatures and enthalpies are summarized in Table 4.8. The treatment of LDPE with VTES slightly decreased the crystallization temperature, but observably decreased the crystallization enthalpy, of LDPE. The crystallization peaks of the VTES treated samples are also observably broader. The decrease in enthalpy as well as the peak broadening is due to the presence of crosslinking. Zhang *et al*. [27] attributed the decrease in crystallization temperature to crosslinking that occurs in the amorphous region of polyolefins, which restrained the movement of the polymer chains, making the crystallization of the polymer difficult. Figure 4.35 shows that the addition of clay had no effect on the crystallization temperature of VTES treated LDPE, which again shows that the crosslinking has the largest effect on LDPE crystallization. Figures 4.36 show little change and no trend in the crystallization enthalpy with the addition of clay.

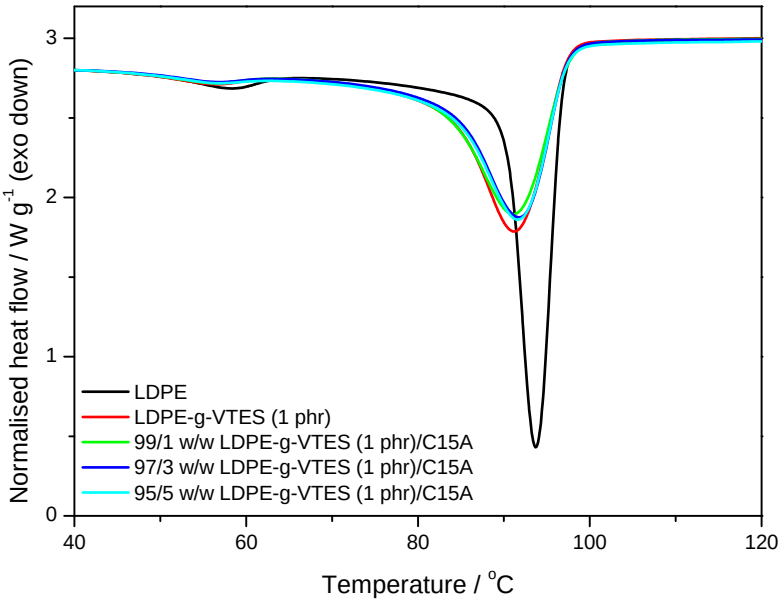

Figure 4.35 DSC cooling curves of LDPE, VTES (1 phr) treated LDPE and the different nanocomposites (System A)

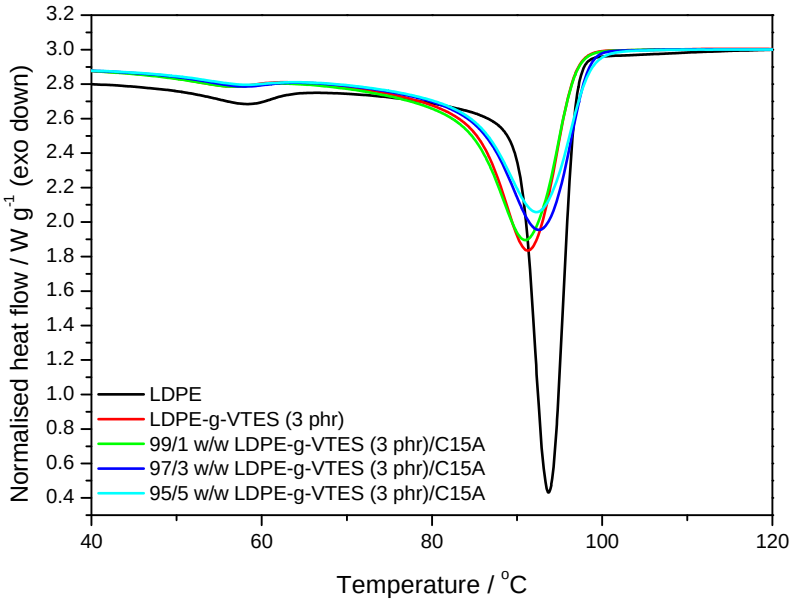

Figure 4.36 DSC cooling curves of LDPE, VTES (3 phr) treated LDPE and the different nanocomposites (System A)

Table 4.8 Summary of the DSC cooling results for all the investigated LDPE-based samples

Composition	$T_{p,c}$ / °C	ΔH_c^{obs} / J g^{-1}	ΔH_c^{norm} / J g^{-1}
LDPE	93.5 ± 0.2	-67.3 ± 2.9	-67.3
LDPE/C15A (w/w)			
97/3	92.7 ± 0.2	-66.9 ± 0.1	-69.0
95/5	92.3 ± 0.1	-66.1 ± 0.4	-69.6
LDPE/Ca^{2+}MMT (w/w)			
97/3	92.6 ± 0.2	-72.8 ± 0.7	-75.1
95/5	92.8 ± 0.5	-68.7 ± 0.8	-72.3
System A			
LDPE-g-VTES (1 phr)	91.1 ± 0.1	-64.5 ± 2.6	-64.5
LDPE-g-VTES (1 phr)/C15A (w/w)			
99/1	91.0 ± 0.2	-64.0 ± 1.4	-64.6
97/3	91.2 ± 0.8	-61.9 ± 1.3	-63.8
95/5	91.2 ± 0.5	-58.0 ± 4.2	-61.1
97/3 w/w LDPE-g-VTES (1 phr)/ Ca^{2+}MMT	91.8 ± 0.5	-59.3 ± 1.0	-61.1
LDPE-g-VTES (3 phr)	91.3 ± 0.3	-57.1 ± 0.2	-57.1
LDPE-g-VTES (3 phr)/C15A (w/w)			
99/1	91.1 ± 1.5	-58.3 ± 1.1	-59.0
97/3	92.7 ± 0.2	-55.8 ± 1.1	-57.5
95/5	92.3 ± 0.3	-50.7 ± 1.4	-53.4
97/3 w/w LDPE-g-VTES (3 phr)/ Ca^{2+}MMT	91.8 ± 0.4	-57.8 ± 0.9	-59.6

$T_{p,c}$, ΔH_c^{obs}, and ΔH_c^{norm} are respectively the peak temperature of crystallization, observed crystallization enthalpy, and the calculated normalised crystallization enthalpy

Figures 4.37 and 4.38 show the DSC heating curves of HDPE, VTES treated HDPE and the different nanocomposites. The results from the DSC curves are summarized in Table 4.9. The melting temperatures slightly decrease, and the melting enthalpies significantly decrease, in the presence of and with an increase in VTES content. The presence of VTES/DCP initiates crosslinking. The formation of crosslinks while the polymer is in the molten state disrupts the

reorientation and chain folding during crystallization and this results in lower crystallinity, and the formation of smaller and more imperfect crystallites. Figures 4.37 and 4.38 show no influence on the melting temperature and melting enthalpy of VTES treated HDPE with the addition of clay. Pakdaman *et al.* [29], who studied the same system, observed that the melting temperature of the samples did not change considerably with grafting of the matrix or with the incorporation of clay. Hence, increasing interaction between the nanoclay and the grafted matrix were likely to occur in the amorphous phase and did not change the melting behaviour of treated HDPE. Figures 4.39 and 4.40 show the cooling curves of the HDPE/C15A nanocomposites treated with different VTES contents, and the results are summarized in Table 4.10. The VTES treatment and the addition of clay had little effect on the crystallization temperature of VTES treated HDPE. However, there is a significant decrease in the crystallization enthalpy of HDPE treated with VTES. This is due to crosslinking of the HDPE matrix. Since HDPE is much more crystalline than LDPE, crosslinking of the molten polymer in the presence of VTES/DCP will have a much more significant influence on the polymer crystallinity. The increase in clay loading had no significant influence on the crystallization enthalpy.

Table 4.9 Summary of the DSC heating results for all the investigated HDPE-based samples

Sample	$T_{p,m}$ / °C	ΔH_m^{obs} / J g^{-1}	ΔH_n^{norm} / J g^{-1}
System A			
HDPE	127.8 ± 0.1	173.9 ± 2.0	173.9
HDPE-g-VTES (1 phr)	126.7 ± 0.8	140.4 ± 2.7	140.4
HDPE-g-VTES (1 phr)/C15A (w/w)			
99/1	126.5 ± 1.3	141.5 ± 2.0	142.9
97/3	126.2 ± 0.5	138.6 ± 7.0	142.8
95/5	125.0 ± 0.8	130.6 ± 2.7	137.5
HDPE-g-VTES (3 phr)	125.4 ± 0.3	136.0 ± 3.6	136.0
HDPE-g-VTES (3 phr)/C15A (w/w)			
99/1	125.4 ± 0.4	131.1 ± 2.1	132.4
97/3	125.6 ± 0.3	130.1 ± 2.4	134.1
95/5	125.5 ± 1.7	125.4 ± 1.7	132.0

$T_{p,m}$, ΔH_m^{obs}, and ΔH_m^{norm} are respectively the peak temperature of melting, observed melting enthalpy, and the calculated normalised melting enthalpy.

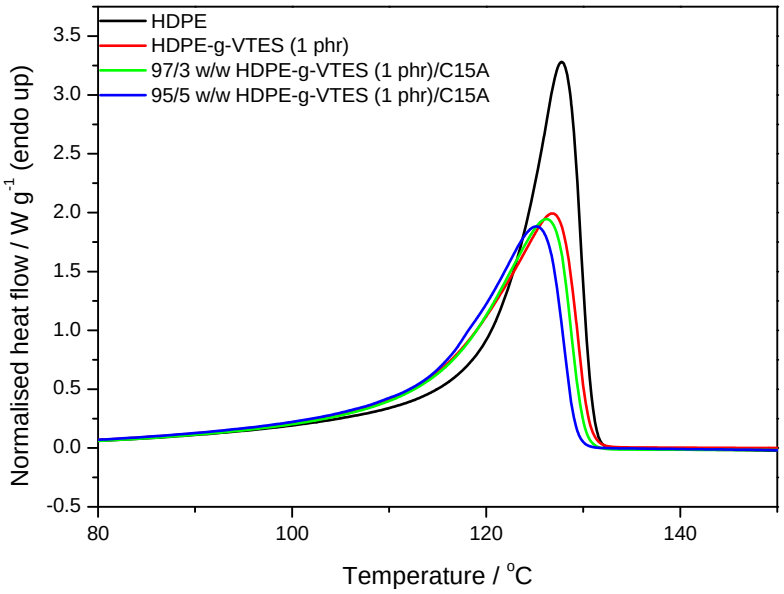

Figure 4.37 DSC heating curves of HDPE, VTES treated LDPE (1 phr) and the different nanocomposites (System A)

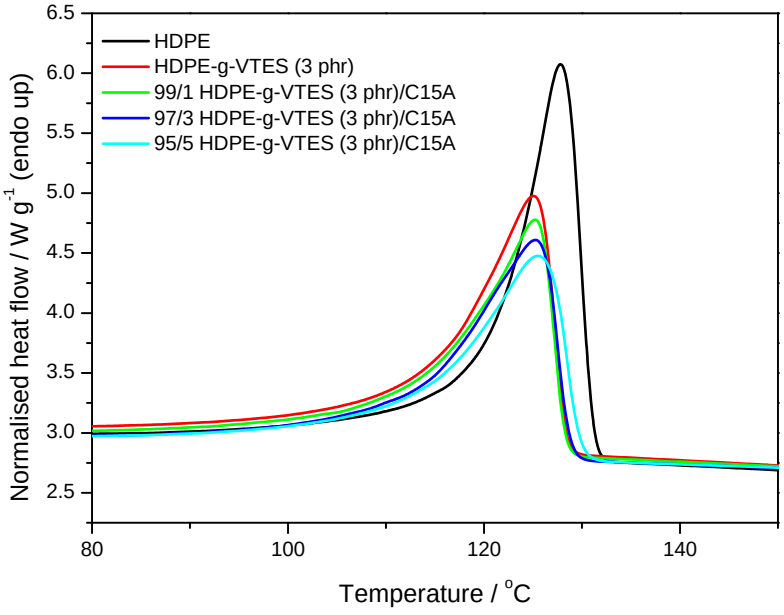

Figure 4.38 DSC heating curves of HDPE, VTES treated LDPE (3 phr) and the different nanocomposites (System A)

Table 4.10 Summary of the DSC cooling results for all the investigated HDPE-based samples

Sample	$T_{p,c}$ / °C	ΔH_c^{obs} / J g^{-1}	ΔH_c^{norm} / J g^{-1}
System A			
HDPE	113.4 ± 0.4	-160.8 ± 2.3	-160.8
HDPE-g-VTES (1 phr)	112.7 ± 0.2	-129.1 ± 2.6	-129.1
HDPE-g-VTES (1 phr)/C15A (w/w)			
99/1	112.2 ± 0.8	-130.6 ± 0.5	-132.0
97/3	112.9 ± 0.6	-131.3 ± 6.0	-135.4
95/5	112.8 ± 0.9	-120.4 ± 6.2	-126.7
HDPE-g-VTES (3 phr)	112.6 ± 0.5	-124.1 ± 2.9	-124.1
HDPE-g-VTES (3 phr)/C15A (w/w)			
99/1	112.7 ± 0.5	-122.8 ± 3.0	-124.0
97/3	111.8 ± 0.8	-124.6 ± 3.0	-128.5
95/5	112.1 ± 0.7	-120.1 ± 3.0	-126.4

$T_{p,c}$, ΔH_c^{obs}, and ΔH_c^{norm} are respectively the peak temperature of melting, observed melting enthalpy, and the calculated normalised crystallization enthalpy

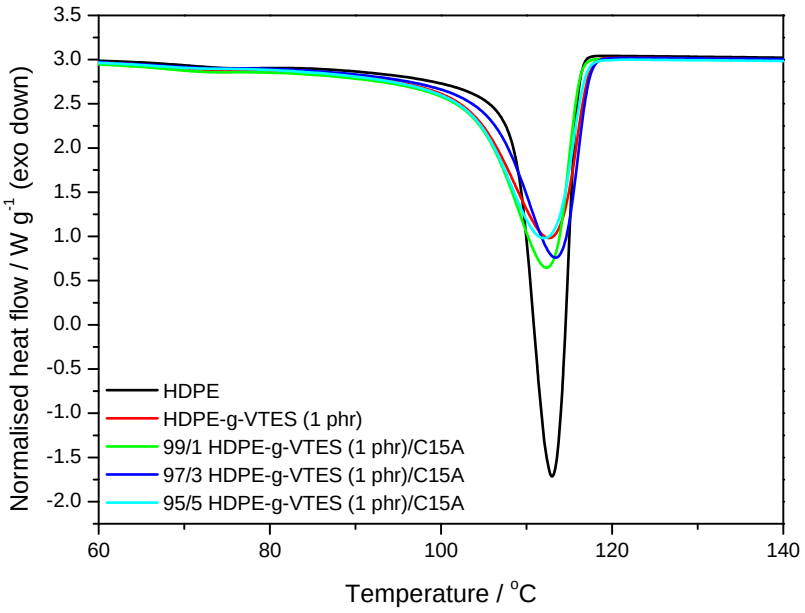

Figure 4.39 DSC cooling curves of HDPE, VTES treated LDPE (1 phr) and the different nanocomposites (System A)

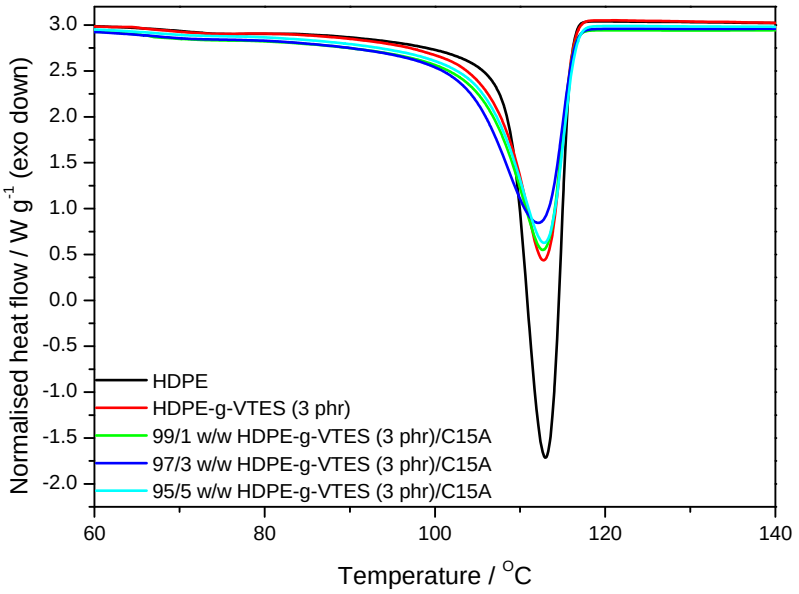

Figure 4.40 DSC cooling curves of HDPE, VTES treated LDPE (3 phr) and different nanocomposites (System A)

4.6 Dynamic mechanical analysis (DMA)

The dynamic mechanical behaviour of all the samples is shown in Figures 4.41 to 4.62. Figure 4.1 shows the storage modulus versus temperature curves of LDPE, and the LDPE/C15A and LDPE/Ca^{2+}MMT nanocomposites. The storage modulus increases with the addition of clay, and all the nanocomposites show higher values than the neat LDPE. This increase in storage modulus is because of the higher modulus of the clay, which contributes to the increase in stiffness of the nanocomposites. This is a common observation for most polymer composites. The increase in clay loading for both C15A and Ca^{2+}MMT results in a decrease in storage modulus, which is probably due to the formation of clay tactoids in the polymer. The enhancement of the storage modulus in polymer-clay nanocomposites normally depends on the aspect ratio of the dispersed clay particles, and on the clay dispersion (intercalation or exfoliation) [30]. The LDPE/C15A nanocomposites have higher storage moduli than the LDPE/Ca^{2+}MMT nanocomposites at the same clay loadings. The modified clay had a slightly better interaction with the polymer which improved the reinforcing effect of the clay. This was observed in the XRD and TEM results that showed more intercalated

structures for LDPE/C15A, while LDPE/Ca^{2+}MMT showed more agglomerates. Chow *et al.* [31] observed that modified MMT-polymer nanocomposites show higher storage moduli than the unmodified nanocomposites. The improvement was associated with the stiffness of the modified MMT, the constraining effect of the clay layers on the molecular motions of the polymer chains, the aspect ratio of the clay platelets, and the degree of dispersion of the modified MMT in the matrix. The storage modulus curves of our pure LDPE and its nanocomposites show a peak around 49 ^{o}C, which can be associated with the melting of thinner lamellae [32].

Figure 4.42 shows the storage modulus curves of LDPE treated with different VTES contents. The treated LDPE shows higher storage modulus values than pure LDPE. This behaviour is probably due to the crosslinking of the polymer (discussed in section 4.4), which contributes to the increase in stiffness of LDPE. However, there is virtually no difference between the E' curves for LDPE and LDPE-g-VTES (3 phr). This is possibly caused by two competing effects, crosslinking by the VTES/DCP combination, which would increase the modulus, and plasticization by the unreacted VTES which would decrease the modulus. The two effects probably balance each other for LDPE-g-VTES (3 phr). McCorimick *et al.* [33] studied the dynamic rheological behaviour of a metallocene copolymer. They observed a decrease in the complex viscosity with addition of VTMS. This behaviour was attributed to the unreacted residual silane which remained in the matrix and acted as a plasticizing agent. Figure 4.43 shows a decrease in the storage modulus with the addition of clay below the glass transition temperature. Ngu *et al.* [34] attributed this behaviour to the development of voids and pores that were formed by nanoparticles agglomeration and to a decrease in crystallinity of the matrix. However, at higher temperatures the storage modulus increases with an increase in clay loading. This behaviour is due to the reinforcing effect of the clay which increases the stiffness of the nanocomposites. Figure 4.44 shows that the addition of clay had very little effect on the storage modulus, and only the 5% clay loading increased the storage modulus. Figure 4.45 clearly shows that the VTES treated nanocomposites have lower storage moduli than the untreated nanocomposites. This observation is in line with the Young's modulus values, which will be discussed in the next section. This behaviour is probably due to the decrease in the crystallinity of the polymer matrix after VTES treatment, which was observed previously in the DSC results (section 4.5).

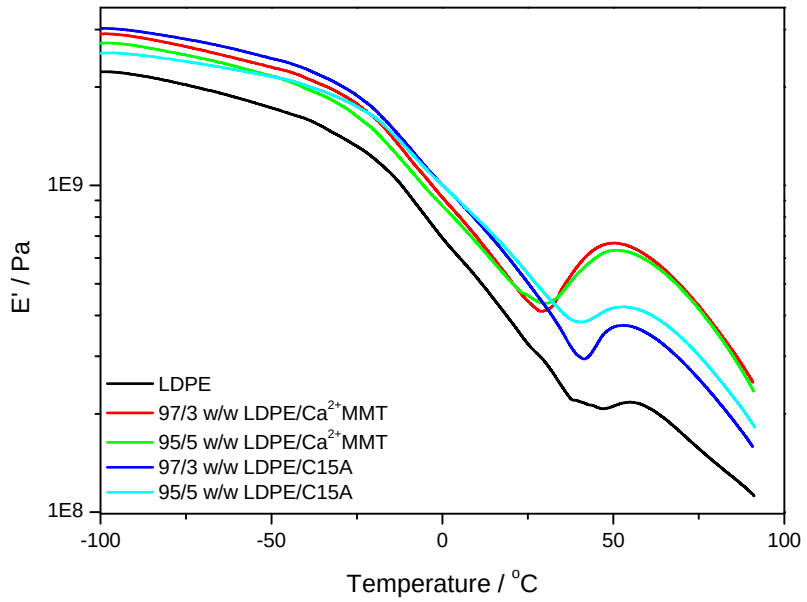

Figure 4.41 Storage modulus of the LDPE/C15A and LDPE/Ca^{2+}MMT nanocomposites

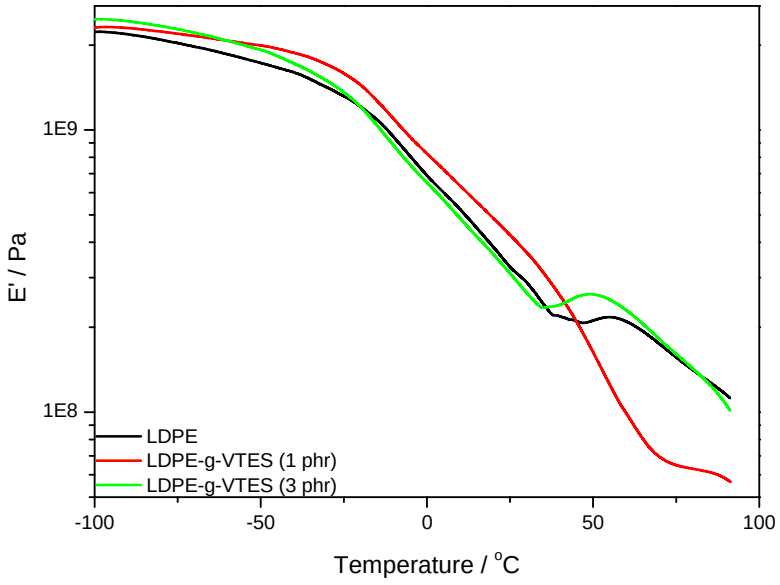

Figure 4.42 Storage modulus of LDPE and LDPE with different VTES contents

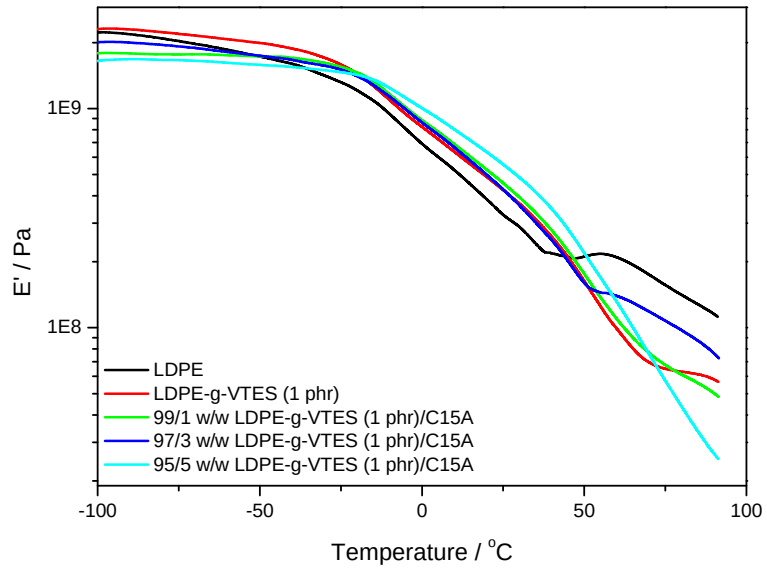

Figure 4.43 Storage modulus of LDPE, LDPE-g-VTES (1 phr)/C15A and the different nanocomposites

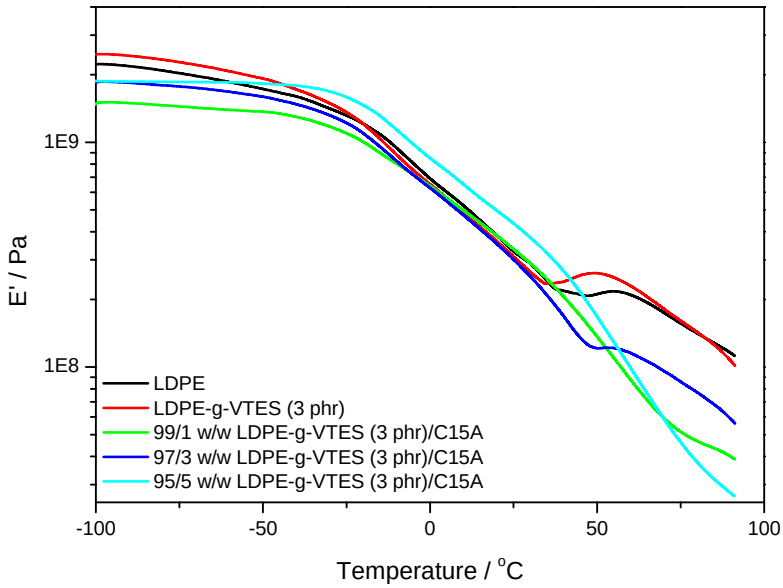

Figure 4.44 Storage modulus of LDPE, LDPE-g-VTES (3 phr)/C15A and the different nanocomposites

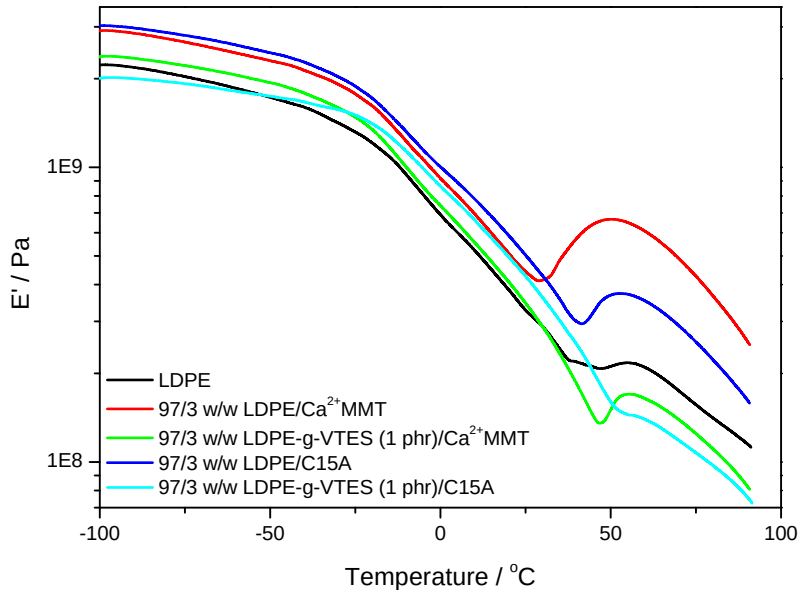

Figure 4.45 Storage modulus of LDPE and the different LDPE/clay nanocomposites containing 3 wt. % of clay

The loss modulus of polyethylene generally shows three transitions in the order of decreasing temperature below the melting temperature. These transitions or relaxations have been designated α, β and γ. The γ transition is usually observed around – 120 °C, the β transition in the range -50 to +20 °C, and the α transition is found between 30 and 120°C. In Figure 4.46, the loss modulus curve of pure LDPE shows two well-defined peaks around -25 °C and 60 °C. These transitions are attributed to the β- and α-relaxations. The β- relaxation is attributed to the main dispersion of the amorphous portion and is mostly referred to as the glass transition temperature, and the α-relaxation is attributed to crystal relaxations [32,35,36]. Contradictory results were reported by different authors on the influence of clay on the glass transition temperature of different polymer matrices. Some found that the presence of clay had no effect on the glass transition temperature [37], others observed a shift to lower temperature [38] or a strong shift to higher temperature [39-40], whereas some observed an increase at low clay content (1-5 wt %) and a decrease at higher contents [41,42]. Figure 4.46 shows that the addition of clay increased the loss modulus of LDPE due to the increasing stiffness of the nanocomposites. However, the presence of clay had no effect on the glass transition temperature and the α-relaxation of LDPE. The α-transition is related to the lamellar thickness, and our DSC results show that the addition of clay had no significant

influence on the lamellar thickness of LDPE. This behaviour can be attributed to the lack of interaction between the polymer and the clay. The nature of the clay had no effect in the glass transition temperature.

Figure 4.47 shows the effect of different VTES contents on the loss modulus of LDPE. The treatment of LDPE with VTES increased the loss modulus, and the glass transition shifted to lower temperatures. The increase in modulus may have been due to increased crosslinking in the presence of higher amounts of VTES, but there was also unreacted VTES which may have played a plasticizing role and decreased the glass transition temperature. There was little effect and no trend of the presence of clay on the glass transition temperature of treated LDPE, as shown in Figures 4.48 and 4.49. This shows that the presence of clay did not significantly influence the chain mobility of the polymer. Figure 4.50 confirms that VTES treatment and the addition of clay had very little influence on the glass transition temperature of LDPE.

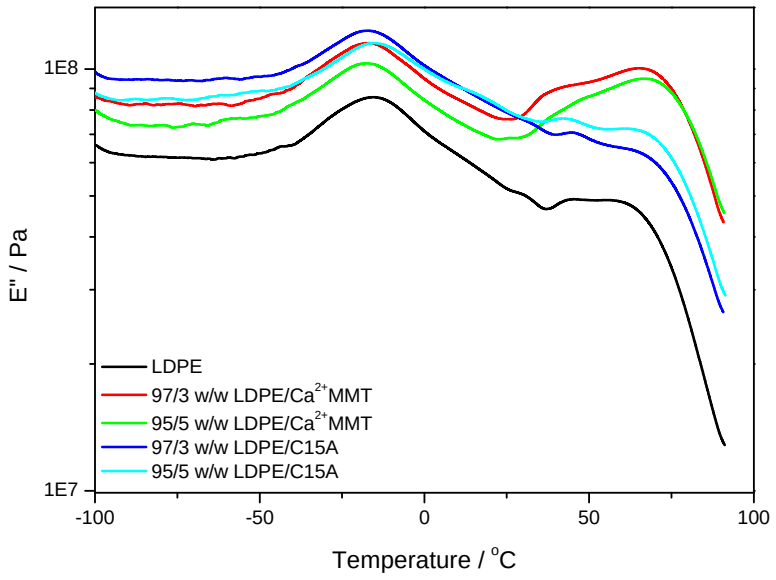

Figure 4.46 Loss modulus of LDPE/C15A and LDPE/Ca^{2+}MMT nanocomposites

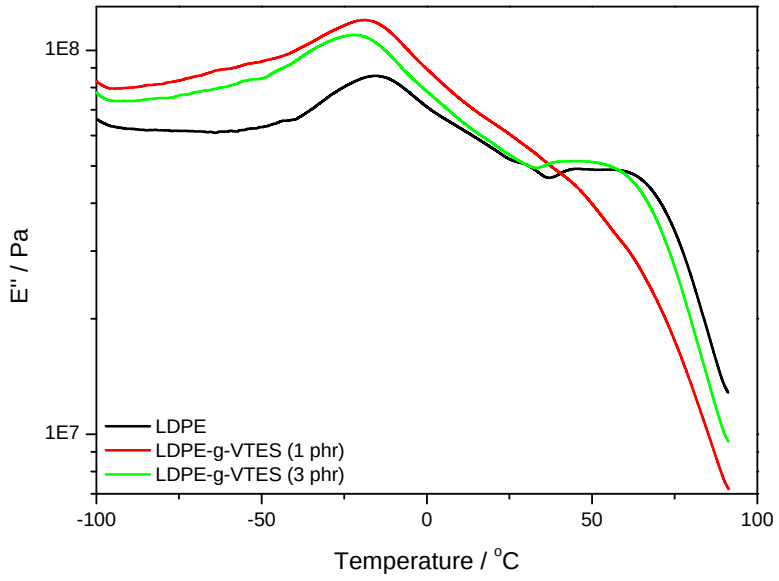

Figure 4.47 Loss modulus of LDPE and LDPE-g-VTES prepared with different VTES contents

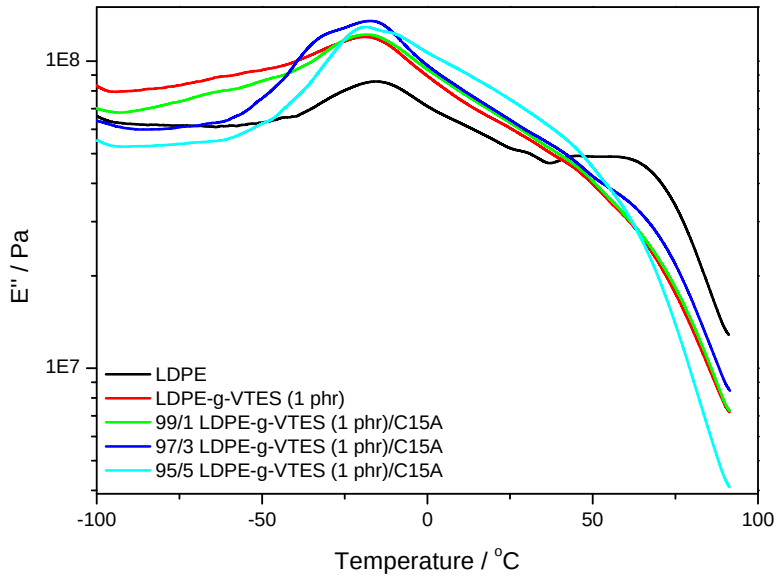

Figure 4.48 Loss modulus of LDPE, LDPE-g-VTES (1 phr)/C15A and the different nanocomposites

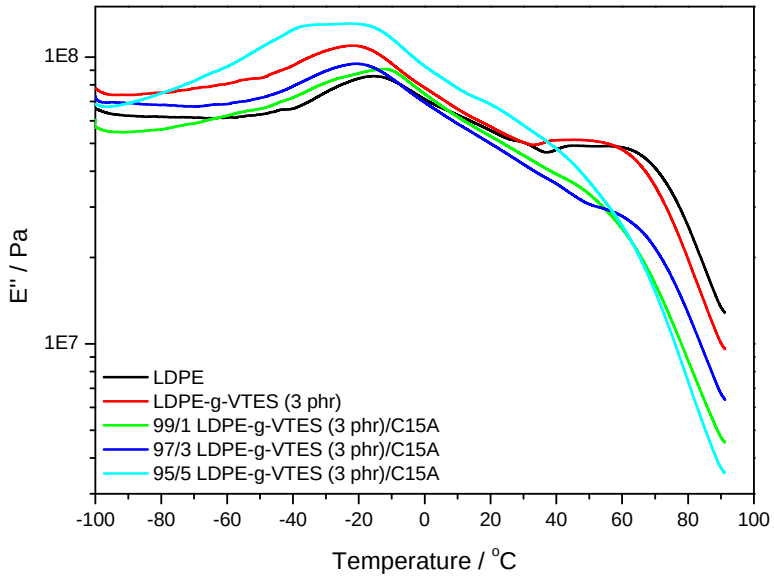

Figure 4.49 Loss modulus of LDPE, LDPE-g-VTES (3 phr)/C15A and the different nanocomposites

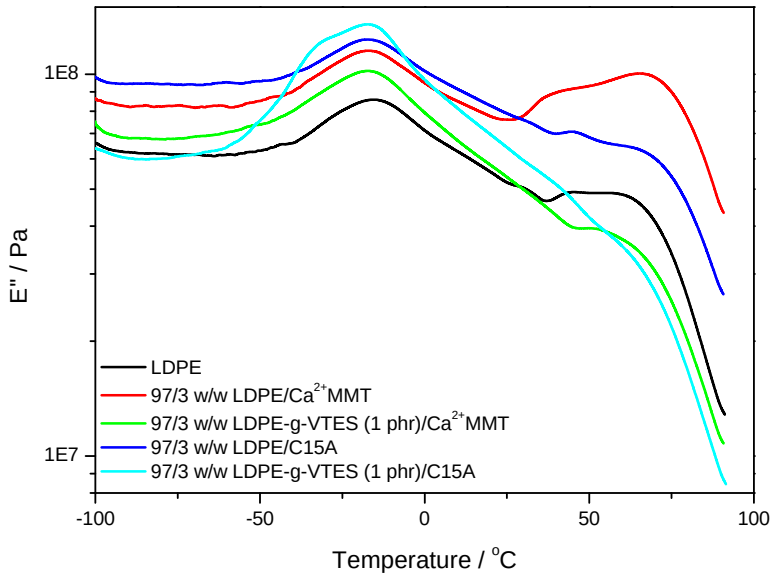

Figure 4.50 Loss modulus of LDPE and the different LDPE/clay nanocomposites containing 3 wt. % of clay

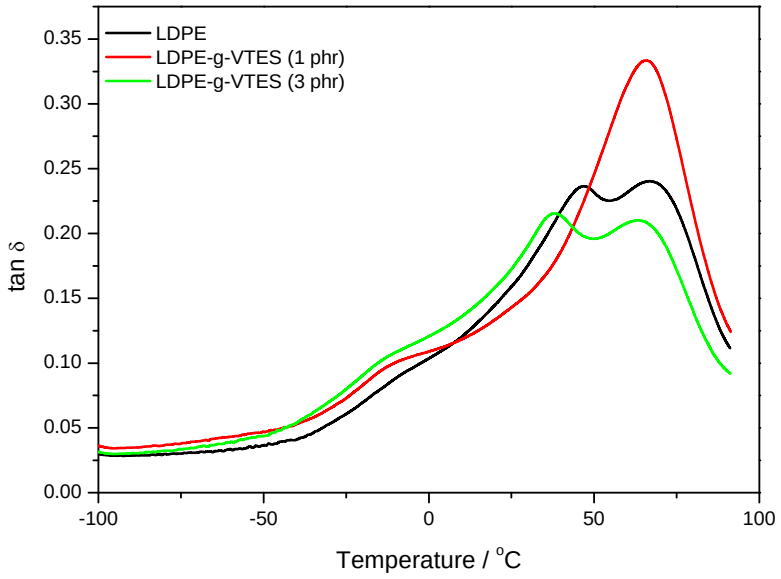

Figure 4.51 tan δ of LDPE treated with different contents of VTES

Figure 4.51, 4.52 and 4.53 show the damping factor (tan δ) of LDPE, LDPE treated with different contents of VTES and the LDPE-g-VTES/C15A nanocomposites. Pure LDPE shows a small peak around -25 – 0°C and is due to the β-relaxation or glass transition. Figure 4.52 and 4.53 show that the glass transition temperature is not significantly affected by the addition of and increase in clay loading. LDPE shows two overlapping peaks around 47 and 67 °C. The peaks can be assigned to the α- transition and the melting of thinner lamellae/smaller crystallites [32,47]. The positions of these peaks changed, and in some cases they merged into a single peak with observable differences in the tan δ maximum. Since there is no trend, it is almost impossible to relate these differences to changes in the morphology as a result of VTES treatment and/or clay loading.

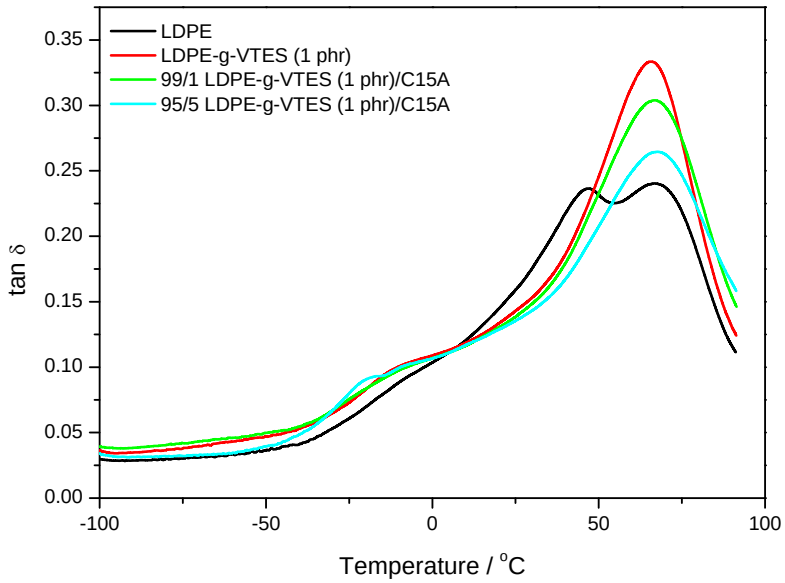

Figure 4.52 tan δ of LDPE, LDPE-g-VTES (1 phr)/C15A and the different nanocomposites

Figure 4.54 shows the storage modulus of VTES treated LDPE clay nanocomposites prepared using System A and System B. The System B samples show lower storage moduli than the System A samples above the glass transition temperature of LDPE. The same behaviour was also observed for the Young's modulus, which will be discussed in the next section. In both systems, the storage modulus decreased with the addition of clay below the glass transition temperature. This observation was discussed earlier in this section. Above the glass transition temperature the presence of clay slightly increased the storage modulus. This is due to the reinforcing effect of the clay layers intercalated into the polymer matrix, and possibly to the immobilization of polymer chains [42]. Figure 4.55 shows a slight decrease in the glass transition temperature of LDPE with VTES treatment in both systems. Mark and colleagues [35] reported that the T_g depends, *inter alia*, on the crystallinity of a polymer. They observed that there is less constraint on the non-crystalline chain segments which increases the entropy, causing T_g to decrease. In our case, the addition of clay had no significant influence on the glass transition temperature. The relaxation resulting from the melting of thinner lamellae/smaller crystallites disappeared for the clay-containing samples. The crystallization

of the polymer around the clay particles probably led to more effective crystal growth and a reduction in the number of small crystallites.

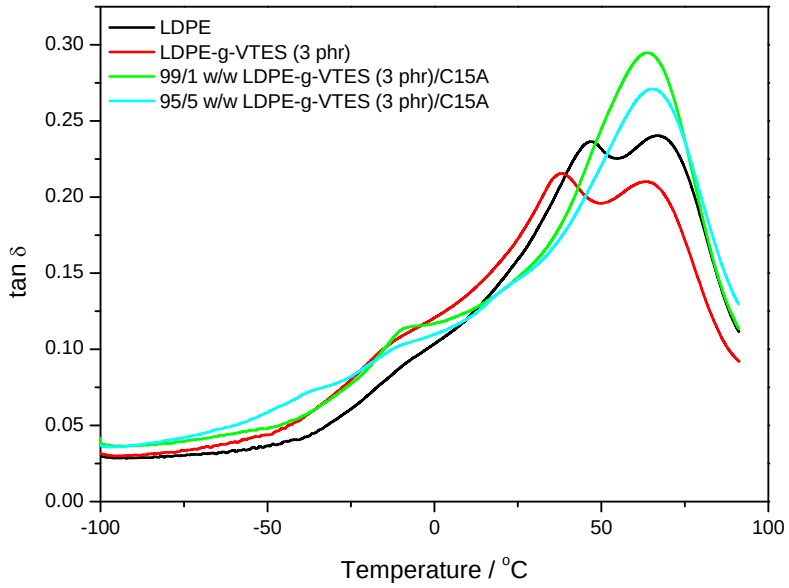

Figure 4.53 tan δ of LDPE, LDPE-g-VTES (3 phr)/C15A and the different nanocomposites

Figures 4.56 to 4.62 show the dynamic mechanical behaviour of HDPE, HDPE treated with different contents of VTES, and the HDPE-g-VTES/C15A nanocomposites. HDPE has the highest storage modulus over the whole investigated temperature range. Around -25 °C there is an increase in the storage modulus of the 1 phr VTES treated nanocomposites (Figure 4.56). This is probably due to a cold crystallization effect where the clay platelets acted as nucleation sites for further crystallization of the HDPE above its glass transition temperature.

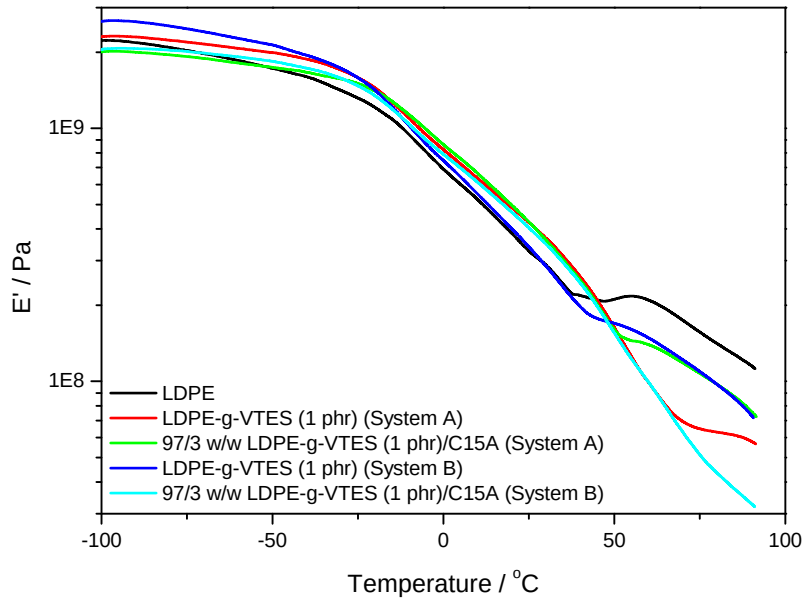

Figure 4.54 Storage modulus of LDPE and the different LDPE/clay nanocomposites

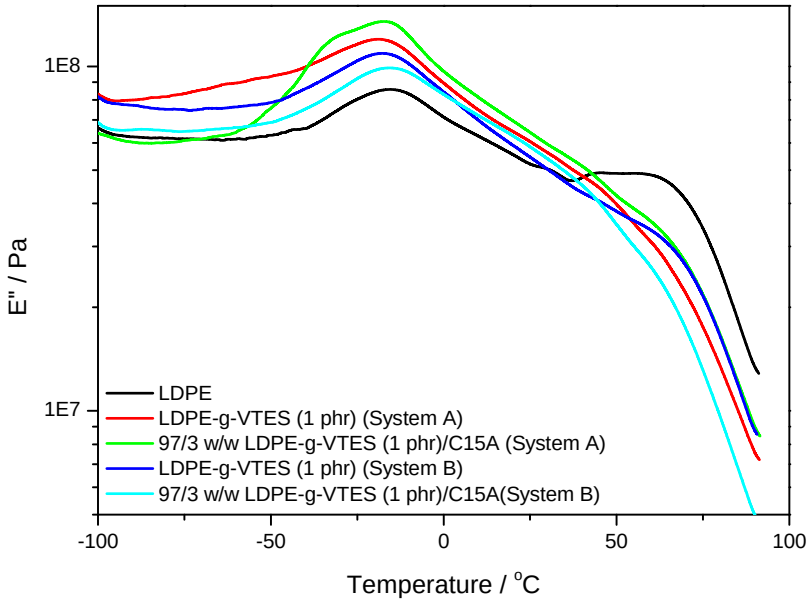

Figure 4.55 Loss modulus of LDPE and the different LDPE/clay nanocomposites

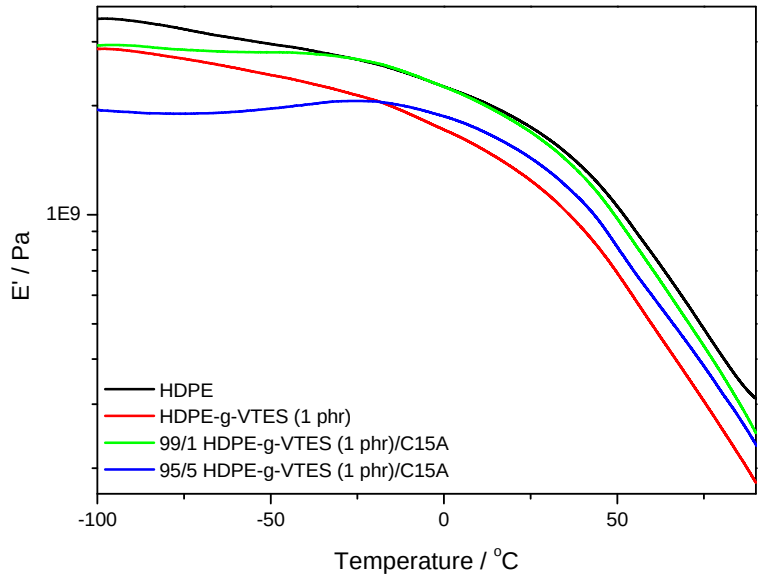

Figure 4.56 Storage modulus of HDPE and the HDPE-g-VTES (1 phr)/C15A nanocomposites

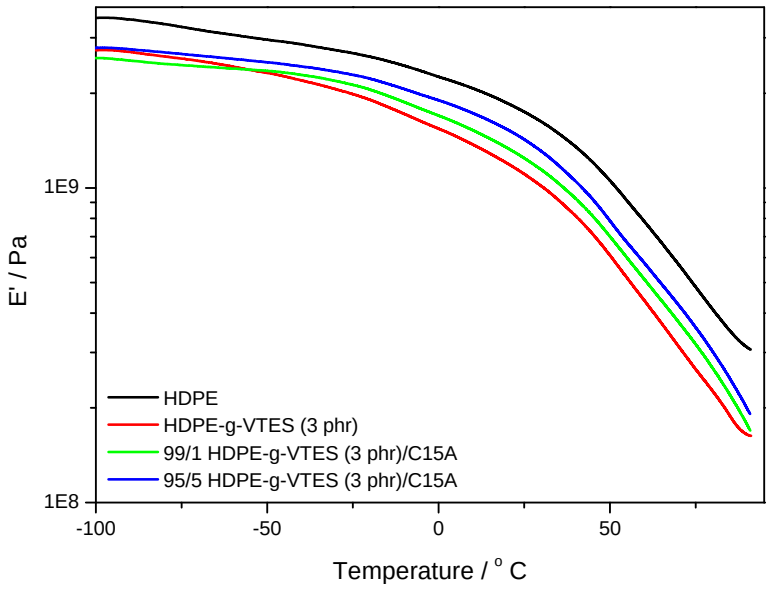

Figure 4.57 Storage modulus of HDPE and the HDPE-g-VTES (3 phr)/C15A nanocomposites

Figure 4.58 shows the loss modulus of HDPE and HDPE treated with different VTES contents. HDPE normally shows only two transitions, a γ- and an α-transition. The transition at about 49 °C is attributed to the α-transition, which is related to chain motions within the crystalline phase. It has been shown that the intensity of the transition increases as the lamellar thickness increases [43]. This transition slightly shifted to lower temperatures after treatment with VTES and with increasing VTES content. This behaviour can be due to the reduced lamellar thickness of HDPE as observed in DSC. The β-transition is absent in HDPE, since it is due to a relaxation in the amorphous or interfacial phase of especially branched polyethylenes [32,43,44], and its magnitude has been shown to decrease as the crystallinity increases. Djoković *et al*. [44] reported that the amount of interfacial content that can produce a visible β-peak in the DMA curve of polyethylene is about 10% of the semicrystalline material. In LPE the interfacial content is about 3-4%, whereas in BPE (with only 0.6 mol % branches) it is about 11%. Long branches affect this relaxation more than shorter ones. An increase in the VTES content results in the development of a peak at -50 °C, which can be associated to a β- transition. This is probably the result of an increase in the amount of the interfacial amorphous content as the VTES content increases. The addition of clay and increase in clay loading also cause the appearance of a β-transition (Figure 4.59 and 4.60). This behaviour can be attributed to the presence of more amorphous material in the polymer due to the decrease in crystallinity (earlier observed in DSC, section 4.5). Figures 4.61 and 4.62 show the tan δ curves of HDPE, HDPE treated with different VTES contents, and the clay containing samples. These curves show the same transitions and trends as the loss modulus curves.

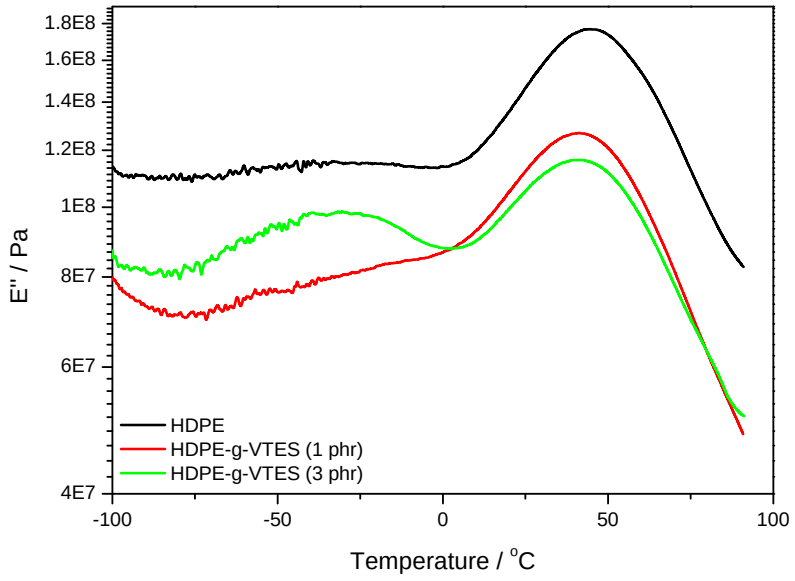

Figure 4.58 Loss modulus of HDPE and HDPE treated with different VTES contents

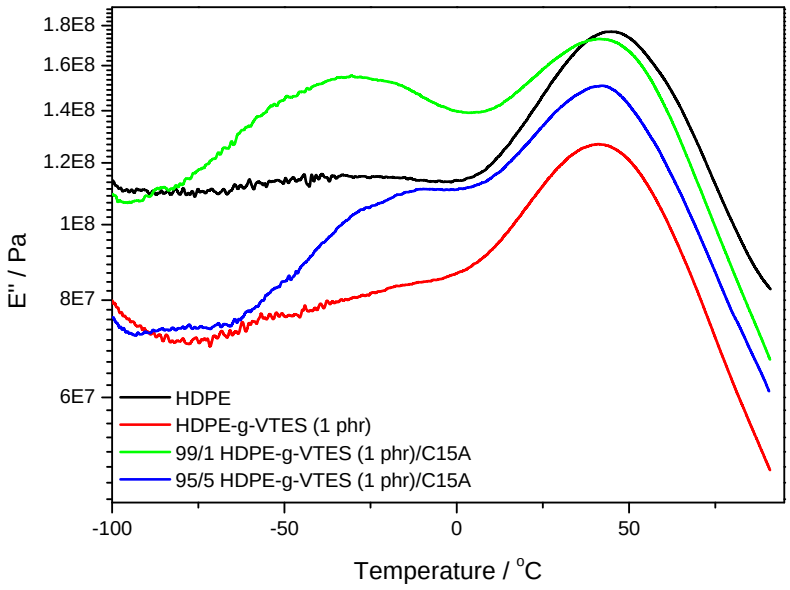

Figure 4.59 Loss modulus of HDPE and the HDPE-g-VTES (1 phr)/C15A nanocomposites

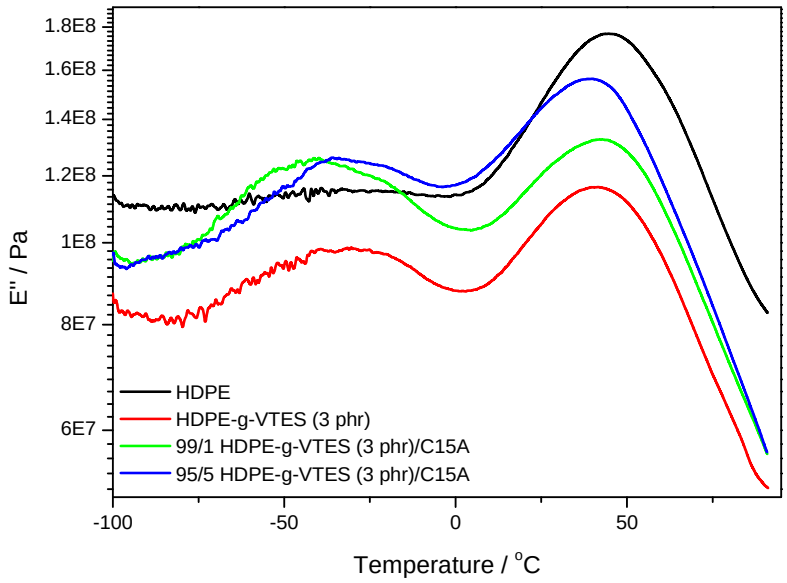

Figure 4.60 Loss modulus of HDPE and the HDPE-g-VTES (3 phr)/C15A nanocomposites

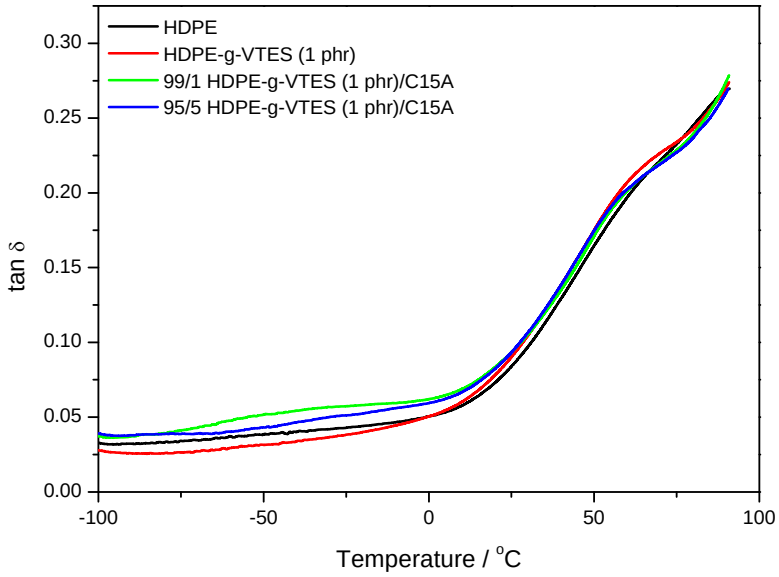

Figure 4.61 tan δ of HDPE and the HDPE-g-VTES (1 phr)/C15A nanocomposites

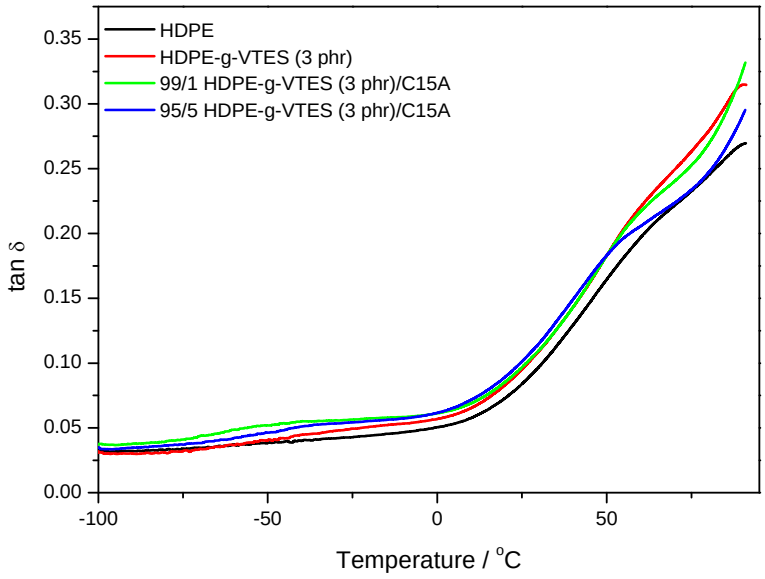

Figure 4.62 tan δ of HDPE and the HDPE-g-VTES (3 phr)/C15A nanocomposites

4.7 Tensile testing

The tensile properties of all the investigated samples are shown in Figures 4.63 to 4.68. The actual values of these properties are summarized in Tables 4.11 and 4.12. All the stress-strain curves are presented in the Appendix. Figure 4.63 shows that the stress at break of LDPE slightly increased with the addition of clay and increase in clay loading. LDPE/C15A nanocomposites show higher stress at break values than LDPE/Ca^{2+}MMT at the same clay loading. The presence of modifier slightly improved the interfacial interaction between LDPE and C15A (XRD and TEM showed a more intercalated structure, section 4.2). The treatment of LDPE with VTES significantly increased the stress at break of LDPE, which is due to the crosslinking of the polymer chains. Zhang *et al.* [27] studied the effect of VTMS concentration (0, 0.5, 1, 1.5, and 2 phr) on the mechanical properties of silane-crosslinked polyethylene-octene elastomer (POE), where DCP content remained constant at 0.1 phr. The tensile strength increased slowly with increase in VTMS content and reached a maximum at 1.5 phr, and then sharply decreased at 2.0 phr. This was due to the excess unreacted VTMS which remained in the polymer, and acted as a plasticizing reagent. In our case the addition of clay had no effect or decreased the stress at break. Mohanty *et al*. [10] observed a decrease in

tensile strength at high clay loadings. They attributed this behaviour to more filler-filler interaction which results in agglomerates and induces local stress concentrations in the nanocomposites, because of a reduction in clay aspect ratio and resultant reduction in the contact surface between the organoclay and the polymer matrix. The VTES treated LDPE nanocomposites still show higher stress at break values than the untreated nanocomposites at the same clay loading. This is due to a weaker interaction between the clay and the polymer in the case of untreated nanocomposites, although the interaction is still strong enough to allow an increase in stress at break with increasing clay content for the untreated samples.

The elongation at break of LDPE decreased with the addition of clay and increase in clay loading (Figure 4.64). This behaviour is common for (nano)composites and is the result of filler particles forming defect centres for the formation and development of crazes and cracks. The treatment of LDPE with VTES increases the elongation at break of LDPE. Contrary to our results, Hidalgo *et al.* [45] observed an initial increase in elongation at break, which decreased as the concentration of organosilane increased. This behaviour was explained through the formation of a very weak crosslinked network at low VTES concentrations that allows the polymer chains to slip without breaking the sample, leading to higher elongation. At high organosilane concentration, the dense network formed prevented the chains from slipping, leading to a decrease in the elongation at break. In our case the VTES content was probably not high enough to form such a dense crosslinked network. The addition of and increase in clay loading reduced the elongation at break. This is probably due to a reduction in the number of crosslinks because of a higher extent of grafting in the presence of the clay, and to the clay particles acting as defect centres where crazes and cracks were initiated. Figure 4.65 shows that the incorporation of both modified and unmodified clay significantly increases the tensile modulus of the LDPE. This increase in tensile modulus is due to the reinforcing effect of the clay on the nanocomposites. The LDPE/C15A nanocomposites have higher tensile modulus values than the LDPE/Ca^{2+}MMT nanocomposites at the same clay loading. Kusmono *et al.* [9] also observed that modified clay nanocomposites showed high tensile modulus values than unmodified clay nanocomposites. The improvement was attributed to the presence of immobilized or partially mobilized polymer chains as a consequence of interaction of the polymer chains with the organic modification of the clay. Although this is possible, in our case it is more probably the result of the more effective intercalation of the modified clay in LDPE.

Figure 4.65 also shows a decrease in tensile modulus of LDPE with the addition and increase in VTES content. The presence of VTES decreases the stiffness of LDPE, probably because of a plasticizing effect of the unreacted VTES. The addition of clay increases the tensile modulus of the VTES treated LDPE. This is due to the reinforcement of the dispersed clay which increases the stiffness of the polymer matrix. However, the tensile moduli of the untreated LDPE/C15A nanocomposites are higher than those of the VTES treated LDPE/C15A nanocomposites at the same clay loading. This is probably due to the competing effect of the presence of the VTES and that of the clay. The presence of VTES decreases the stiffness and that of C15A increases the stiffness of the nanocomposites. Morawiec *et al.* [46] also observed that untreated LDPE/MMT-ODA showed higher tensile modulus values than the PE-g-MA treated nanocomposites at the same clay loading. They concluded that the presence of MMT-ODA clay causes an increase in tensile modulus, while the presence of the relatively soft compatabilizer caused a decrease in the tensile modulus.

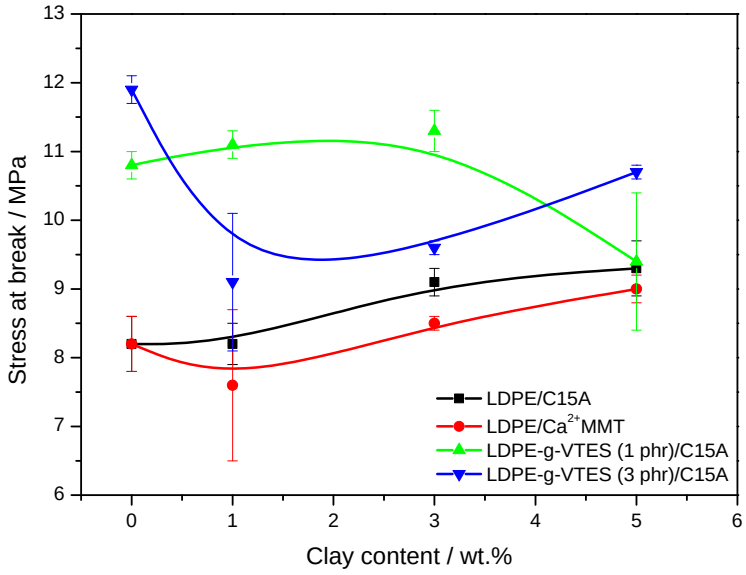

Figure 4.63 Stress at break of LDPE/C15A, LDPE/Ca^{2+}MMT and the LDPE-g-VTES/C15A nanocomposites

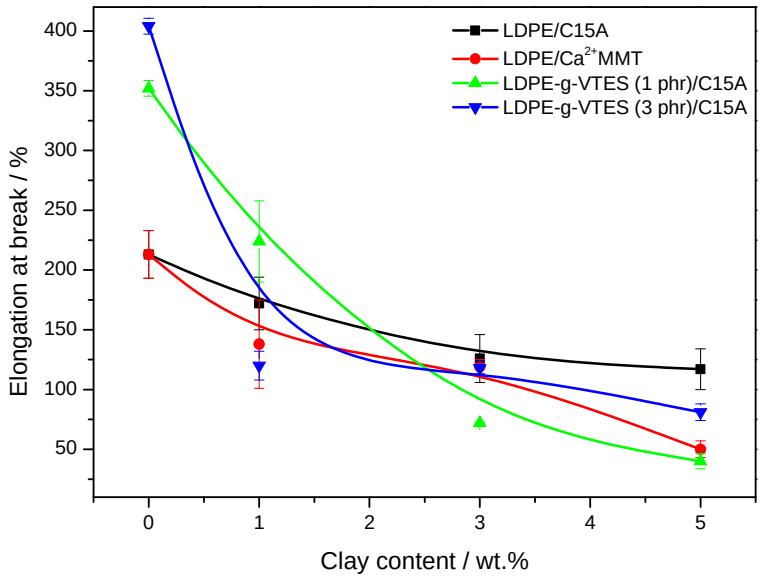

Figure 4.64 Elongation at break of LDPE/C15A, LDPE/Ca^{2+}MMT and the LDPE-g-VTES/C15A nanocomposites

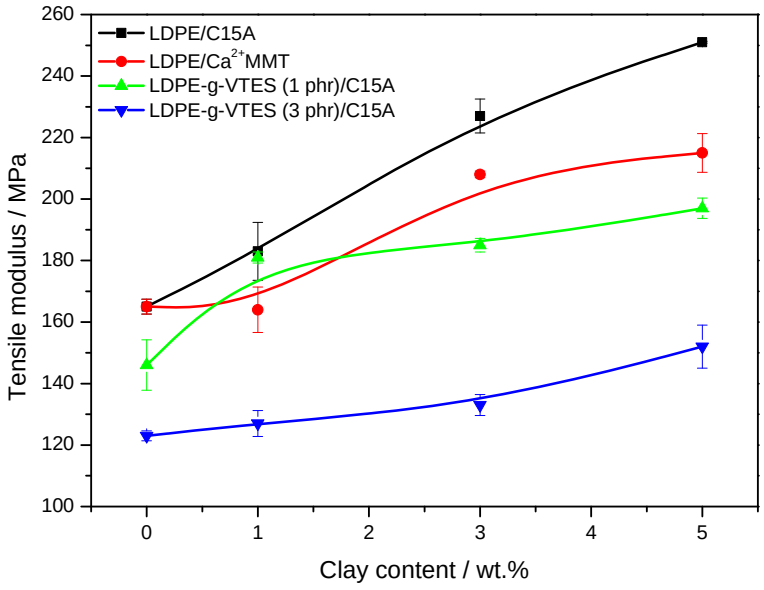

Figure 4.65 Tensile modulus of LDPE/C15A, LDPE/Ca^{2+}MMT and the LDPE-g-VTES/C15A nanocomposites

Table 4.11 Summary of the tensile results of LDPE samples

Sample	ε_b / %	σ_b / MPa	E / MPa
LDPE	213 ± 20	8.2 ± 0.4	165 ± 2
System A			
99/1 w/w LDPE/C15A	172 ± 22	8.2 ± 0.3	183 ± 9
97/3 w/w LDPE/C15A	126 ± 20	9.1 ± 0.2	227 ± 6
95/5 w/w LDPE/C15A	117 ± 17	9.3 ± 0.4	251 ± 0
99/1 w/w LDPE/Ca^{2+}MMT	138 ± 37	7.6 ± 1.1	164 ± 7
97/3 w/w LDPE/Ca^{2+}MMT	119 ± 6	8.5 ± 0.1	208 ± 1
95/5 w/w LDPE/Ca^{2+}MMT	50 ± 7	9.0 ± 0.2	215 ± 6
LDPE-g-VTES (1 phr)	352 ± 7	10.8 ± 0.2	145 ± 8
99/1 w/w LDPE-g-VTES (1 phr)/C15A	224 ± 34	11.1 ± 0.2	181 ± 2
97/3 w/w LDPE-g-VTES (1 phr)/C15A	72 ± 0	11.3 ± 0.3	185 ± 2
95/5 w/w LDPE-g-VTES (1 phr)/C15A	40 ± 6	9.4 ± 1.0	197 ± 3
97/3 w/w LDPE-g-VTES (1 phr)/Ca^{2+}MMT	339 ± 8	12.4 ± 0.5	161 ± 5
LDPE-g-VTES (3 phr)	403 ± 7	11.9 ± 0.2	121 ± 2
99/1 w/w LDPE-g-VTES (3 phr)/C15A	120 ± 12	9.1 ± 1.0	127 ± 4
97/3 w/w LDPE-g-VTES (3 phr)/C15A	118 ± 5	9.6 ± 0.1	133 ± 3
95/5 w/w LDPE-g-VTES (3 phr)/C15A	81 ± 7	10.7 ± 0.1	152 ± 7
97/3 w/w LDPE-g-VTES (3 phr)/Ca^{2+}MMT	379 ± 19	11.0 ± 0.8	139 ± 3
System B			
LDPE-g-VTES (1 phr)	253 ± 15	11.3 ± 0.3	110 ± 4
97/3 w/w LDPE-g-VTES (1 phr)/C15A	233 ± 19	11.4 ± 0.3	137 ± 3
97/3 w/w LDPE-g-VTES (1 phr)/ Ca^{2+}MMT	259 ± 43	11.3 ± 0.1	106 ± 1
LDPE-g-VTES (3 phr)	333 ± 32	11.2 ± 0.2	93 ± 4
97/3 w/w LDPE-g-VTES (3 phr)/C15A	170 ± 14	11.0 ± 0.4	111 ± 6
97/3 w/w LDPE-g-VTES (3 phr)/ Ca^{2+}MMT	299 ± 40	11.1 ± 0.6	104 ± 4

ε_b, σ_b and E are elongation at break, stress at break, and Young's modulus of elasticity.

Table 4.11 shows that the stress at break values of LDPE treated according to System A and System B do not differ much within experimental error, but the values are significantly higher than that of untreated LDPE. These higher values are probably the result of the crosslinking of the polymer chains. The addition of clay did not significantly influence the

tensile strength of VTES treated LDPE in both systems. However, the elongation at break decreased with increasing DCP concentration because the crosslinks restricted the polymer chain motion during extension. Jiao *et al.* [47] observed an increase in tensile strength and a decrease in elongation at break with increasing DCP concentration. Their explanation was that, after crosslinking, ethylene-octene copolymer formed three-dimensional network, leading to an increase in strength and a decrease in elongation resulting in a restriction of molecular chain movement caused by the crosslinked network. No trend could be observed in the elongation at break values when comparing the nanocomposites prepared according to Systems A and B. This is probably due to a balance between a number of factors that will influence the elongation at break, e.g. extent of crosslinking of the polymer chains, nature and dispersion of the clay, interaction between the clay and the polymer, etc. The tensile moduli of the LDPE nanocomposites treated according to System B are observably lower than those treated according to System A at the same VTES content and clay loading. This is surprising, because one would expect the modulus to be higher because of the higher crosslink densities of the System B samples. This observation may be explained as being the result of the lower crystallinity of the System B samples (see discussion in section 4.5).

Table 4.12 Summary of the tensile results of HDPE samples

Sample	ε_b / %	σ_b / MPa	E / MPa
HDPE	953 ±12	16.6 ± 0.9	361 ± 9
HDPE-g-VTES (1 phr)	432 ± 3	14.4 ± 1.0	491 ± 84
99/1 w/w HDPE-g-VTES (1 phr)/C15A	364 ± 5	15.3 ± 1.3	526 ± 42
97/3 w/w HDPE-g-VTES (1 phr)/C15A	201 ± 49	16.3 ± 0.3	563 ± 35
95/5 w/w HDPE-g-VTES (1 phr)/C15A	90 ± 13	15.8 ± 1.4	535 ± 23
HDPE-g-VTES (3 phr)	578 ± 4	18.2 ± 0.4	421 ± 0
99/1 w/w HDPE-g-VTES (3 phr)/C15A	220 ± 3	14.7 ± 0.6	493 ± 7
97/3 w/w HDPE-g-VTES (3 phr)/C15A	232 ± 4	13.4 ± 2.5	500 ± 16
95/5 w/w HDPE-g-VTES (3 phr)/C15A	81 ± 12	10.8 ± 0.2	495 ± 2

ε_b, σ_b and E are elongation at break, stress at break, and Young's modulus of elasticity.

Table 4.12 shows the tensile properties of HDPE and the HDPE-g-VTES/C15A nanocomposites. Figure 4.66 shows that the tensile strength values decreased after 1 phr VTES treatment, and increased with the addition of clay and an increase in clay loading. The

increase in tensile strength is directly attributed to the dispersion of the clay layers in the HDPE matrix and the strong interaction between the HDPE and the clay. The tensile strength increased with increasing VTES content, but the addition of and increase in clay loading decreased the tensile strength. The increase with increasing VTES content is probably due to the formation of crosslinks between the polymer chains, while the decrease with increasing clay content is probably the result of several factors, amongst which are the decreasing crystallinity and crosslink density of the samples, and the fact that the clay may have formed defect centres for the formation and propagation of crazes and cracks. As can be seen in Table 4.12 and Figure 4.67, the tensile modulus increased with VTES treatment, but decreased at the higher VTES content. This will also be due to the increased crosslinking in the VTES treated samples. The addition of and increase in clay loading increased the tensile modulus, but only up to about 2% clay loading. This is due to the reinforcement of the polymer by the dispersed clay which. The levelling off at higher clay contents is probably due to the formation of agglomerates as a result of more filler-filler interaction, which was also observed in the TEM micrographs. Mohan *et al*. [28] stated that the possible reasons for the development of agglomerates in nanocomposites are the high concentration of clay, improper processing methods, and particle-particle interaction. According to them the agglomerates act as crack initiators and reduce the properties of the polymer. Generally the elongation at break decreases with VTES treatment and with increasing clay content (Figure 4.68 and Table 4.12). The reasons will be the same as discussed for the LDPE samples.

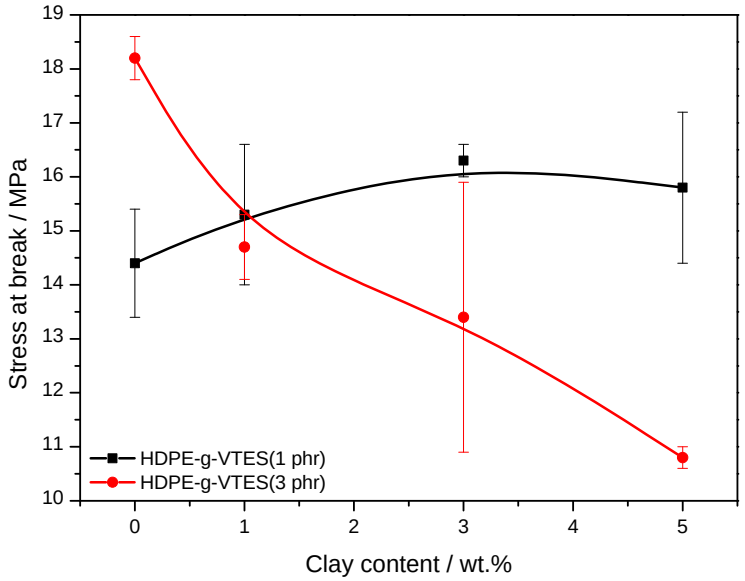

Figure 4.66 Stress at break of HDPE-g-VTES and the HDPE-g-VTES/C15A nanocomposites

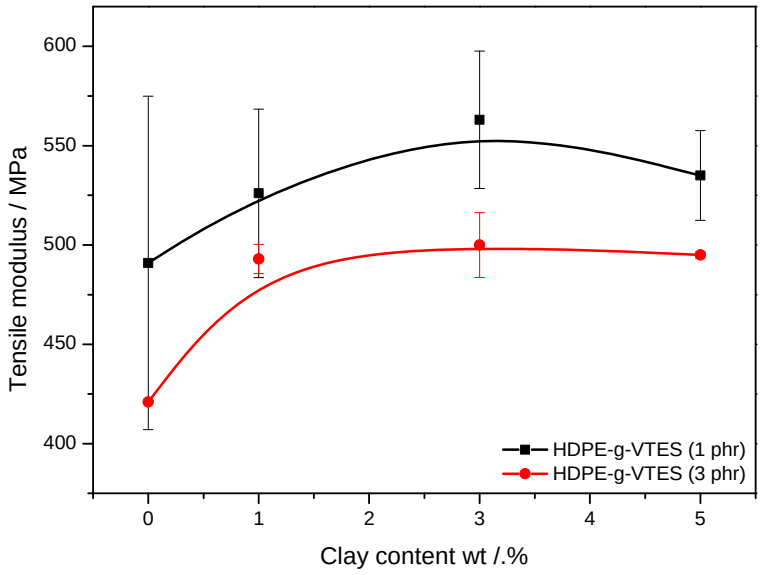

Figure 4.67 Tensile modulus of HDPE-g-VTES and the HDPE-g-VTES/C15A nanocomposites

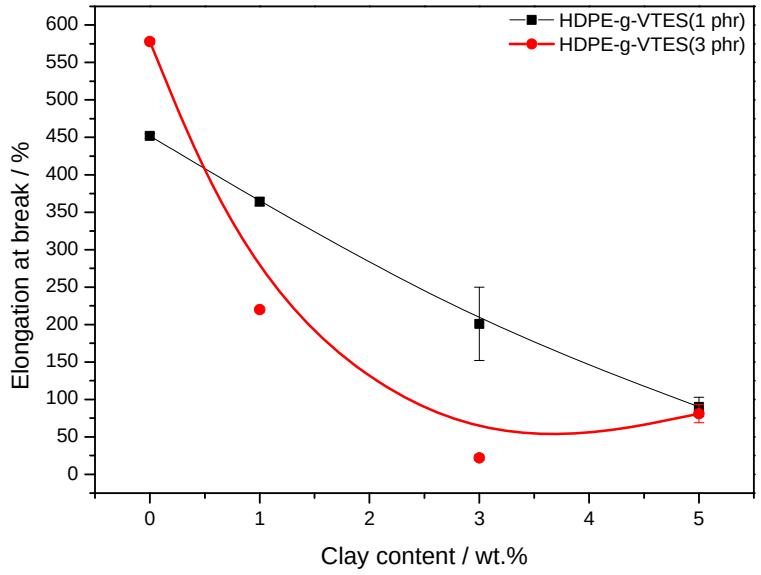

Figure 4.68 Elongation at break of HDPE and HDPE-g-VTES/C15A nanocomposites

4.8 References

1. Kusmono, Z.A. Mohd Ishak, W.S. Chow, T.T. Rochmadi. Effect of clay modification on the morphology, mechanical, and thermal properties of polyamide 6/polypropylene/montmorillonite nanocomposites. Polymer Composites 2010; 31:1156-1167.
   DOI 10.1002/pc.20902
2. D.R. Katti, K.S. Katti, M. Raviprasad, C. Gu. Role of polymer interactions with clays and modifiers on nanomechanical properties and crystallinity in polymer clay nanocomposites. Journal of Nanomaterials 2012; 2012:1-15.
   DOI;10.1155/2012/341056
3. F.G. Alabarse, R.V. Conceicao, N.M. Balzaretti, F. Schenato, A.M. Xavier. In-situ FTIR analyses of bentonites under high-pressure. Applied Clay Science 2011; 51:202-208.
   DOI:10.1016/j.clay.2010.11.017
4. S.K. Kim, H.D. Kwen, S.H. Choi. Radiation-induced synthesis of vinyl copolymer based nanocomposites filled with reactive organic montmorillonite clay. Radiation Physics and Chemistry 2012; 81:519-523.
   DOI:10.1016/j.radphyschem.2012.01.027
5. R.K. Gupta, E. Kennel, K. Kwang-Jea. Polymer nanocomposites handbook. CRC Press Taylor and Francis Group, New York (2010).
   ISBN: 978-0-8493-9777-6
6. H. Lu, Y. Hu, M. Li, Z. Chen, W. Fan. Structure characterization and thermal properties of silane-grafted-polyethylene/clay nanocomposites prepared by reactive extrusion. Composites Science and Technology 2006; 66:3035-3039.
   DOI: 10.1016/j.compscitech.2006.01.018
7. A.H. Navarchian, K.M. Ardakani. Processing of transmission electron microscope images for quantification of the layered dispersion degree in polymer-clay nanocomposites. Journal of Applied Polymer Science 2009; 114:531-542.
   DOI 10.1002/app.30534
8. L. Xie, X.Y. Lv, Z.J. Han, J.H. Ci, C.Q. Fang, P.G. Ren. Preparation and performance of high-barrier low density polyethylene/organic montmorillonite nanocomposites. Polymer-Plastics Technology and Engineering 2012; 51:1251-1257.
   DOI; 10.1080/03602559.2012.699131

9. Kusmono, Z.A. Mohd Ishak, W.S. Chow, T. Takeichi, Rochmadi. Effect of clay modification on the morphological, mechanical, and thermal properties of polyamide 6/polypropylene/montmorillonite nanocomposites. Polymer Composites 2010; 31:1156-1167.
DOI:10.1002/pc.20902

10. S. Mohanty, S.K. Nayak. Melt blended polystyrene/layered silicates nanocomposites: Effect of clay modification on the mechanical, thermal, morphological and viscoelastic behaviour. Journal of Thermoplastic Composites Materials 2007; 20:175-193.
DOI: 10.1177/0892705707073180

11. L. Dun, G.S. Sur. Comparison of Na^{+}-MMT and Ca^{2+}-MMT for the preparation and characterization of poly(ethylene-*co*-acrylic acid) ionomer/MMT nanocomposites. Macromolecular Research 2011; 19:1035-1040.
DOI 10.1007/s13233-011-1016-4

12. B. Aldousiri, H.N. Dhakal, S. Onuh, Z.Y. Zhang, N. Bennett, M.O.W. Richardson. Effect of layered silicate reinforced on the structure and mechanical properties of spend polyamide-12 nanocomposites. Composites: Part B 2012; 43:1363-1367.
DOI:10.1016/j.compsitesb.2011.08.005

13. Y.Y. Choi, S.H. Lee, S.H. Ryu. Effect of silane functionalization of montmorillonite on epoxy/montmorillonite nanocomposite. Polymer Bulletin 2009; 63:47-55.
DOI 10.1007/s00289-009-0068-5

14. A.K. Nikolidis, D.S. Achilias, G.P. Karayannidis. Effect of the type of organic modifier on the polymerization kinetics and the properties of poly(methyl methacrylate)/organomodified montmorillonite nanocomposites. European Polymer Journal 2012; 48:240-251.
DOI:10.1016/j.eurpolymj.2011.11.004

15. B. Singh, N. Sharma. Mechanistic implications of plastic degradation. Polymer Degradation and Stability 2008; 93:561-584.
DOI:10.1016/j.polymdegradstab.2007.11.008

16. M. Abdelwahad, T. Agag, A. Akelah, T. Takeichi. Synthesis and characterization of methyl methacrylate modified vinylester resin-clay nanocomposites. The Open Macromolecules Journal 2012; 6:20-27.

17. M. Kaci, C. Remili, A. Benhamida, S. Bruzaud, Y. Grohens. Recyclability of polystyrene/clay nanocomposites.Molecular Crystals and Liquid Crystals 2012; 556:94-106.
DOI: 10.1080/15421406.2012.635922

18. C. Zhao, H. Qin, F. Gong, M. Feng, S. Zhang, M. Yang. Mechanical, thermal and flammability of polyethylene/clay nanocomposites. Polymer Degradation and Stability 2005; 87:183-189.
DOI:10.1016/j.polymdegradstad.2004.08.005

19. S.V. Krishna. G. Pugazhonthi. Influence of processing conditions on the properties of polystyrene (PS)/organomontmorillonites (OMMT) nanocomposites prepared via solvent blending method. International Journal of Polymeric Materials 2011; 60:144-162.
DOI: 10.1080/00914037.2010.504167

20. A.A. Onischuk. V.N. Panfilov. Mechanism of thermal decomposition of silanes. Russian Chemical Reviews 2001; 70:321-332.
DOI: 10.1070/RC2001v070n04ABEH000603

21. A. Nese, S. Sen, M.A. Tasdelen, N. Nugay, Y. Yagci. Clay-PMMA nanocomposites by radical polymerization using intercalated phenacyl pyridinium salt initiators. Macromolecular Chemistry and Physics 2006; 207:820-826.
DOI: 10.1002/macp.200500511

22. R. Rezanavaz, M.K.R. Aghjeh. Relationship between morphology and physico-mechanical properties of polyethylene/clay nanocomposites. Materials Science and Engineering 2012; 40:1-10.
DOI:10.1088/1757-899X/40/1/012047

23. A. Olad, M. Hayasi. A comparative study of polystyrene/layered silicate nanocomposites, synthesis by emulsion and bulk polymerization methods. Polymer-Plastics Technology and Engineering 2011; 50:1487-1495
DOI: 10.1080/03602559.2011.593083

24. H. Azizi, J. Morshedian, M. Barikani. Silane grafting and moisture crosslinking of polyethylene: The effect of molecular structure. Journal of Vinyl and Additive Technology 2009; 15:184-190.
DOI: 10.1002/vnl.20194

25. K. Sirisinha, D. Meksawat. Preparation and properties of metallocene ethylene copolymer crosslinked by vinyltrimethoxysilane. Polymer International 2005; 54:1014-1020.
DOI: 10.1002/pi.1800

26. Z. Wang, X. Wu, Z. Gui, Y. Hu, W. Fan. Thermal and crystallization behaviour if silane-crosslinked polypropylene. Polymer International 2005; 54:442-447.
DOI:10.1002/pi.1715

27. G. Zhang, G. Wang, J. Zhang, P. Wei, P. Jing. Performance evaluation of silane crosslinking of metallocene-based polyethylene-octene elastomer. Journal of Applied Polymer Science 2006; 102:5057-5061.
DOI: 10.1002/app.25169

28. D.A D'Amico. L.B. Manfredi, V.P. Cyras. Crystallization behaviour of poly(3-hydroxybutyrate) nanocomposites based on modifiers clays. Thermochimica Acta 2012; 544:47-53.
DOI.org/10.1016/j.tca.2012.06012

29. A. Sharif-Pakdaman, J. Morshedian, Y. Jahani. Influence of the silane grafting of polyethylene on the morphology, barrier, thermal, and rheological properties of high-density polyethylene/organoclay nano composites. Journal of Applied Polymer Science 2012; 125:E305-E313.
DOI:10.1002/app.36367

30. K. Grigoriadi, A. Giannakas, A. Ladavos, N.M. Barkoula. Thermomechanical behaviour of polymer/layered silicate clay nanocomposites based on unmodified low density polyethylene. Polymer Engineering and Science 2012; 00:000-000.
DOI: 10.1002/pen.23264

31. W.S. Chow, S.S. Neoh. Dynamic mechanical, thermal, and morphological properties of silane-treated montmorillonite reinforced polycarbonate nanocomposite. Journal of Applied Polymer Science 2009; 114:3967-3975.
DOI:10.1002/app.30977

32. J.A. Molefi, A.S. Luyt. Comparison of the influence of copper micro- and nano-particles on the mechanical properties of polyethylene/copper composites. Journal of Materials Science 2010; 45:82-88.
DOI: 10.1007/s10853-009-3894-9

33. J.A. McCormick, J.R. Royer, C.R. Hwang, S.A. Khan. Tailored rheology of a metallocene polyolefin through silane grafting and subsequent silane crosslinking. Journal of Polymer Science: Part B: Polymer Physics 2000; 38:2468-2479.
DOI: 10.1002/1099-0488(20000915)

34. J.L.S. Ngu, I. Noshida, M. Akmil, A.L. Chuah, R.C. Thevy. Thermal properties of low-density polyethylene/ALPHA-alumina nanocomposites. Journal of Thermoplastic Composite Material 2011; 25:415-426.
DOI:10.1177/0892705711411340

35. J. Mark, K. Ngai, W. Graessley, L. Mandelkern, E. Samulski, J. Koenig, G. Wignall. Physical Properties of Polymers, 3rd Edition. Cambridge University Press (2003).

36. M.R. Nouri. Thermal and dynamic mechanical properties of a polypropylene random copolymer. Iranian Polymer Journal 2005; 14:485-493.

37. G.S. Venkatesh, A. Deb, A. Karmarkar, S.S. Chauhan. Effect of nanoclay content and compatibilizer on viscoelastic properties of montmorillonite/polypropylene nanocomposites. Materials and Design 2012; 37:285-291.
DOI:10.1016/j.matdes.2011.12.034

38. J.I. Velasco, M. Ardanuv, V. Realinho, M. Antunes, A.I. Fernandez, J.I. Gonzalez-Pena, M.A. Rodriquez-Perez, J.A. de Saja. Polypropylene/clay nanocomposites: Combined effects of clay treatment and compatibilizer polymers on the structure and properties. Journal of Applied Polymer Science 2006; 102:1213-1223.
DOI: 10.1002/app.24419

39. M. Ataeefard, S. Moradian. Polypropylene/organoclay nanocomposites: Effects of clay content on properties. Polymer-Plastics Technology and Engineering 2011; 50:732-739.
DOI: 10.1080/03602559.2010.551438

40. S.J. Ahmadi, H. Yadong, W. Li. Synthesis of EPDM/organoclay nanocomposites: Effect of the clay exfoliation on structure and physical properties. Iranian Polymer Journal 2004; 13:415-422.

41. X. Qiao, W. Zhong, K. Sun, X. Chen. Effect of clay content on the dynamic mechanical and rheological properties of polypropylene/MAH-g-POE/clay composites. Journal of Applied Polymer Science 2009; 114:1702-1702.
DOI: 10.1002/app.30218

42. L. Wang, K. Wang, L. Chen, Y. Zhang, C. He. Preparation, morphology and thermal/mechanical properties off epoxy/nanoclay composite. Composites: Part A 2006; 37:1890-1896.
DOI:10.1016/j.compsitesa.2005.12.020

43. R.O Sirotkin, N.W. Brooks. The dynamic mechanical relaxation behaviour of polypropylene copolymers cast from solution. Polymer 2001; 42:9801-9808.
PII: S0032-3861(01)00535-3

44. V. Djokivic, D. Kostoski, M.D. Dramicanin. Viscoelastic behaviour of semicrystalline polymers at elevated temperature on the basis of a two-process model for stress relaxation. Journal of Polymer Science: Part B: Polymer Physics 2000; 38:3239-3246.
DOI: 10.1002/1099-0488(20001215)

45. M. Hidalgo, M.I. Beltran, H. Reinecke, C. Mijango. Thermal and mechanical properties of silane-crosslinked poly (vinylchloride). Journal of Applied Polymer Science 1998; 70:865-872.

46. J. Moraweic, A. Pawlak, M. Slouf, A. Galeski, E. Piorkowska, N. Krasnikowa. Preparation and properties of compatibilized LDPE/organo-modified montmorillonite nanocomposites. European Polymer Journal 2005; 41:1115-1122.
DOI: 10.1016/j.eurpolymj.2004.11.011

47. C. Jiao, Z. Z. Wang, A. Gui, Y. Hu. Silane grafting and crosslinking of ethylene-octene copolymer. European Polymer Journal 2005; 41:1204:1211.
DOI:10.1016/j.eurpolymj.2004.12.008

Chapter 5: Conclusions

The purpose of this study was to improve the thermal and mechanical properties of low-density polyethylene (LDPE) and high-density polyethylene (HDPE) by filling both matrices with nanoclays, and by modifying the polymer with an organic silane. The properties of the polymer-clay nanocomposites strongly depend on the morphology and level of clay dispersion in the polymer matrix. The effect of clay modifier and vinyltriethoxysilane (VTES) grafting/crosslinking treatment was investigated as means to improve the interfacial interaction and clay dispersion in both matrices.

The extent of grafting was controlled by the amounts of DCP and VTES. FTIR analysis clearly showed that grafting in System A (where a lower amount of DCP was used) was not very effective, and that the 'grafted' LDPE contained an appreciable amount of ungrafted (pure or hydrolysed) VTES. However, sufficient grafting was achieved in System B (where a higher amount of DCP was used), but here the extent of crosslinking was also higher. Despite these treatments, complete dispersion (exfoliation) of the clay layers in the polymer matrices was not achieved, and only mixed morphologies (exfoliated and intercalated structures) where successfully produced.

Although complete exfoliation was not achieved in the different systems that we investigated, there were observable improvements in the mechanical properties and thermal stability of LDPE. The presence of both modified and unmodified clay increased the storage modulus, loss modulus and tensile modulus of LDPE. This was due to the reinforcement of the clay which increased the stiffness of the polymer. The thermal stability of LDPE was significantly improved by the introduction of modified clay, but the unmodified clay did not have a significant influence on the thermal stability. An increase in stress at break was observed with the addition of both modified and unmodified clay. The presence of both clays did not significantly influence the melting temperature and melting enthalpy of LDPE. This showed that the crystallization of the polymer was not influenced by the presence of the clay.

The results obtained from most techniques indicated that the presence of DCP/VTES did not significantly improve the interfacial interaction in the LDPE/C15A and HDPE/C15A nanocomposites to the extent of achieving fully exfoliated structures. The presence of

DCP/VTES initiated crosslinking between the polymer chains. Since HDPE is more crystalline than LDPE, the crosslinking had a more significant influence on its crystallinity. The presence of VTES grafting/crosslinking significantly decreased the melting temperature and the crystallinity of LDPE and HDPE, but the presence of clay reduced this influence for both matrices. This is probably because silane grafting was more prevalent in the presence of clay. Crosslinking increased the thermal stability of LDPE and HDPE, and the addition of and increase in clay loading further increased the thermal stability of the polymers. The presence of clay in the DCP/VTES treated matrices improved the tensile modulus due to the reinforcing effect and fairly good interaction between the treated polymers and the clay. In both polymer matrices the thermal stability, storage modulus and tensile modulus decreased at higher VTES contents, and the addition of and increase in clay loading slightly improve these properties. The thermal stability of the LDPE nanocomposites prepared according to Systems A and B did not differ much, but the mechanical and thermomechanical properties of the nanocomposites prepared according to System B where significantly lower, probably because of the reduced crystallinity of the polymer after being crosslinked. It is expected that the difference in properties will be even more prevalent in HDPE, because of the significantly higher crystallinity of this polymer.

Overall it was found that VTES treatment slightly improved the interaction between the polymer and the clay, and the clay modification did not play a significant role in this case. In the absence of clay VTES treatment led to grafting onto and crosslinking between the polymer chains, with crosslinking being more prevalent. However, in the presence of clay the grafting seemed to have been more prevalent, although there was still some crosslinking. This crosslinking had a stronger influence on the HDPE properties because of its higher crystallinity than the presence of the clay. It is therefore clear that a more detailed study will be needed where the influence of each of several parameters can be quantified. These parameters are the morphology of the polymer, the type of clay used, the extent of grafting and/or crosslinking, and the extent of interaction between the different types of clay and the silane grafted chains of the polymer(s).

ACKNOWLEDGEMENTS

I would like to pass my sincere gratitude to the Lord Almighty for seeing me through this journey and giving me the strength, wisdom, patience, and courage to persevere throughout this project.

My gratitude and appreciation to my supervisor **Prof. Adriaan Stephanus Luyt**, for his consistent supervision, guidance, encouragement and patience during all stages of this project. His overly enthusiasm and integral view on research and his mission for providing 'only high-quality work and not less', has made a deep impression on me. Throughout my thesis-writing period, he provided encouragement, very good advice, good teaching and lots of good ideas.

Special thanks to **Puseletso Julia Mofokeng**, who has been a friend, sister, mother and a mentor. For her support, advice, encouragement and most for being there in times of troubles through the course of this project. You have been a pillar of my strength and always a shoulder to cry on. **Cheryl-Anne (Zanele)**, I am happy I got to know someone so warm and down to earth. Your door was always open, you inspired me and encouraged me to believe in myself and do my best all the time. **Mr Tsietsi Tsotetsi and Mrs Malimabe** thank you for believing in me and giving me the chance to expand my horizon and reach for the stars.

I am also grateful to my mentors **Dr Mohammad Essah Ahmad** and **Dr Maithufi Nora** for giving valuable advice and providing technical guidance and valuable contributions throughout the research program. To my best friend **Mohanuwa Mofokeng** thank you for always supporting and encouraging me to further my studies and for helping me get through the tough times, and for all the good ideas shared.

I am also grateful to the staff and colleagues in the Faculty of Natural and Agricultural sciences for their assistance in every aspect of my project. To the entire polymer research team (PhD, M.Sc and Honours). Special thanks to Dr. He Wei, Dr. Nagi Greesh, Mr. Mfiso Mngomezulu, Mr. Tshwafo Motaung, Mr Shale Sefadi, Mr. Thabang Mokhothu, Mr. Teboho Motsoeneng. Mr. Teboho Mokhena, Mr. Jonas Mochane, Mr. Tladi Mofokeng, Mrs Nomampondomise Molefe, for all their help, support, interest and valuable inputs.

And last but definitely not least, thanks to my parents (Mr Matebesi Daniel Sibeko and Mrs Mantseke Marie Sibeko) for raising me with their love, guidance, support, responsibility and a lot of encouragement.

APPENDIX

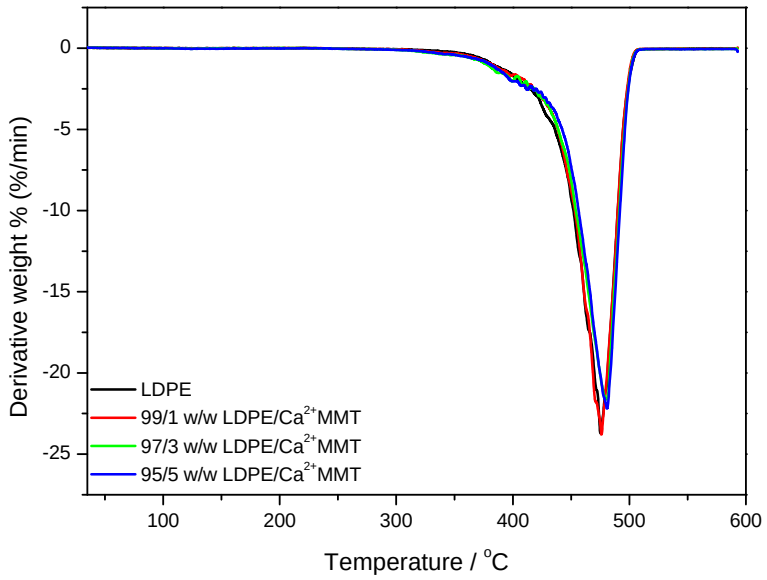

Figure A.1 DTGA curves of LDPE and LDPE/Ca^{2+}MMT nanocomposites

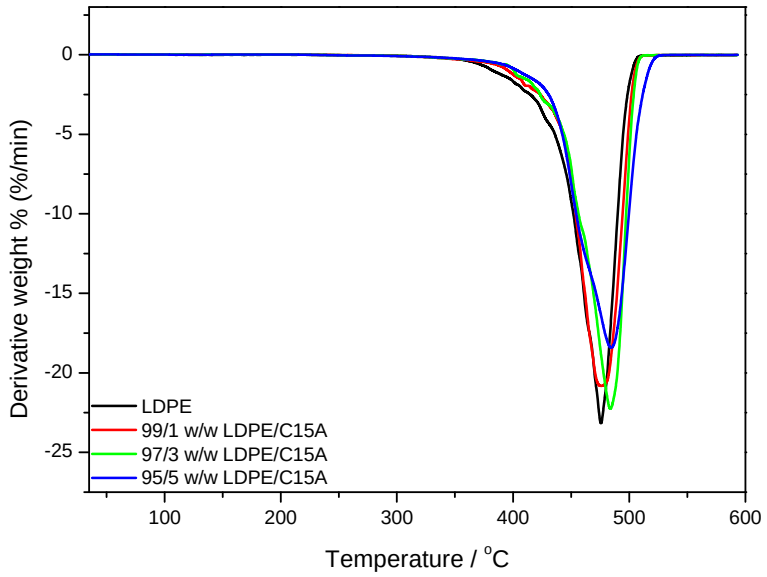

Figure A.2 DTGA curves of LDPE and LDPE/C15A nanocomposites

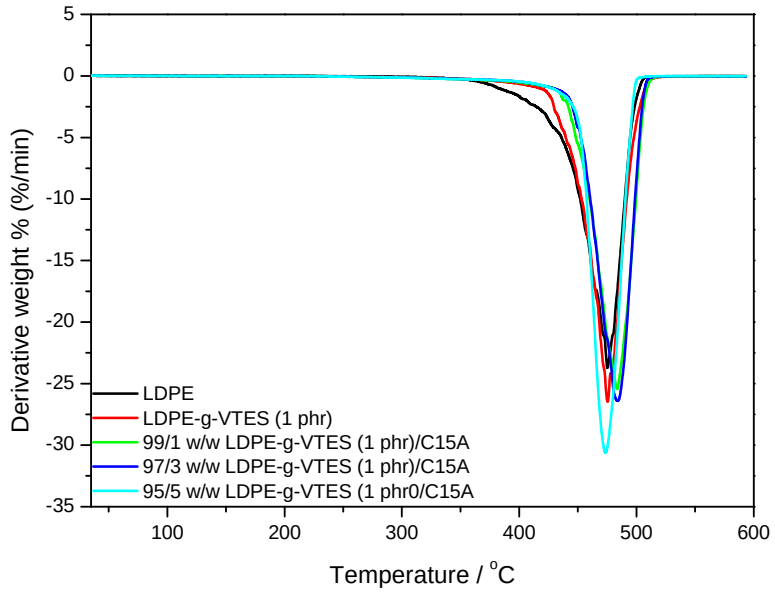

Figure A.3 DTGA curves of LDPE, VTES grafted LDPE (1 phr, System A) and the different nanocomposites

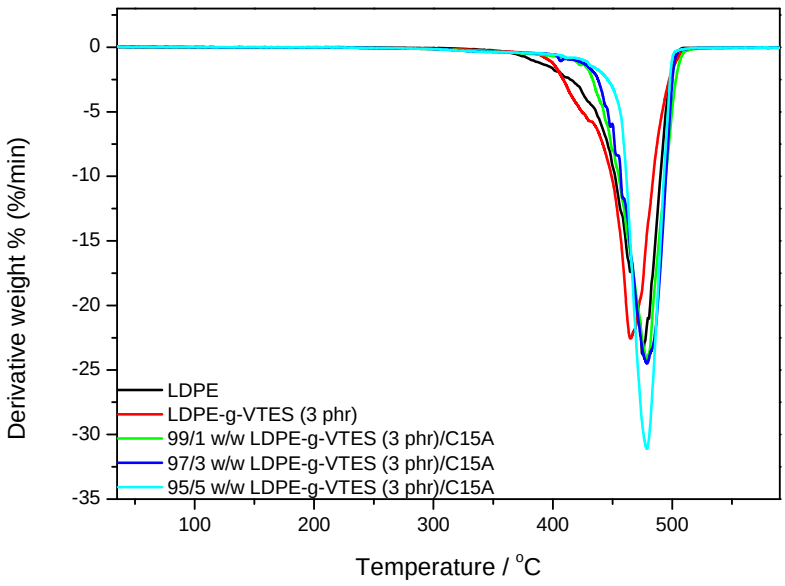

Figure A.4 DTGA curves of LDPE, VTES grafted LDPE (3 phr, System A) and the different nanocomposites

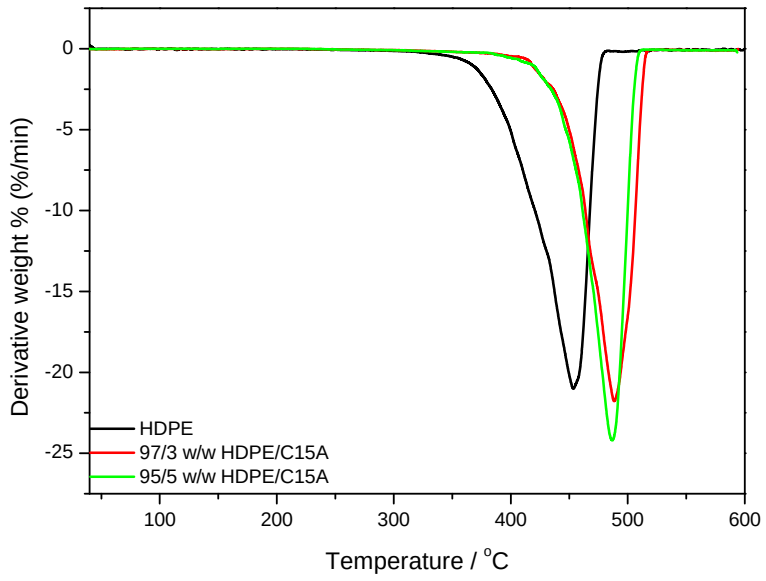

Figure A.5 DTGA curves of HDPE and HDPE/C15A nanocomposites

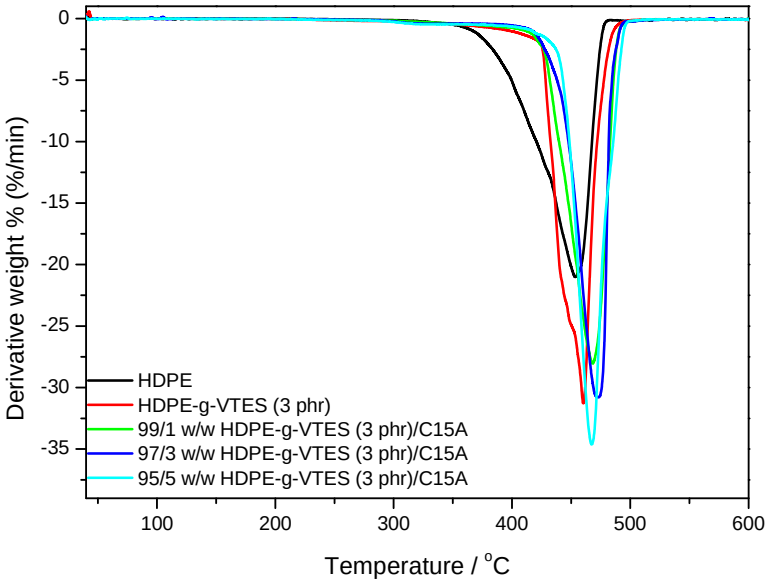

Figure A.6 DTGA curves of HDPE, VTES grafted HDPE (3 phr, System A) and the different nanocomposites

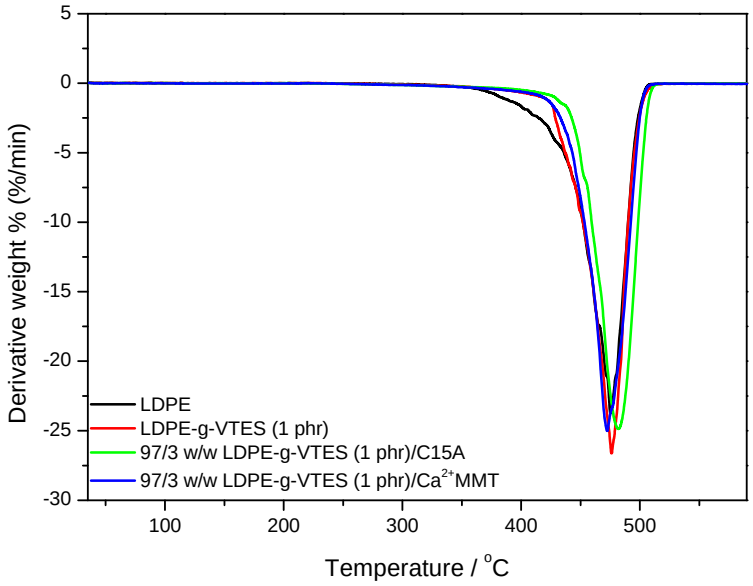

Figure A.7 DTGA curves of LDPE, VTES grafted LDPE (1 phr, System B) and the different nanocomposites

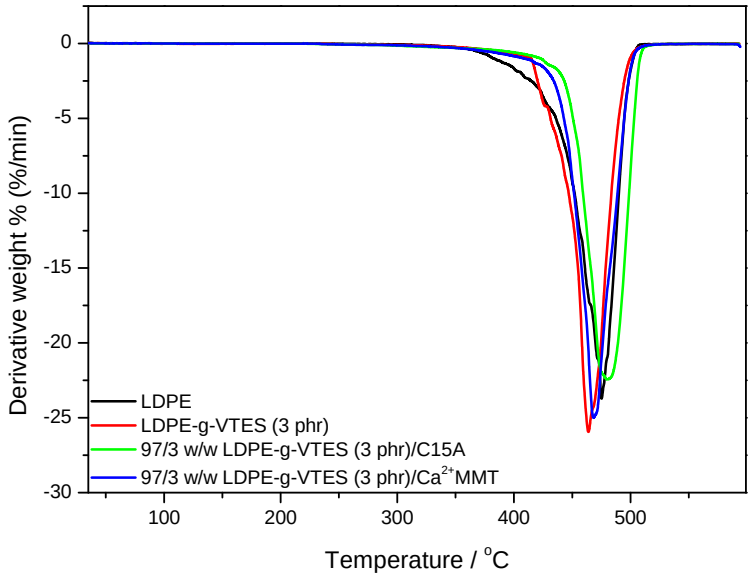

Figure A.8 DTGA curves of LDPE, VTES grafted LDPE (3 phr, System B) and the different nanocomposites

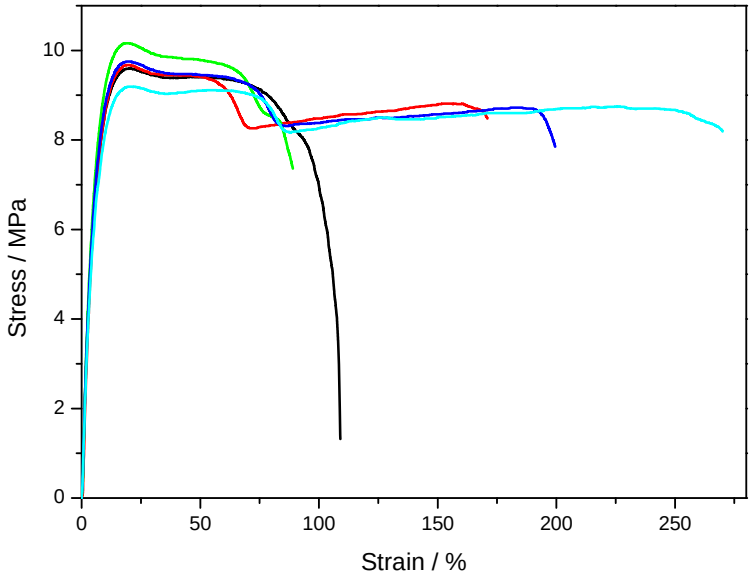

Figure A.9 Stress-strain curves for the LDPE

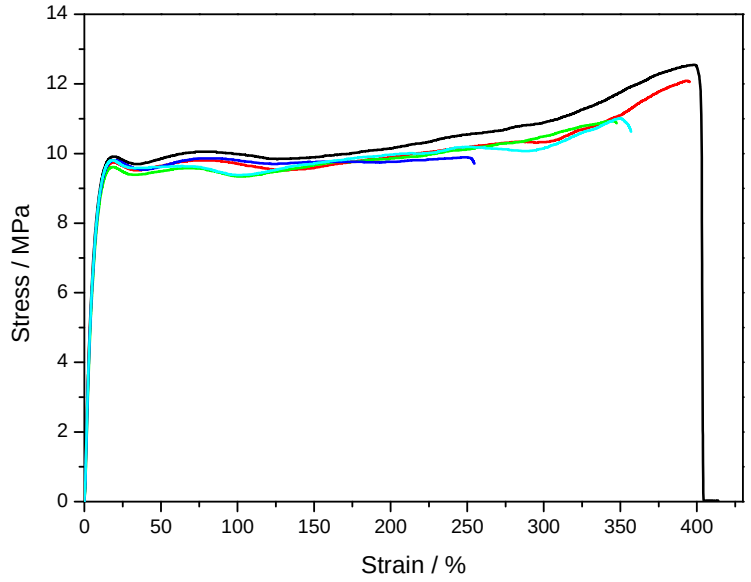

Figure A.10 Stress-strain curves for the LDPE-g-VTES (1 phr)

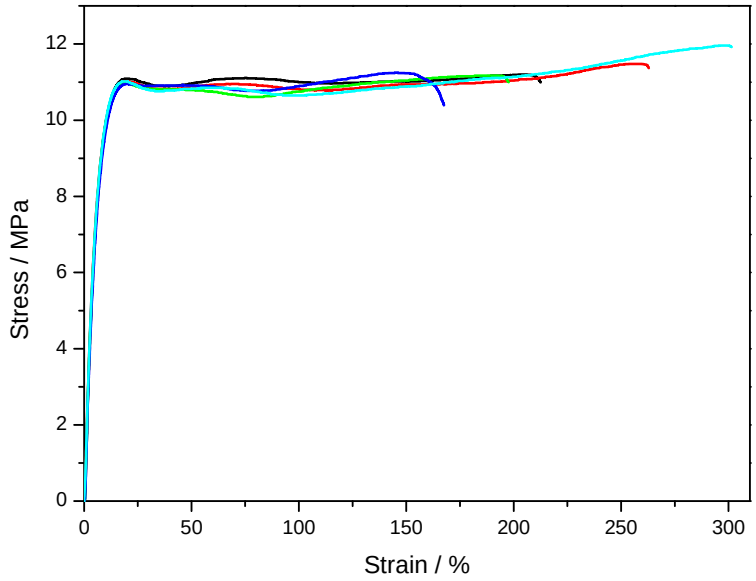

Figure A.11 Stress-strain curves for the 99/1 w/w LDPE-g-VTES (1 phr)/C15A nanocomposite

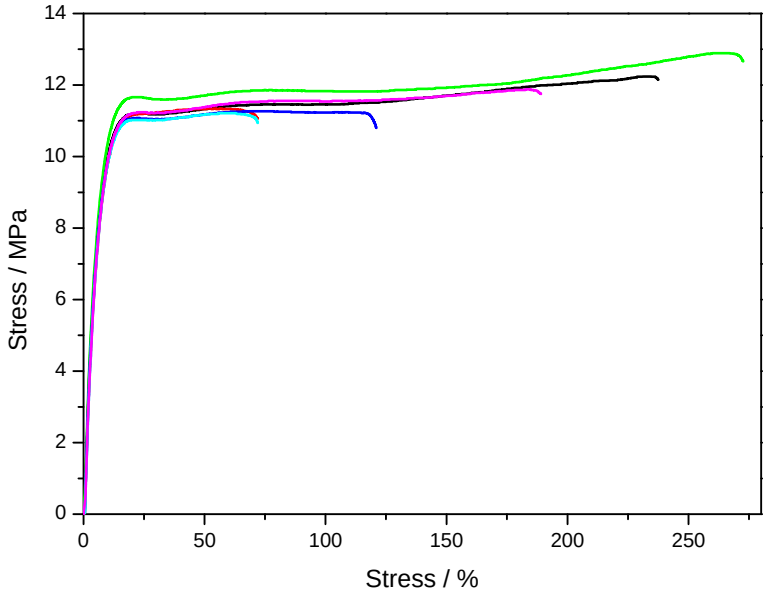

Figure A.12 Stress-strain curves for the 97/3 w/w LDPE-g-VTES (1 phr)/C15A nanocomposite

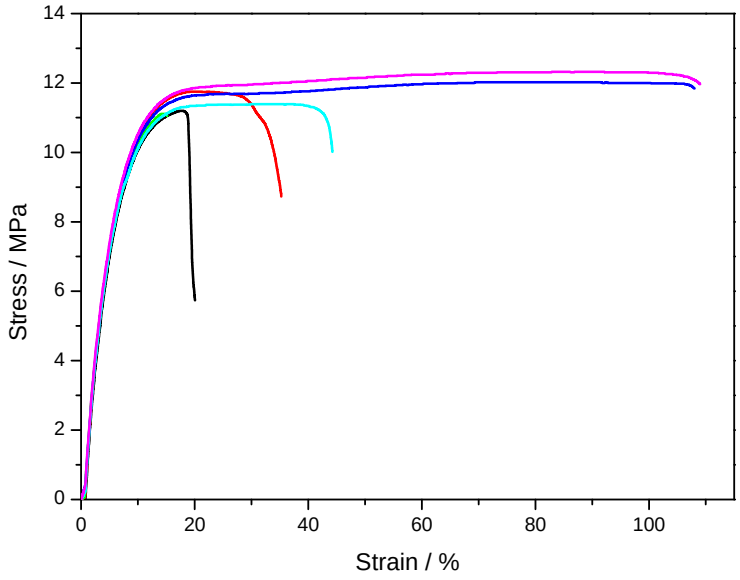

Figure A.13 Stress-strain curves for the 95/5 w/w LDPE-g-VTES (1 phr)/C15A nanocomposite

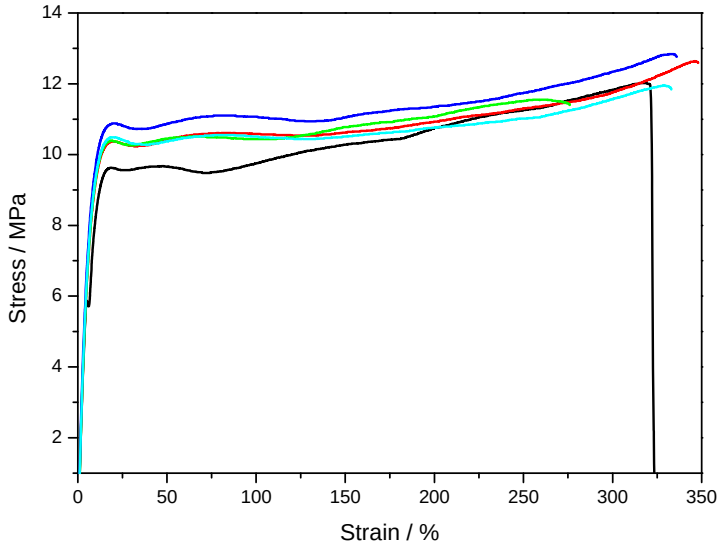

Figure A.14 Stress-strain curves for the 97/3 w/w LDPE-g-VTES (1 phr)/Ca^{2+}MMT nanocomposite

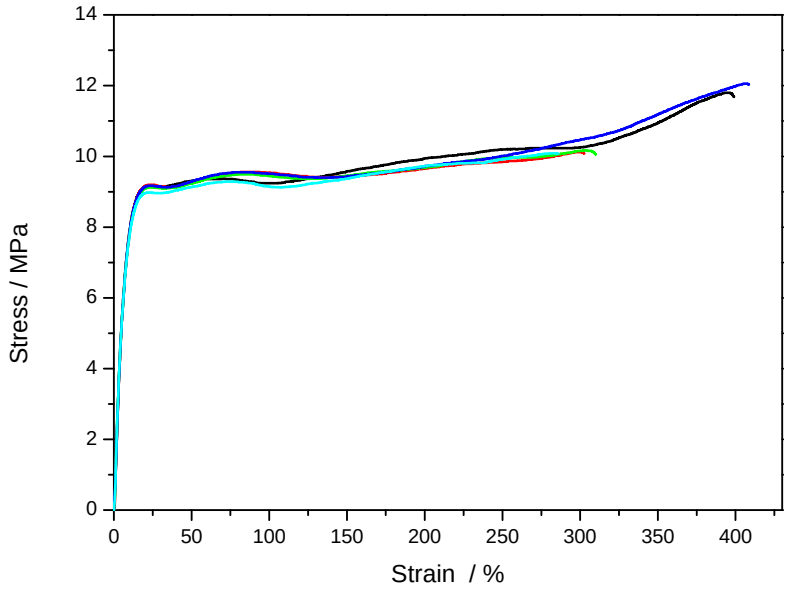

Figure A.15 Stress-strain curves for the LDPE-g-VTES (3 phr)

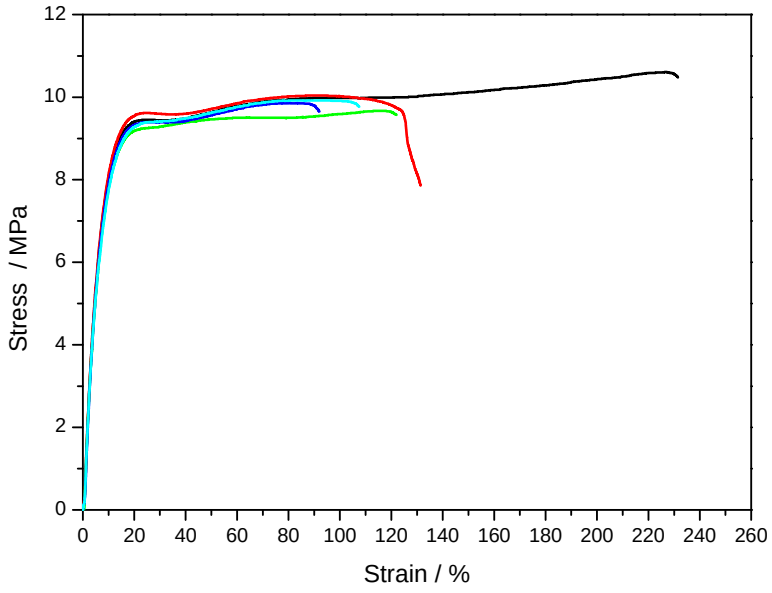

Figure A.16 Stress-strain curves for the 99/1 w/w LDPE-g-VTES (3 phr)/C15A nanocomposite

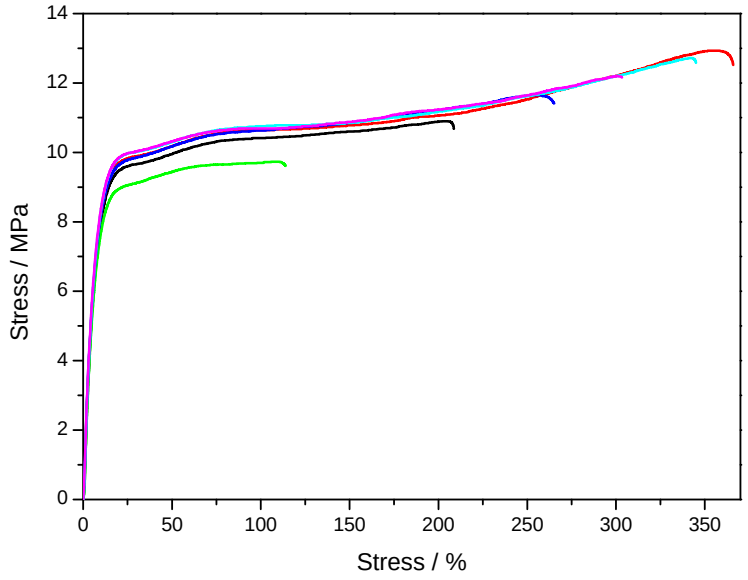

Figure A.17 Stress-strain curves for the 97/3 w/w LDPE-g-VTES (3 phr)/C15A nanocomposite

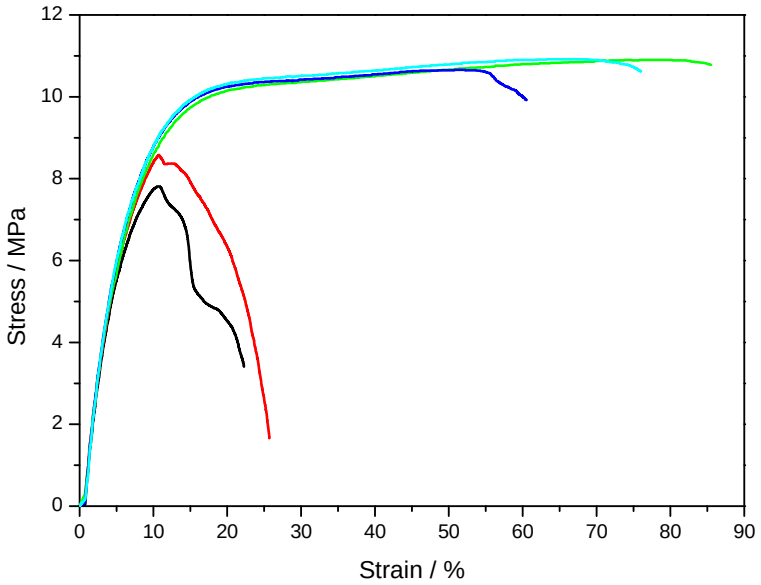

Figure A.18 Stress-strain curves for the 95/5 w/w LDPE-g-VTES (3 phr)/C15A nanocomposite

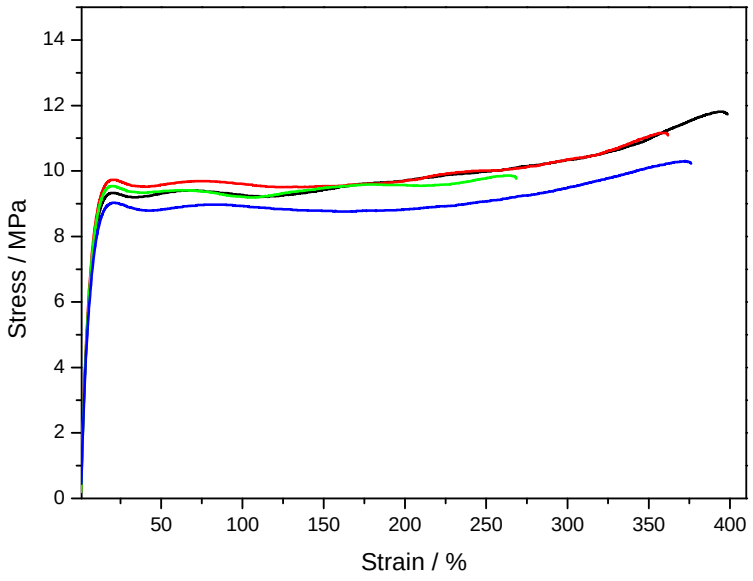

Figure A.19 Stress-strain curves for the 97/3 w/w LDPE-g-VTES (3 phr)/Ca^{2+}MMT nanocomposite

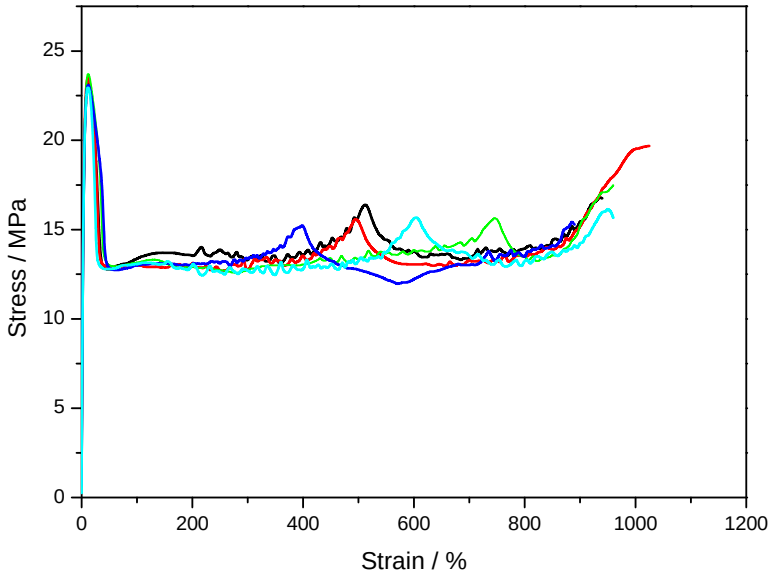

Figure A.20 Stress-strain curves for the HDPE

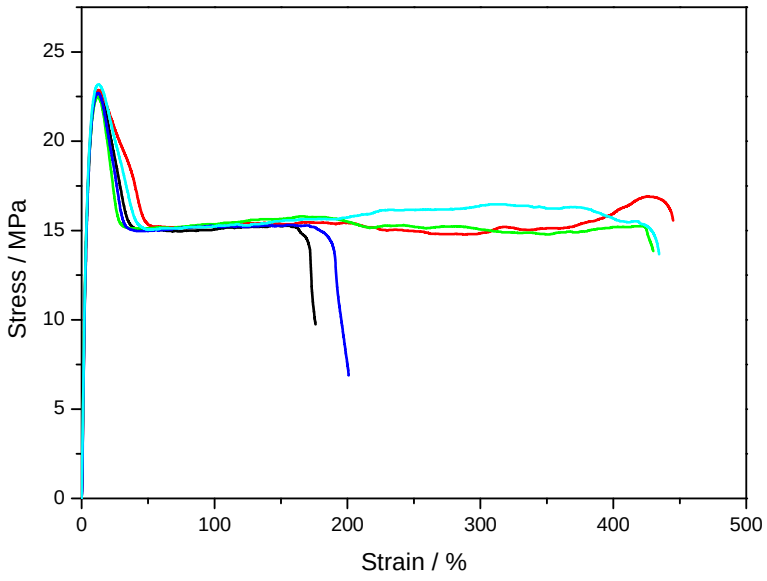

Figure A.21 Stress-strain curves for the HDPE-g-VTES (3 phr)

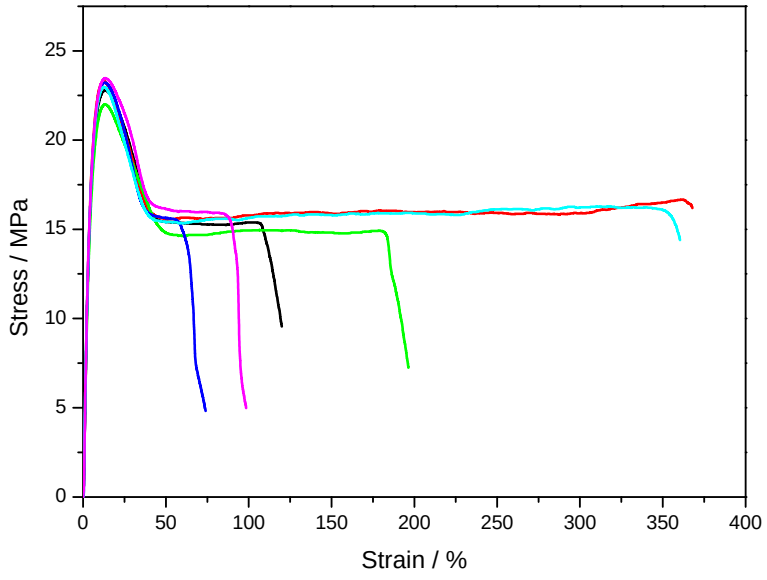

Figure A.22 Stress-strain curves for the 99/1 w/w HDPE-g-VTES (1 phr)/C15A nanocomposite

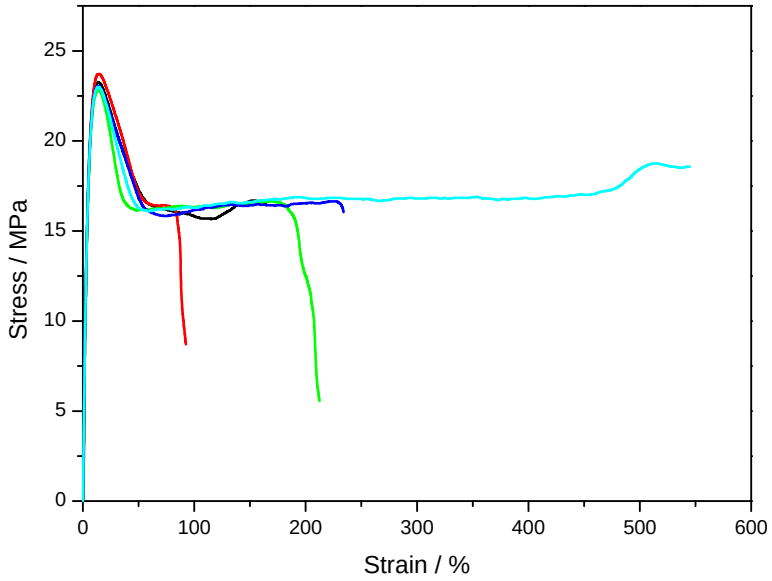

Figure A.23 Stress-strain curves for the 97/3 w/w HDPE-g-VTES (1 phr)/C15A nanocomposite

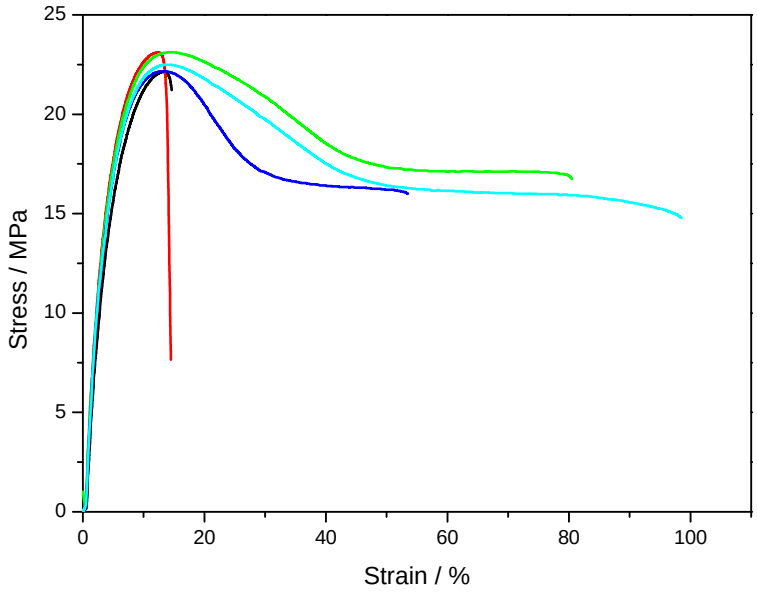

Figure A.24 Stress-strain curves for the 95/5 w/w HDPE-g-VTES (1 phr)/C15A nanocomposite

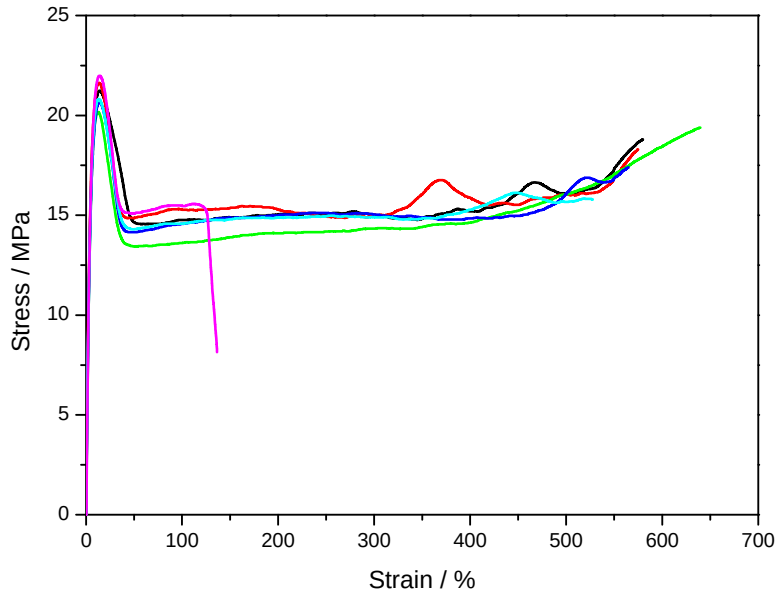

Figure A.25 Stress-strain curves for the HDPE-g-VTES (3 phr)

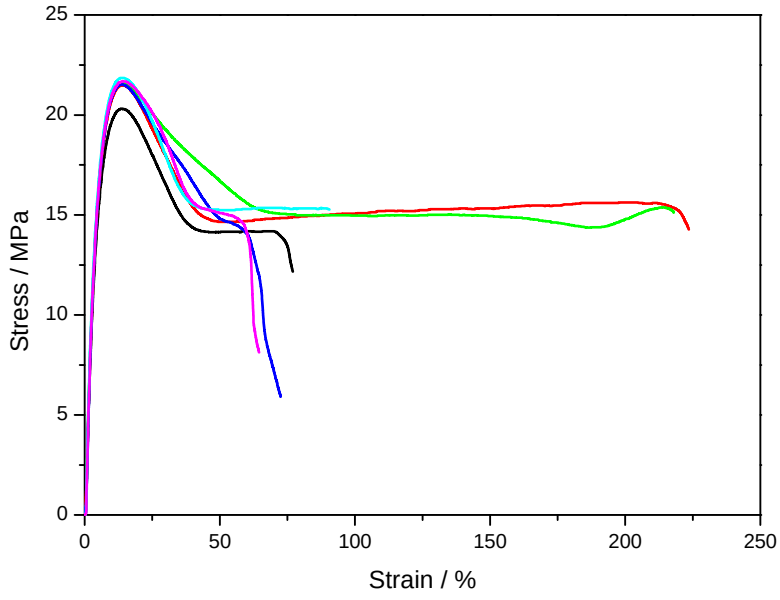

Figure A.26 Stress-strain curves for the 99/1 w/w HDPE-g-VTES (3 phr)/C15A nanocomposite

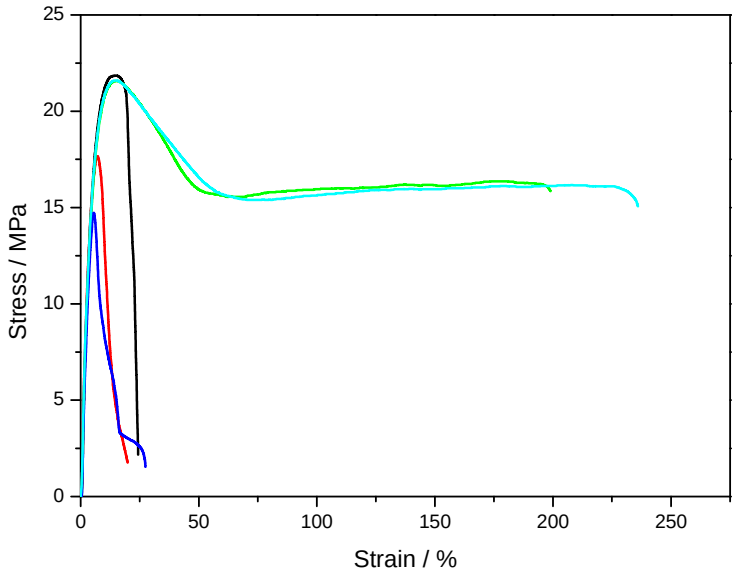

Figure A.27 Stress-strain curves for the 97/3 w/w HDPE-g-VTES (3 phr)/C15A nanocomposite

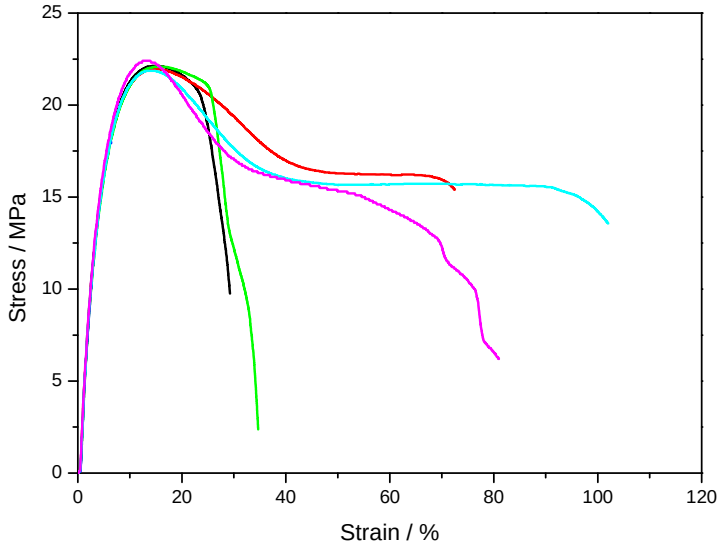

Figure A.28 Stress-strain curves for the 95/5 w/w HDPE-g-VTES (3 phr)/C15A nanocomposite